siRNA Loaded Lipidoid Nanoparticles and the Immune System

Submitted in partial fulfillment of the requirements for
the degree of

Doctor of Philosophy

in

Chemical Engineering

Lisa N. Kasiewicz

B.S., Chemical Engineering, Columbia University

Carnegie Mellon University
Pittsburgh, PA

May 2018

Acknowledgments

First I thank my adviser, Dr. Kathryn Whitehead. I definitely am a better presenter, writer, and scientific communicator after working with her these five years, and am grateful for the opportunity to work on such interesting research. I also thank my labmates (all of you, how could I possibly single anyone out), who have helped a great deal through the years, and been wonderful friends besides. Himali Ranade as well, my undergraduate mentee, who helped with my first paper. I thank my committee: Dr. Kris Dahl, Dr. Todd Przybycien, Dr. Newell Washburn, and Dr. Whitehead (Chair), for advising me during the proposal and thesis defense exams.

I would like to thank my funding sources, namely the Disruptive Health Technology Institute and the Wadhwani Foundation (proposal number 161842). The latter has made the immune response project possible, and facilitated the collaboration with Indian Institute of Technology Bombay. I would also like to thank the Purwar group at IIT Bombay, especially Dr. Rahul Purwar and Sushant Kumar, for sharing their expertise with immunology and immunological techniques. They were extremely gracious hosts when I visited their lab and I am fortunate to have had the ability to travel there. Last but not least, I owe so much to my husband, Dr. Nicholas Chisholm, who has supported me in so many ways through my PhD and been my rock when I needed him most. We met, married, and Doctored at Carnegie Mellon, and I really couldn't have done it without him.

Abstract

Delivery vehicles are necessary for many therapeutics to overcome the various challenges in their path. It is clear, however, that the relationship between delivery vehicles and the immune system is a complex one. One such delivery vehicle is the lipidoid nanoparticle, which has been shown to be potent in several cell types. This thesis details the first time lipidoids have been used for wound delivery, and demonstrates the successful silencing of an inflammatory protein, TNFα, in the context of diabetic ulcers. Knockdown is seen in an in vitro macrophage-fibroblast coculture model, as well as in non-diabetic and diabetic mice wound models. Lipidoids silence roughly half of the TNFα gene expression in the diabetic wound and have been shown to help the wound close faster than untreated controls. Of course, immune activation can decrease therapeutic efficacy or trigger dangerous reactions in the patient. Learning more about what chemical moieties cause an immune response would allow for the design of a particle that could better resist immune clearance and avoid the creation of a secondary response. This thesis investigated the effect of a lipidoid library on the immune system using a two pronged approach. The lipidoids were first tested against human peripheral blood mononuclear cells and then were injected into mice to probe the in situ immune response. Several types of B cells were examined in this latter case, namely germinal center B cells, plasma cells, and memory B cells. A T cell dependent response occurred, favoring memory B cells for most of the lipidoids tested. There was an increase in free antibody in the blood that reflected this increase in antibody producing cells. Nitrogen rings and carbon tail lengths of eleven and twelve carbons were particularly reactive, though it appears that the amine head group determines immune response more than the tail. Further work will analyze whether these increases in immune cells reflect a loss of therapeutic efficacy, as current ramifications are unclear. An in-depth T cell subset analysis with flow cytometry would also help complete the picture.

Table of Contents

List of Figures and Illustrations

Chapter 1

Introduction

While a drug might be extremely useful, the unfortunate truth is that many are unable to traverse the various barriers in the body to get where they are needed most. They might have difficulty extravasating from the bloodstream or entering the target organ. Once there they may not be taken up by the proper cells or trafficked intracellularly to their intended destination. Fortunately the encapsulation or complexation of therapeutic molecules with a delivery vehicle can help overcome these challenges. The field of drug delivery focuses on how to optimally package a variety of compounds in a way that augments or complements their therapeutic abilities.

Many different types of delivery vehicles have been developed, ranging from polymers to gold nanoparticles to liposomes. These vehicles are essential for everything from vaccines to cancer therapeutics, and often make therapy possible at all. Sometimes delivery is targeted to the immune system itself, both for vaccines and for inflammatory diseases like rheumatoid arthritis. Regrettably for the drug delivery field, millions of years of evolution have trained our bodies to destroy that which is not self, and the immune system cannot tell the difference between a harmful invader like a virus and a beneficial therapeutic. This complicates not only therapeutic delivery to the immune system, but the delivery of any drug to any organ. Ultimately it is clear that a better understanding of the interplay between drug delivery vehicles and the immune system would benefit delivery vehicle design.

Our lab specializes in a class of lipid nanoparticles called lipidoids. These synthetic lipid-like molecules are composed of a tertiary amine head group conjugated to acrylate tails. They can be used

to either deliver a therapeutic to the immune system (Chapters 2 and 3) or probe the immune response to certain surface chemistries (Chapter 4). This thesis will examine the intended and unintended effects of drug delivery and the lipidoid nanoparticles' ability to modulate the immune system.

While more specific background will be given in each chapter's introduction, Chapters 2 and 3 detail the use of lipidoid nanoparticles loaded with siRNA against tumor necrosis factor α (TNFα) topically applied to diabetic ulcers. TNFα is a master cytokine in the inflammation response, and is a contributor to the chronic inflammation which prevents diabetic ulcers from closing in a timely manner. Delivery is examined first in an in vitro macrophage-fibroblast coculture and then in in vivo non-diabetic and diabetic mouse models. This marks the first time lipidoid nanoparticles have been used for delivery to wounds (or topical delivery at all). Chapter 4 uses a library of different lipidoid chemistries to mount a large-scale screen of the B cell and cytokine response to surface chemistry. The hope is that learning what moieties provoke immune response can contribute to the design of a less immunostimulatory particle. This may help with immune system evasion and preserve the efficacy of therapeutics in vivo.

Chapter 2

Silencing TNFα with lipidoid nanoparticles downregulates both TNFα and MCP-1 in an *in vitro* co-culture

Much, but not all, of this chapter can be found in Kasiewicz and Whitehead [1].

Diabetes is one of the most formidable diseases facing the world today, with the number of patients growing every year. Poor glycemic control yields a host of complications, such as impaired wound healing. This often results in the formation of diabetic foot ulcers, which carry a poor prognosis because they are notoriously difficult to treat. Current therapies do not address the increased number of infiltrating macrophages to the wound bed that overproduce tumor necrosis factor α (TNFα), which increases fibroblast apoptosis and collagen dismantling and decreases angiogenesis. In this study, we investigated the potential of RNA interference therapy to reduce the inappropriately high levels of TNFα in the wound bed. Although TNFα is a challenging gene silencing target, our lipidoid nanoparticles potently silence TNFα mRNA and protein expression at siRNA doses of 5 - 100 nM without inducing vehicle-related gene silencing or cell death. We also describe the creation of an *in vitro* macrophage-fibroblast co-culture model, which reflects the TNFα and monocyte chemotactant protein-1 (MCP-1/CCL2) cross-talk that exists in diabetic wounds. Because TNFα induces fibroblasts to produce MCP-1, we show that

silencing TNFα results in a downregulation of MCP-1, which should inhibit the recruitment of additional macrophages to the wound. In co-culture experiments, a single lipidoid nanoparticle dose of 100 nM siTNFα downregulated TNFα and MCP-1 by 64% and 32%, respectively. These data underscore the potential of lipidoid nanoparticle RNAi treatment to inhibit a positive feedback cycle that fuels the pathogenesis of diabetic foot ulcers.

2.1 Introduction

Diabetes is one of the most prevalent diseases worldwide and is reaching epidemic proportions, especially in the United States. The number of those afflicted grows each year as the population ages, and a recent study by the American Medical Association posits that 50% of Americans now have pre-diabetes or diabetes [2]. Approximately 90% of diabetics suffer from Type II Diabetes, which is characterized by hyperglycemia and resultant complications [3]. These complications include ischemia, peripheral neuropathy, kidney failure, and impaired wound healing—the last of which can lead to the formation of a chronic non-healing foot ulcer. Each diabetic has up to a 25% lifetime risk of developing a foot ulcer, with many requiring lower leg amputation [4]. Unfortunately, these amputations carry a 50% three year survival rate due to the unresolved biological pathologies [5].

Unlike acute wounds, diabetic foot ulcers do not proceed normally through the general stages of wound healing [6]. Instead, they become entrenched in a state of chronic inflammation characterized by macrophage and cytokine dysfunction [7]. A greater than normal number of macrophages has been shown to persist within diabetic wounds, and these macrophages overproduce a key inflammatory cytokine: tumor necrosis factor α (TNFα) [8, 9, 10, 11]. In normal wound beds, TNFα is produced by activated macrophages in carefully controlled amounts to induce fibroblast migration, proliferation, and matrix remodeling, as well as to stimulate angiogenesis [12]. Overproduction of TNFα, however, disturbs this balance and results in chronic levels of cellular apoptosis and matrix degradation [13, 9, 14, 15, 10]. Currently the most common method of treatment is the use of biocompatible polymer bandage materials, hyperbaric oxygen therapy, and antibiotics [16, 17]. There has also been some research into the use of growth factors [18], neuropeptides [19, 20], and small molecule drugs [21] to help heal these

ulcers.

RNA interference (RNAi) is an alternative therapeutic approach that can be used to reduce the expression of proteins that prolong the wound healing process. For example, there have been several reports of improved wound healing outcomes upon gene silencing of matrix metalloproteinase 9 (MMP-9), an enzyme involved in extracellular matrix remodeling [22, 23]. In this study, we asked whether or not RNAi therapy can correct macrophage dysfunction through the downregulation of TNFα. Historically, other inflammatory diseases such as inflammatory bowel disease and arthritis have benefited from the use of agents against common inflammatory cytokines such as TNFα [21, 24, 25]. In the case of diabetic wound healing, systemic anti-TNFα therapies [26] and antibody-based neutralization [27] have been shown to ameliorate symptoms. Unfortunately, systemic anti-TNFα therapies suppress a patient's entire immune system and can result in an increased risk of infection and severe liver damage [28, 29, 27, 25]. Although such risks prevent the widespread use of systemic anti-TNFα therapy [30], local downregulation of the inflammatory cytokine may improve wound healing times without causing unwanted side effects.

In this paper, we demonstrate an alternative therapy using topically applied lipidoid nanoparticles (LNPs) loaded with siRNA against TNFα to improve diabetic foot ulcer healing in an *in vitro* co-culture model. Because the overexpression of TNFα underpins the deregulated immune response in diabetic foot ulcers, it is a particularly suitable choice of a gene target for siRNA. Furthermore, we have previously developed LNPs that potently deliver siRNA *in vivo* without provoking the immune system [31, 32, 33]. LNPs contain ionizable amine groups that facilitate receptor-mediated endocytosis and endosomal escape under the reduced pH conditions of the endosome [34, 35]. Herein, we show that LNPs transfect macrophages and fibroblasts in cell culture, and that sustained TNFα knockdown is possible at low doses of siRNA without loss of cell viability.

In order to more accurately mimic the wound bed environment, we also describe the creation of an *in vitro* co-culture model that facilitates the assessment of multiple components of the inflammatory cycle present in the wound bed (fig. 2.1). Although co-cultures have been used for biomaterial and fundamental biology studies, their use in drug delivery applications or diabetic silencing work has been very limited [36, 37, 38, 39]. Nevertheless, both cell types are present within the wound bed and engage

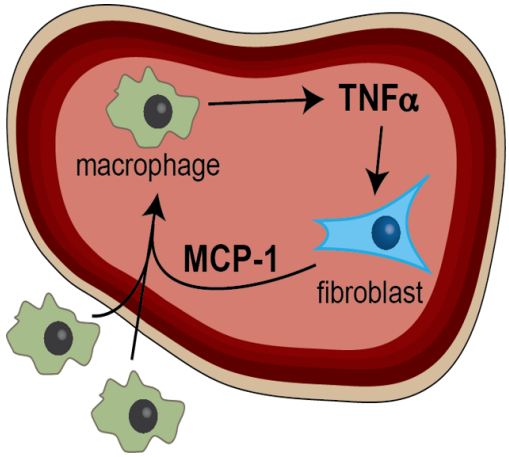

Figure 2.1: **Cycle of inflammatory cytokine/chemokine upregulation in diabetic foot ulcers.** Macrophages, which respond to the initial wound damage, produce TNFα, which triggers fibroblasts to produce MCP-1. MCP-1 recruits additional activated inflammatory macrophages to the wound site, which fuel the inflammatory cycle. Our approach involves knocking down the expression of TNFα, which is expected to result in the downregulation of MCP-1 and inhibition of the inflammatory cycle.

in important cytokine cross-talk [40, 36]. In particular, fibroblasts produce monocyte chemotactant protein-1 (MCP-1/CCL2) upon TNFα stimulation, which summons monocytes and macrophages to the wound site and contributes to vasculature inflammation [36, 38]. Given the chronic upregulation of TNFα in diabetic foot ulcers, MCP-1 is also overproduced and helps to further the positive feedback cycle of inflammation [36, 40]. Putting an end to the TNFα/MCP-1 cycle as demonstrated in a co-culture would not only decrease the effects of TNFα in the foot ulcer, but reduce the recruitment of further activated monocytes.

Using this co-culture, we show that siTNFα not only suppresses the expression of TNFα in macrophages but also inhibits the expression of MCP-1 in neighboring fibroblasts. By down-regulating MCP-1, we expect that anti-TNFα RNAi therapy will reduce the number of macrophages infiltrating the wound bed and promote rapid wound healing.

2.2 Materials and Methods

2.2.1 Cell culture

RAW 264.7 macrophages (ATCC, Manassas, VA) were maintained in High Glucose (4.5 g/L) Dulbecco's Modified Eagle's Medium (Gibco, Carlsbad, CA), 10% Fetal Bovine Serum (Invitrogen, Carlsbad, CA), and 1% Penicillin-Streptomycin (Invitrogen) at 37°C and 5% carbon dioxide. 3T3-NIH fibroblast cells (ATCC) were cultured in Dulbecco's Modified Eagle's Medium (Gibco), 10% Newborn Calf Bovine Serum (Invitrogen), and 1% Penicillin-Streptomycin (Invitrogen). Fibroblasts were used below passage 25 and macrophages below passage 9.

2.2.2 Cell viability

The MTT Cell Proliferation Assay (ATCC) was used to measure cell viability. Macrophages were seeded at a density of 5×10^4 cells/well and fibroblasts at 2×10^4 cells/well in clear 96-well plates. Approximately five hours after seeding, 100 nM dose of nanoparticles was added for 24 hours where indicated. After 24 hours, 10 uL of MTT reagent was applied per well. Four hours after MTT reagent addition, 100 uL of MTT detergent was added and the plate was allowed to sit covered by aluminum foil overnight at room temperature. Absorption values of treated cells were normalized to untreated cell values.

2.2.3 Nanoparticle formulation

Lipidoids were formulated into nanoparticles for all experiments. All experiments were conducted with the three-tailed version of the lipidoid $306O_{13}$ [32]. The lipidoid was synthesized via the Michael addition of 3,3'-Diaminodipropylamine (Acros Organics) to tridecyl acrylate (Pfaltz and Bauer, Waterbury, CT) at a stoichiometric ratio of 1:3 as described previously [31]. The three-tailed product was purified over a silica column on a Teledyne ISCO chromatography system. For nanoparticle formulation, the lipid solution was formed by mixing the lipidoid, distearoyl-sn-glycerol-3-phosphocholine (DSPC, from Avanti Polar Lipids), cholesterol (Sigma Aldrich, St. Louis, MO), and, where noted, C14-PEG (Avanti Polar Lipids) at a molar ratio of 50:10:38.5:1.5 in the presence of ethanol (Sigma Aldrich), citrate buffer, and

PBS. Silencer Select Pre-Designed siRNA against Tumor Necrosis Factor α (s75248) and CCL2 (151586) was purchased (Life Technologies). The siRNA was diluted in 10 mM sodium citrate and combined with the lipid solution at a final lipid to siRNA weight ratio of 5:1. The solution was vortexed after each reagent addition, and the lipid solution was added to the siRNA solution. The mixture was vortexed to form nanoparticles.

2.2.4 Nanoparticle characterization

Nanoparticles were diluted to a final siRNA concentration of 1 μg/mL in PBS. Percent siRNA entrapment was determined via the Quant-iT Ribogreen assay (Invitrogen), as Ribogreen binds to siRNA and fluoresces. Entrapment was determined by comparing the signal from intact LNP solutions to the signal from an LNP solution that had been ruptured with 2% Triton-X surfactant. Nanoparticle size was measured with a Malvern Zetasizer Nano (Malvern Instruments, UK).

2.2.5 RNA interference

For fibroblast GAPDH mRNA experiments, fibroblasts were seeded at a density of 3×10^5 cells/well in 24-well plates approximately 5 hours before nanoparticle addition. Cells were harvested for RNA extraction 24 hours after nanoparticle addition. For macrophage mRNA experiments, macrophages were seeded at a density of 3.25×10^5 cells/well in 24-well plates approximately 5 hours before nanoparticle addition. In TNFα experiments, twenty hours after nanoparticle addition, 20 ng/mL of Lipopolysaccharide (LPS) from *E. coli* 0111:B4 (Sigma-Aldrich) was added to each well. Macrophages were harvested for RNA extraction an experiment-specified number of hours after LPS addition. For GAPDH silencing, macrophages were harvested 24 hours after nanoparticle addition with no LPS added. In all experiments, three wells of the 24-well plate were grouped into each biological replicate, and there were three biological replicates per sample.

2.2.6 RNA extraction and cDNA synthesis

RNA extraction and purification was accomplished with the QIAshredder and RNeasy Mini Kit (Qiagen, Valencia, CA). RT-PCR was performed with the High Capacity cDNA Reverse Transcription kit (Applied Biosystems) to form 2 μg of cDNA. The quality and quantity of mRNA and cDNA were assessed by the absorbance at 260/280 nm with the Nanodrop 2000 UV-Vis spectrophotometer (Thermo Scientific).

2.2.7 Quantitative PCR

qPCR was performed in a 384-well block on a ViiA^{TM} 7 Real-Time PCR system machine with purchased Taqman Gene Expression Master Mix (Applied Biosystems), along with GAPDH (Mm99999915_g1), TNFα (Mm00443258_m1), CCL2 (Mm00441242_m1), and β-Actin (Mm00607939_s1) Taqman probes (Life Technologies). 10 uL of Master Mix, 1 uL of endogenous control probe, and 1 uL of target gene probe was used per well. All runs utilized the comparative Ct method and the following run protocol: 50°C (2 min), 95°C (10 minutes), 40 cycles of 95°C (15 sec) and 60°C (1 min). qPCR experiments consisted of three biological replicates and two technical replicates per each biological. The target gene was normalized to the endogenous control gene for each sample, and then normalized again to the nanoparticle-free control sample. GAPDH was compared to β-Actin, while TNFα and MCP-1/CCL2 were both compared to GAPDH.

2.2.8 TNFα ELISA

Culture supernatants were collected, divided into single use aliquots, frozen at -80°C, and thawed just before use in the Mouse TNFα ELISA kit (Invitrogen). Culture samples were diluted 1:99 and added to the antibody coated well plate, along with the serial dilution of the provided standard. The experiment was then carried out according to the kit protocol.

2.2.9 Juxtacrine co-culture

3T3 cells were removed with trypsin and pelleted by centrifugation. They were then re-suspended in DMEM and 10% FBS media (macrophage media). 250 uL of 6×10^5 cells/mL were plated into wells of a 24-well plate, along with fibroblast only wells. RAW 264.7 macrophages were scraped and diluted to a density of 5×10^5 cells/mL, and 250 uL was plated into fibroblast containing and macrophage only wells. All fibroblast only and macrophage only wells received 250 uL of fresh FBS containing media, to bring all well volumes to 500 uL. Nanoparticles were added 5 hours later, and 20 ng/mL LPS was added 20 hours after that to all wells. In one experiment, where indicated, mRNA was extracted from all wells 4 hours after LPS addition. In another experiment, mRNA was extracted from all wells 16 hours after LPS addition.

2.2.10 Paracrine co-culture

The same seeding procedure was used as in juxtacrine co-culture experiments (above), except fibroblasts and macrophages were plated in separate wells. Fibroblasts were seeded at a density of 3×10^5 cells/mL and macrophages at 2.5×10^5 cells/mL, 500 uL each well. Macrophages were incubated with 100 nM siTNFα nanoparticles for 20 hours, before receiving 20 ng/mL LPS. As indicated in individual experiments, either seven or ten hours later, media was removed from the fibroblast wells and replaced with media directly from the LPS only or nanoparticles/LPS macrophages. Control fibroblasts received 20 ng/mL LPS directly into the original media. mRNA was extracted 12 or 18 hours after the media switch, as indicated.

2.2.11 Statistical Analyses

All mean values are expressed as $\pm$ standard deviation. Unpaired Student's t-tests and one-way ANOVA tests were used where appropriate to evaluate statistical significance. A p value of < 0.05 was considered significant.

2.3 Results

2.3.1 LNP characterization and silencing proof of concept

The lipidoid nanoparticles (LNPs) used in this study comprise five ingredients: the lipidoid $306O_{13}$ (50 mol%), DSPC (10 mol%), cholesterol (40 - X mol%), and mPEG-2000 (X mol%, as indicated). X ranged from 0 to 5, but was 1.5 for most experiments. LNPs are depicted in the first panel of fig:lipidoid-basics. LNPs form spontaneously due to hydrophobic interactions and electrostatic attraction between the protonated lipidoid amine (under reduced pH conditions) and the negatively charged siRNA. siRNA entrapment values within the nanoparticle are comparable across doses, with an average encapsulation percentage of 80-82%, as calculated from four separate experiments using siGAPDH and siTNFα (second panel of fig. 2.2). Nanoparticles were shown to remain stable (same Z-average diameter of about 180 nm, no loss of entrapment) for upwards of seven days at room temperature at a 100 nM dose (fig. 2.3). The nanoparticle is well tolerated by both fibroblasts and macrophages, as measured by an MTT assay in which the absorbance values of treated cells were normalized to those of untreated cells (third panel of fig. 2.2). No statistically significant loss of viability was seen after a 24-hour incubation with a 100 nM dose of control siRNA specific against green fluorescent protein (GFP). GFP is used as a control because it is not natively expressed in either cell line. Before choosing an appropriate diabetic wound gene target, proof-of-concept silencing experiments were conducted on a model housekeeping gene, GAPDH, to assess nanoparticle potency on macrophages and fibroblasts. When siGAPDH was delivered using LNPs, a dose dependent knockdown of GAPDH mRNA was observed in both fibroblasts and macrophages 24 hours post-transfection (fourth panel of fig. 2.2). In fibroblasts, 98% knockdown was achieved with an siGAPDH dose of 100 nM, and the EC_{50} was 5 nM. In macrophages, a 100 nM siGAPDH dose resulted in 89% silencing, with an EC_{50} of 15 nM.

Since many cell types can be sensitive to the presence of ethanol and change their gene expression accordingly, qPCR experiments were conducted to assess whether silencing was due to direct toxicity effects from the ethanol. In this case, macrophages received a volume of ethanol roughly double of that which is found in the final formulation of the lipidoid nanoparticles (22% of the total volume). Addi-

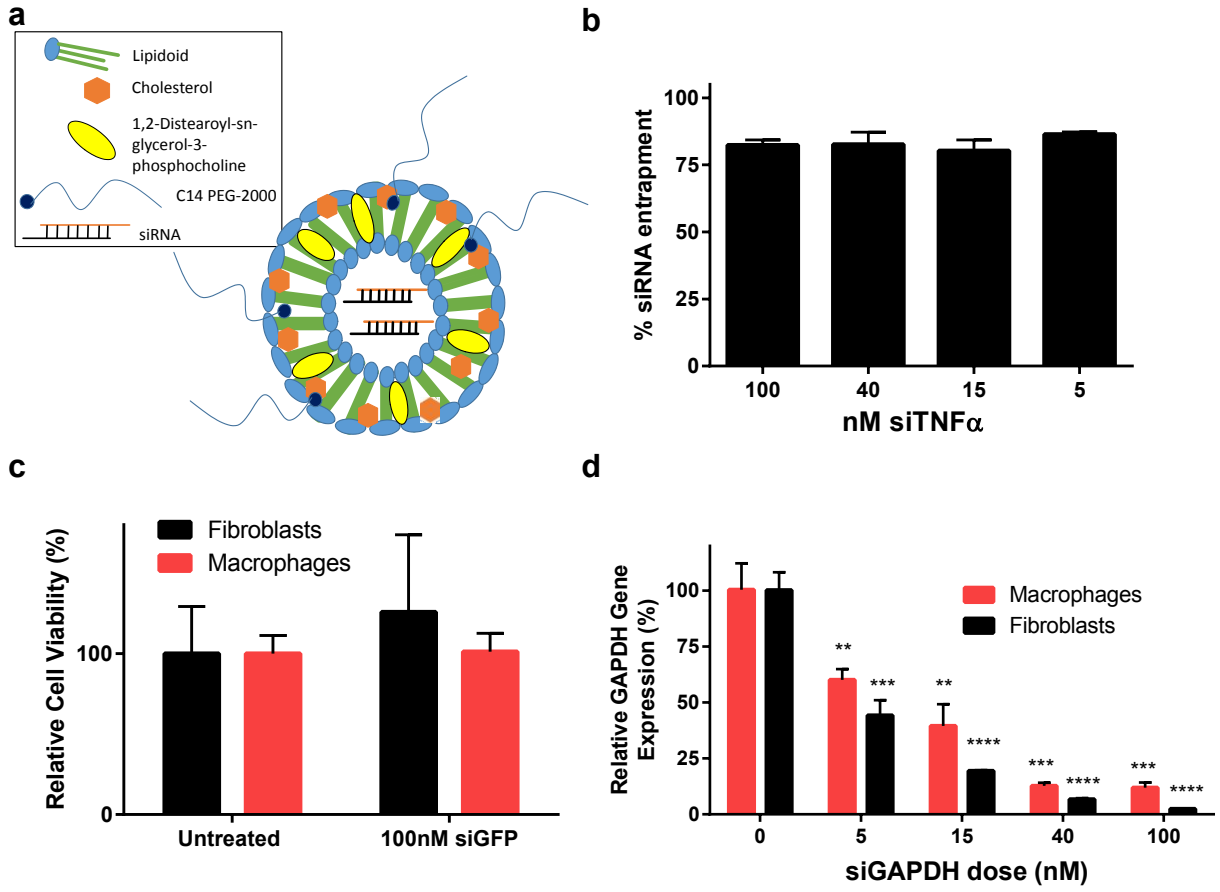

Figure 2.2: **Lipidoid nanoparticles (LNPs) potently deliver siRNA to fibroblasts and macrophages, two important cells found in diabetic foot ulcers.** (a) The lipidoid nanoparticle is composed of five ingredients: the lipidoid, DSPC, cholesterol, mPEG-2000, and siRNA. (b) Regardless of siRNA concentration, LNPs entrapped approximately 80% of siRNA upon formulation. n = 3. (c) Control LNPs containing a 100 nM siRNA dose did not affect the viability of macrophages or fibroblasts after 24 hours of exposure as determined by an MTT assay. $n = 6$ (macrophages), $n = 4$ (fibroblasts). (d) LNPs induced dose-dependent GAPDH silencing in macrophages and fibroblasts 24 hours post-transfection. $n = 3$. Error bars in all panels represent s. d. ($^{*}p < 0.05$, $^{**}p < 0.01$, $^{***}p < 0.001$, $^{****}p < 0.0001$)

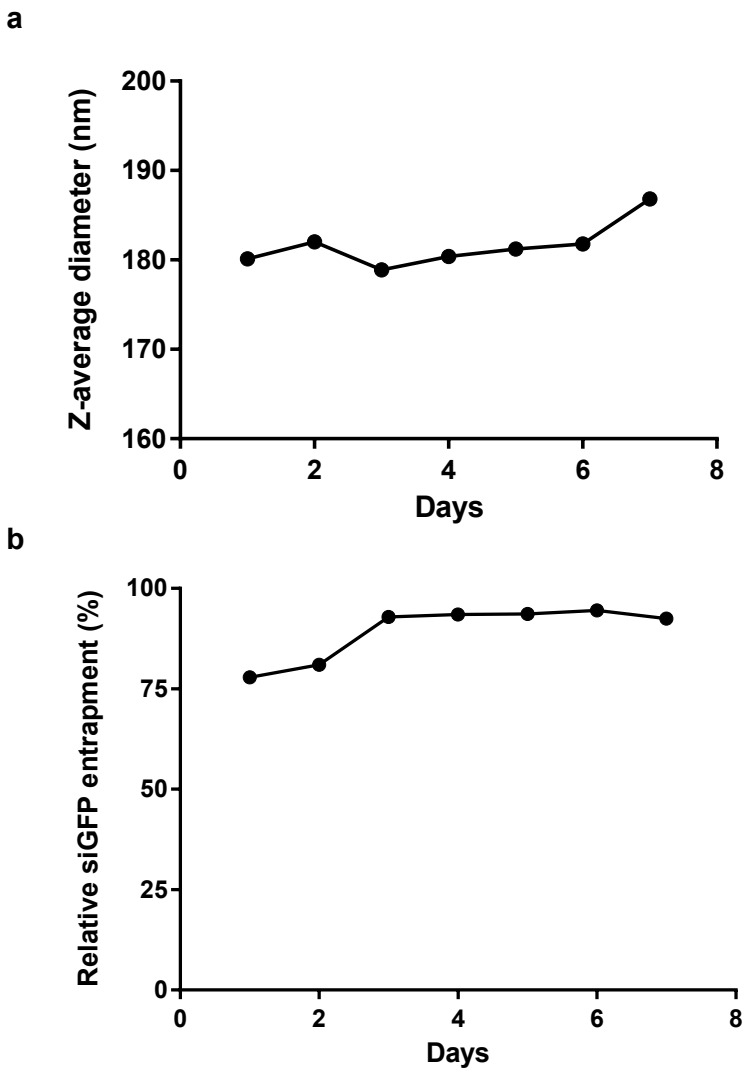

Figure 2.3: **Nanoparticles are stable for at least 7 days at room temperature.** (a) Nanoparticle diameter was measured via Dynamic Light Scattering every day for 7 days. (b) siRNA entrapment efficiency was measured via the Quant-iT Ribogreen assay every day for 7 days. The apparent increase in entrapment efficiency is due to the disintegration of the siRNA that was not originally encapsulated inside the nanoparticles.

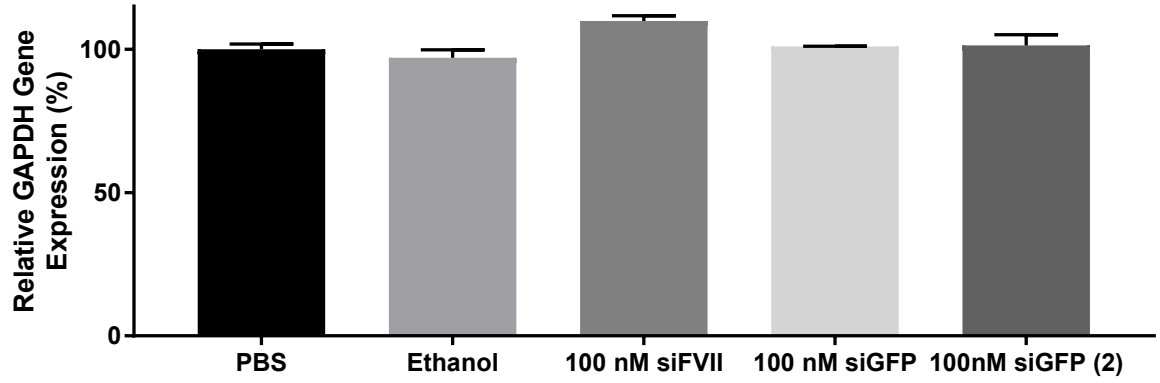

Figure 2.4: **Silencing is not due to toxicity or off-targeting effects.** Macrophages received 2.5 uL of ethanol or 100 nM doses of siFVII or siGFP. When compared to gene expression in cells receiving only PBS control, no knockdown was observed. $n = 3$. Error bars in all panels represent s. d.

tionally, nanoparticles loaded with 100 nM siRNA targeting Factor VII and GFP (both targets which are not expressed in macrophages) were separately delivered to assess off-targeting effects. The siGFP in particular was delivered in two different experiments to confirm the findings. No silencing of the house-keeping gene GAPDH was observed in either the ethanol or siFVII/siGFP treated cells, confirming that all knockdown typically seen is due to the effect of properly targeted siRNA and not coincidence or toxicity.

2.3.2 TNFα silencing in macrophages

Having demonstrated potent GAPDH knockdown in fibroblasts and macrophages, we next selected a disease-relevant protein for gene silencing: the inflammatory cytokine TNFα. Macrophages in cell culture are inactive and need to be stimulated to produce TNFα. Therefore, lipopolysaccharide (LPS), a component of gram negative bacteria, was applied to macrophages in the remainder of experiments in order to stimulate the production of inflammatory cytokines, including TNFα [41]. Based on protocols for macrophage stimulation [41], an initial experiment was conducted to assess the optimal dose of LPS to use (fig. 2.5). TNFα production four hours after treatment varied little between 50 and 100 ng/mL of LPS, while increasing amounts of LPS predictably triggered increasing TNFα production. PBS treated cells received no LPS and serve as a baseline control. Ultimately, a dose of 20 ng/mL LPS was chosen

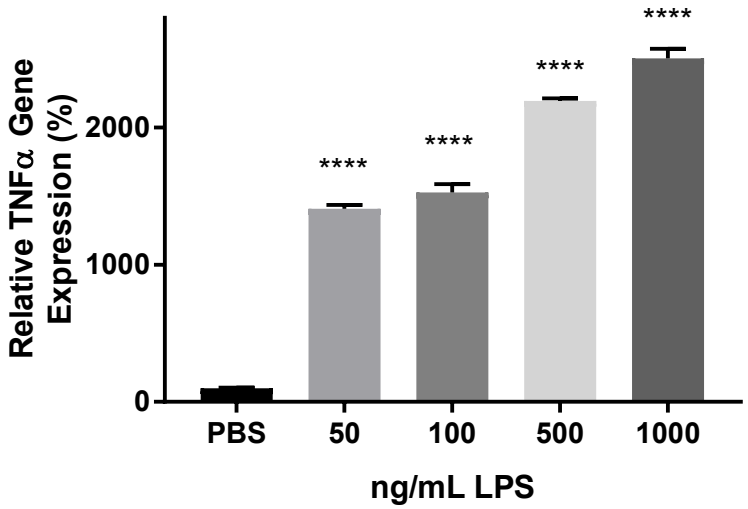

Figure 2.5: **Increasing LPS dose increases macrophage production of TNFα.** Macrophages were plated at 3.3×10^5 cells/well and treated with varying amounts of LPS. As LPS dose increased, so did TNFα production. $n = 3$. Error bars in all panels represent s. d. ($^{****}p < 0.0001$)

to proceed, to avoid issues of LPS-mediated toxicity.

Two separate experiments were conducted to gauge when LPS-stimulated TNFα production by macrophages peaked. They are graphed side by side in fig. 2.6. A dose of 20 ng/mL LPS was applied to macrophages at time t = 0 and cells were harvested for RNA collection at the specified time points following initial stimulation. qPCR reveals that though the production of TNFα can vary from experiment to experiment (no doubt due to the genetic makeup of macrophages present and their specific rate of replication), the dynamics of TNFα production remains largely the same. In fact, this shape will again surface in the longer experiment shown in fig. 2.10. LPS stimulated production of TNFα peaks somewhere between two and four hours following treatment before gradually decreasing over time. As a result, a time point of four hours post LPS addition was chosen for RNA harvest in future fixed point experiments.

The typical dosing timeline for experiments using siTNFα loaded nanoparticles is depicted in the first panel of fig. 2.7, with 20 ng/mL LPS added to wells 20 hours after the addition of LNPs. Four hours later, mRNA was extracted for gene silencing analysis by qPCR. As is shown in the second panel of fig. 2.7, LPS induced a 25-fold increase in TNFα mRNA expression compared to untreated macrophages. In contrast, control LNPs containing 100 nM siGFP were relatively well tolerated and

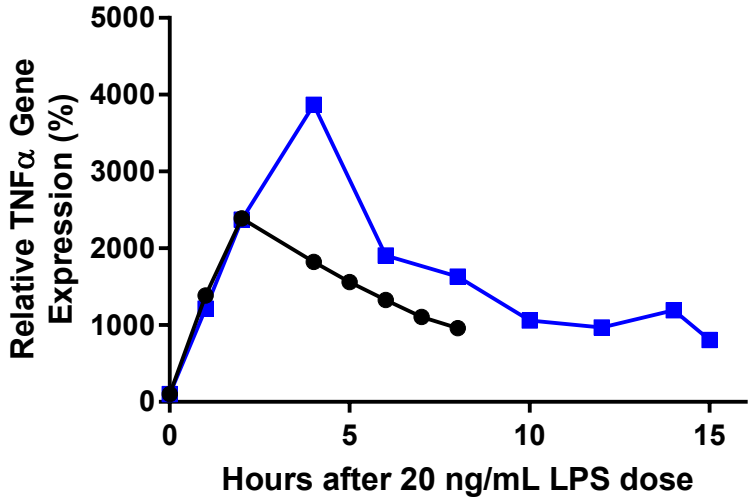

Figure 2.6: **LPS production changes over time.** Macrophages were plated at 3.25 x 10^5 cells/well and treated with 20 ng/mL LPS in two separate experiments, each represented by a different line. The initial time point is represented by PBS-only treated cells. One experiment lasted eight hours and the other lasted fifteen. For both experiments, TNFα production peaked between two and four hours after LPS stimulation. $n = 3$. Error bars in all panels represent s. d.

non-immunostimulatory. Next, we showed that LNPs containing siTNFα silenced TNFα in a dose dependent manner in LPS-stimulated macrophages (third panel of fig. 2.7). A 100 nM siTNFα dose resulted in TNFα silencing of 65%, with an EC_{50} dose of 40 nM.

We also sought to demonstrate that TNFα knockdown did not depend on the order of LNP or LPS addition. The fourth panel of fig. 2.7 shows results when cells were stimulated with LPS prior to LNP addition, as well as afterwards, to mimic the chronic inflammation of an actual ulcer. Macrophages were first dosed with LPS and then with LNPs 15 hours later, with another dose of LPS applied nine hours after that. When mRNA was extracted 15 hours after this second dose, TNFα silencing at 40 nM and 100 nM doses was 65% and 62%, respectively. These levels of mRNA silencing were similar to the results obtained when LNPs were applied prior to LPS.

The ending time point of 24 hours was chosen because it is typical for gene expression studies. Out of curiosity we stimulated macrophages with 20 ng/mL LPS and conducted a dose response 20, rather than 24, hours after original nanoparticle addition. As a method of comparison we ran a parallel experiment where 40 and 100 nM siTNFα were tested 24 hours after nanoparticle addition. They are both

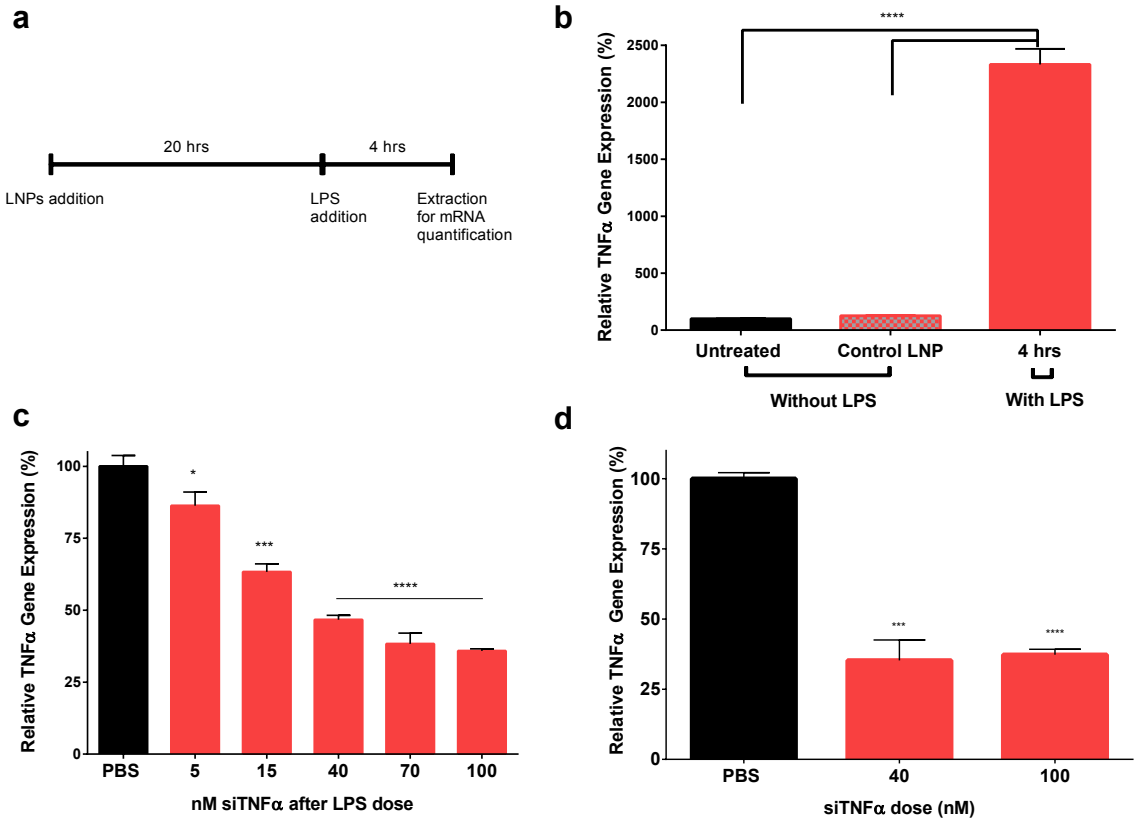

Figure 2.7: **Macrophages produce TNFα upon stimulation with lipopolysaccharide (LPS).** (a) Timeline of nanoparticle and LPS addition for panels (b) and (c). (b) Macrophages subjected to a 100 nM dose of control LNPs did not upregulate TNFα. In comparison, macrophages stimulated with LPS produced nearly 25-fold more TNFα mRNA compared to untreated macrophages 4 hours post-LPS application. (c) TNFα silencing was dose-dependent in macrophages. (d) Macrophages received LPS, then LNPs, and finally a second dose of LPS before mRNA extraction. Silencing at 40 nM and 100 nM doses (65% and 62% respectively) was similar to when LNPs were applied before LPS. Error bars in all panels represent s. d. ($n = 3$, $^{*}p < 0.05$, $^{***}p < 0.001$, $^{****}p < 0.0001$).

shown in fig. 2.8, compared as lines on the same graph. Interestingly, silencing was greatly improved when RNA was extracted 20 hours after nanoparticle addition, with all doses of siTNFα yielding lower gene expression as compared to typical 24 hour data. The 24 hour data matched other dose response data previously shown in fig. 2.7.

Because the timing of mRNA and protein silencing are often different, we used an ELISA assay to assess TNFα silencing at the protein level. In these experiments, cell supernatant was collected 10 hours after LPS dosing (experimental timeline shown in the first panel of fig. 2.9). The ELISA assay showed that 15 nM siTNFα yielded 51% TNFα protein knockdown, while 100 nM yielded a 76% reduction (sec-

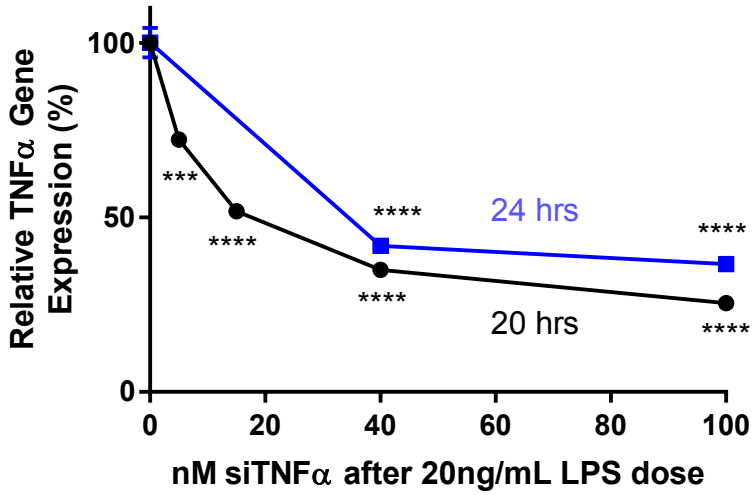

Figure 2.8: **Silencing improves at 20 hours post nanoparticle addition.** Macrophages were plated simultaneously for two experiments at 3.3 cells x 10^5 cells/well. In the first experiment, macrophages received 5, 15, 40, and 100 nM doses of siTNFα. They then received LPS sixteen hours later. Four hours post LPS treatment, the cells were harvested and RNA collected. This time shift demonstrated an improved dose response as compared to the typical 24 hour post nanoparticle addition timeline. As a means of comparison, cells were also treated separately with 40 and 100 nM siTNFα, but the typical timeline of 24 hours between nanoparticle addition and RNA collection was followed. Silencing results from these two doses proved comparable to previous dose responses carried out at the same time point. Error bars in all panels represent s. d. ($n = 3$, $^{***}p < 0.001$, $^{****}p < 0.0001$)

ond panel of fig. 2.9). Percentages are shown in fig. 2.9, and 100% TNFα expression corresponded to 23,600 pg/mL TNFα in the macrophage supernatant.

After showing both a dose dependent silencing at both the mRNA and protein levels, we assessed the kinetics of LNP-mediated TNFα silencing for a period of 24 hours after LPS stimulation (fig. 2.10). In this experiment, macrophages were incubated with either PBS or 40 nM doses of siTNFα for 20 hours and then dosed with LPS. Silencing was measured at 4 hour intervals for 24 hours, at which point TNFα mRNA levels had returned close to baseline. LNPs used in this experiment did not contain PEG. The same data are depicted in two different ways in the first and second panels of fig. 2.10 in order to highlight several aspects of the experiment. The first panel of fig. 2.10 shows that TNFα mRNA expression rapidly increases 4 hours after LPS treatment for both control (black circles) and siTNFα treated macrophages (red squares) before gradually decreasing. However, the relative magnitude of the inflammatory response is ~70% less for the treated group. The second panel of fig. 2.10, which depicts

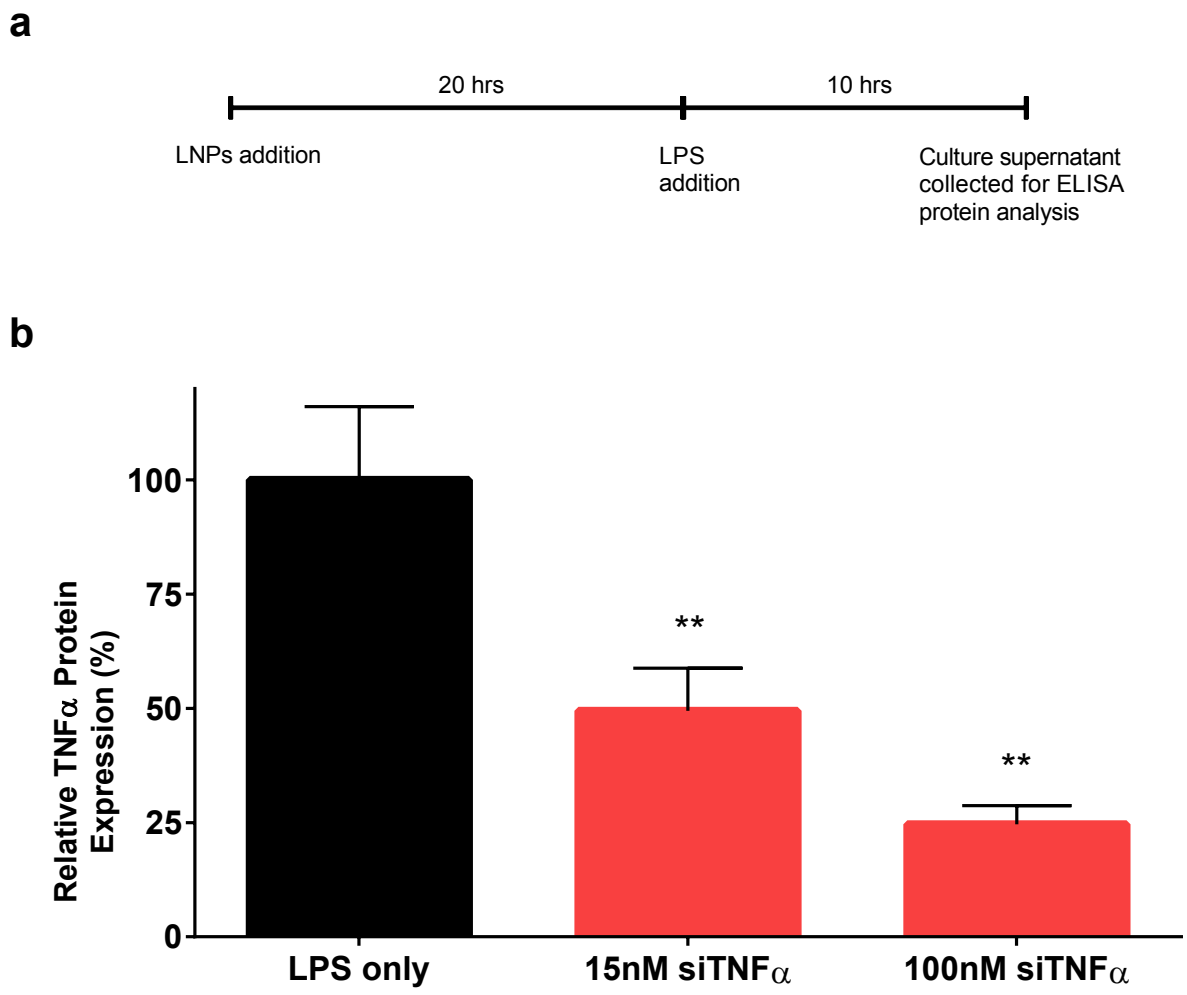

Figure 2.9: **ELISA confirmed knockdown of TNFα protein production.** (a) Nanoparticle and LPS timeline for ELISA experiments. (b) LNPs reduced TNFα protein levels up to 75% in a dose-dependent manner as measured by ELISA, 10 hours after LPS addition. Error bars represent s. d. ($n = 4$, $^{**}p < 0.05$).

the treated group normalized to the control group, shows that silencing holds steady at ~70% throughout the 24 hour experiment.

After analyzing the silencing response over a 24 hour period, the question of how long silencing could persist for arose. LPS silencing largely returns to baseline by 24 hours (fig. 2.10), so repeated dosing of 20 ng/mL LPS became necessary. While macrophages can suffer from LPS fatigue with repeated dosing, once a day did not prove to be an issue. In this case, LPS and 100 nM siTNFα were added to cells at the same time, as opposed to nanoparticles being added twenty hours before (first panel of fig. 2.11). This was to allow the experiment to run for a longer amount of time, as macrophages quickly divide and consume their media's nutrients/overgrow their well plate. Because of this shift in timing, the first day's silencing is worse than it would be if nanoparticles were added in advance: 40% for concurrent addition vs. 65% silencing normally. The second panel of fig. 2.11 shows the TNFα expression for every treatment group for all days normalized to the LPS treatment group on Day 1. This reveals the overall increase or decrease in TNFα production as a function of time. TNFα gene expression for LPS treated cells peaked on Day 3 for both experiments, while silencing was at its maximum. The third panel of fig. 2.11 normalizes each day to its individual LPS only TNFα gene expression. This demonstrates the silencing on each day. Excepting the first day, silencing largely remains between 50-70%. Two separate experiments were run, with paired LPS only and nanoparticle treated cells graphed in the same color.

One of the key components of the nanoparticle formulation is PEG. PEG is typically included in liposomes to prevent the nonspecific binding of serum proteins and to deter the immune system from immediately clearing the foreign therapeutic. Macrophages, as a key part of the immune system, are one of the very cell types most likely to phagocytose and clear naked nanoparticles. However, as our desired target in this case is the macrophage and its overproduction of TNFα, we assessed whether removing the PEG from the nanoparticle formulation would improve uptake and thus TNFα silencing. As shown in fig. 2.12, the removal of PEG from the formulation did not significantly impact the level of silencing seen at any of the doses tried, except for 100 nM siTNFα. This is ultimately not too surprising, as it is specifically the complex and as of yet poorly understood corona of blood serum proteins found only in the body that indicate to the macrophage that a compound should be cleared. This in vitro system is simply not complex enough to replicate this behavior. It is clear from in vivo data, however,

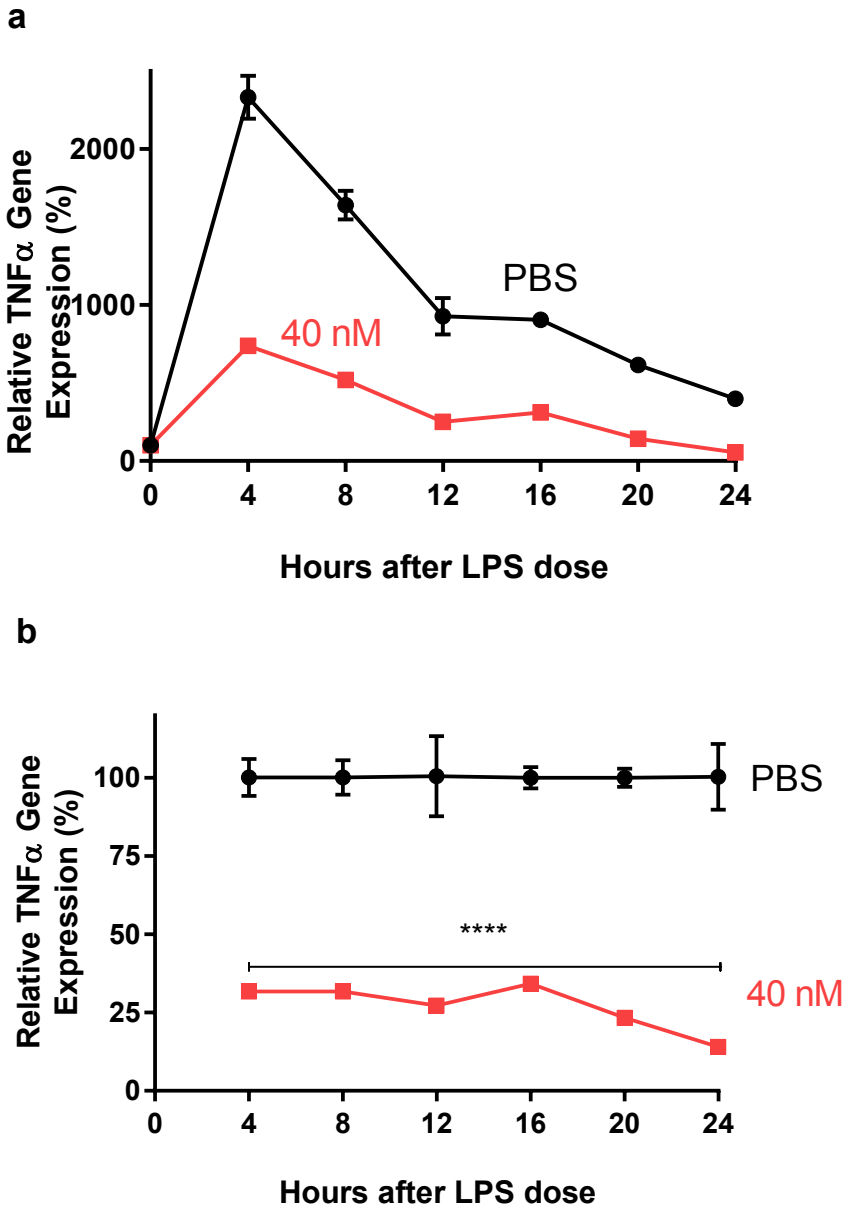

Figure 2.10: **TNFα silencing persists for 24 hours after macrophage stimulation.** The kinetics of TNFα expression and silencing is shown for macrophages treated with either PBS (black circles) or a 40 nM dose of siTNFα (red squares) for 20 hours prior to stimulation with LPS. The same data are depicted in two ways. (a) Normalization of TNFα expression for both treatments to time zero shows that TNFα expression for both groups peaked 4 hours post-LPS application, decreasing thereafter. (b) The normalization of TNFα expression of the siRNA treated group to the control group shows that silencing persisted over 24 hours at a constant level of approximately 70%. Error bars represent s. d. ($n = 3, ^{****}p < 0.0001$).

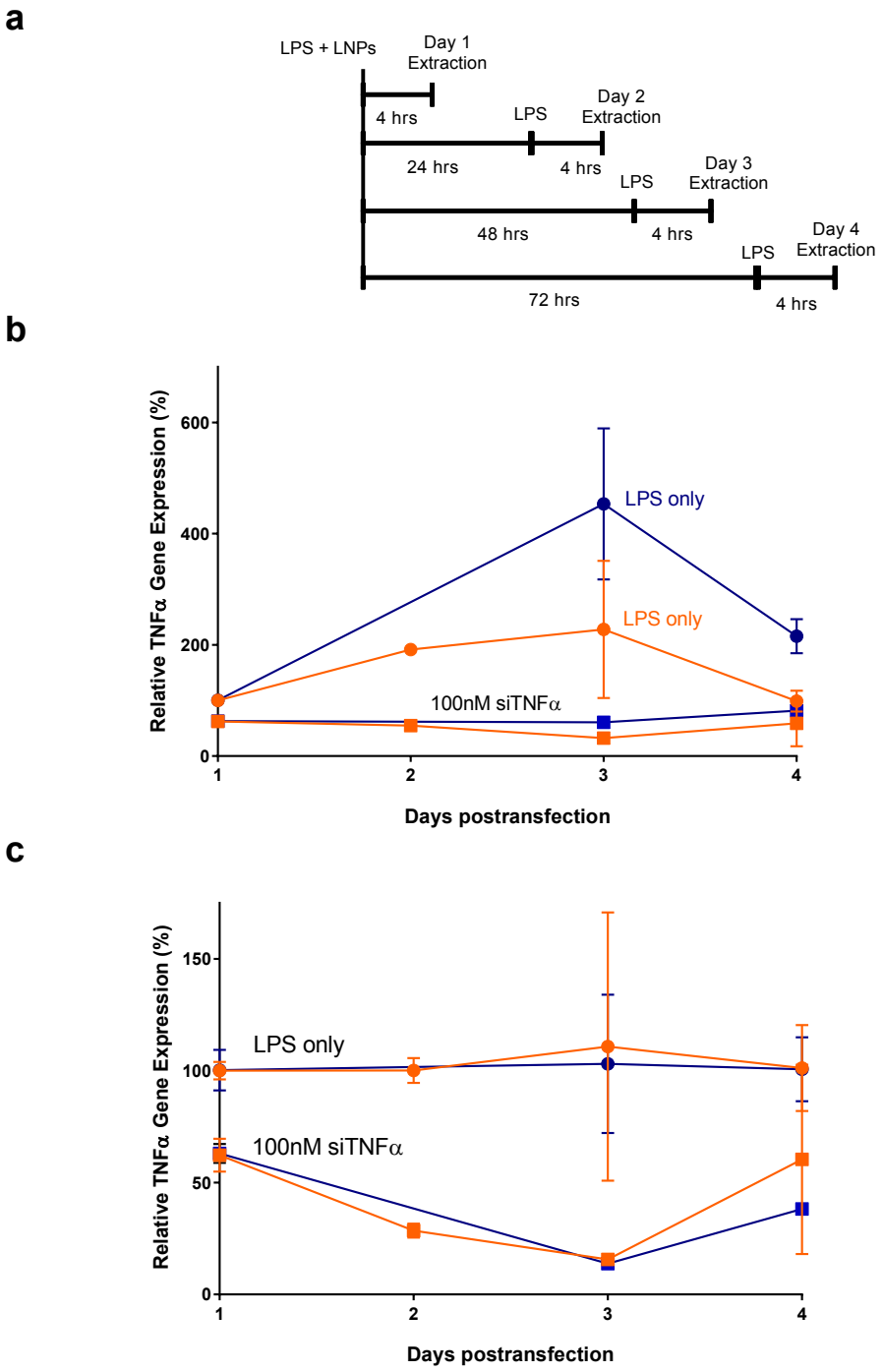

Figure 2.11: **TNFα silencing persists for at least three days.** a) Timeline of LPS and nanoparticle addition for both sets of experiments. Macrophages received 20 ng/mL LPS once a day for four days. RNA was extracted four hours after LPS addition on each day. b) Every data point is normalized to the LPS only treatment group on Day 1 for each separate experiment. This reveals the dynamics of LPS stimulated TNFα gene expression over time. Gene expression peaked on Day 3. c) Every 100 nM siTNFα point is normalized to its LPS only treatment group for that day. This shows the silencing present on each day. Silencing remains largely between 50-70%. Error bars represent s. d. $n = 3$.

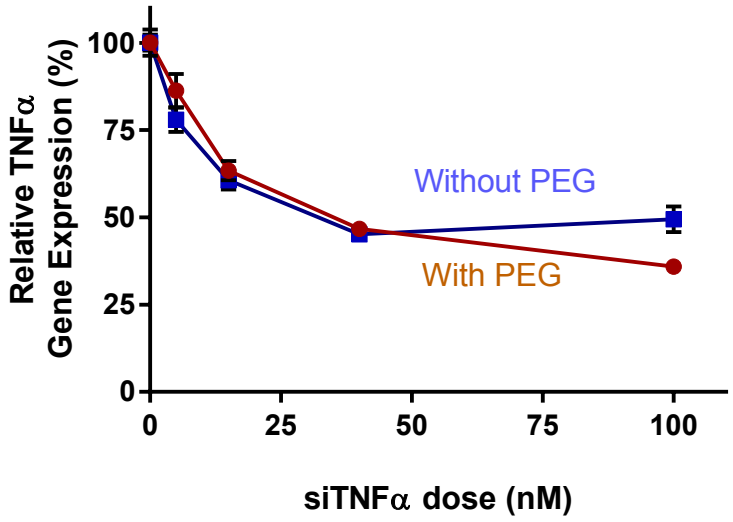

Figure 2.12: **Silencing is similar with or without PEG in the nanoparticle formulation.** Macrophages were plated and treated with different doses of siTNFα. Twenty hours later they received 20 ng/mL of LPS, and RNA was harvested four hours after that. The blue line indicates nanoparticles made without PEG, while the red line includes PEG. Silencing was similar between the two types of treatments, with only modest improvement seen at the 100 nM dose. $n = 3$.

that the removal of PEG does indeed increase the rate of uptake by macrophages.

Though we assessed the effect of the complete removal of PEG, we wanted to determine the effect of different PEG concentrations on TNFα silencing. PEG concentration was varied from 0% to 5% in a 100 nM siTNFα dose, and the resulting TNFα gene expression was measured via qPCR (fig. 2.13). While all PEG formulations knocked down TNFα an average of 70-75%, a one-way ANOVA indicated statistical difference between the different levels. 5% PEG clearly silenced worse than the other formulations, with an average of 60% knockdown. This indicates that 5% PEG inhibits the uptake of nanoparticles by macrophages.

2.3.3 TNFα knockdown causes MCP-1 downregulation in paracrine co-culture experiments

With our ability to silence TNFα well established, we asked whether or not siRNA treatment could also downregulate the expression of monocyte chemotactant protein-1 (MCP-1), another key player in the positive feedback inflammatory cycle depicted in fig. 2.1. Both fibroblasts and macrophages produce

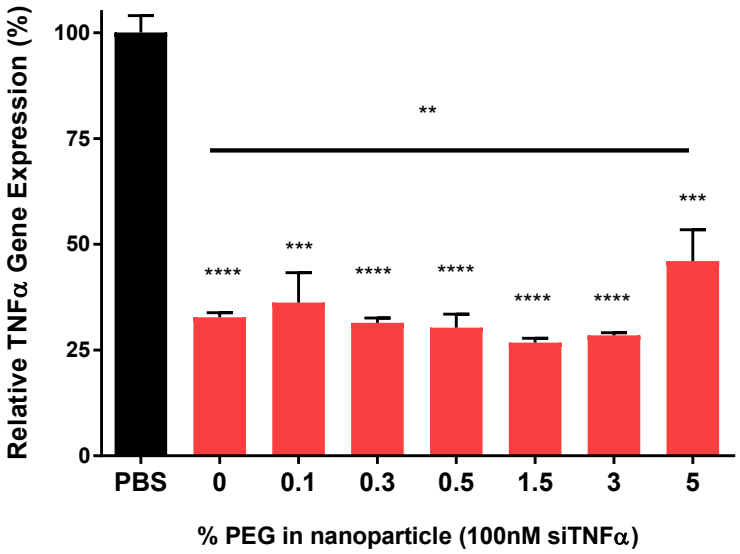

Figure 2.13: **High levels of PEG reduce silencing of TNFα.** Macrophages were plated and treated with formulations that contained varying levels of PEG, stretching from 0% to 5%. Twenty hours later they received a 20 ng/mL dose of LPS and RNA was harvested four hours after that. Unpaired t-tests indicate that the silencing observed is statistically significant for all formulations, while a one-way ANOVA across the different PEG percentages indicate that the silencing between them was also statistically different. 5% PEG performed the worst of all formulations tested. Error bars in all panels represent s. d. ($n = 3$, $^{***}p < 0.001$, $^{****}p < 0.0001$)

MCP-1 in response to LPS and TNFα [42], which results in the recruitment of additional monocytes and macrophages to the wound bed. In order to recapitulate this dynamic system *in vitro*, we used a macrophage/fibroblast co-culture in which the two cell lines were free to engage in the normal cross-talk that exists within a wound bed.

We used two different types of co-culture to capture different aspects of the wound environment: paracrine and juxtacrine. In paracrine co-culture experiments, macrophages and fibroblasts were seeded in distinct wells, and the soluble products from each cell line were transferred to the other. This co-culture mimics the ability of macrophages and fibroblasts that are physically separate within a wound bed to influence each other through the production of cytokines, even though the two cell types are not in close proximity. Removing fibroblasts' media and replacing it with macrophage media from control cells treated with LPS only or cells treated with LPS and 100 nM siTNFα helps to mimic this phenomenon. The first panel of fig. 2.14 illustrates the dosing and switching timeline followed in the paracrine experiment, where four different regimes are tested to ensure that results were independent

of timing. "t1" (7 or 10 hours) represents the number of hours macrophages were allowed to produce TNFα before their media was removed and added to the fibroblasts. "t2" (12 or 18 hours) is the length of time fibroblasts were incubated with the macrophage media before mRNA was extracted. Instead of receiving macrophage media, control fibroblasts were dosed with LPS to account for any changes in gene expression due directly to LPS rather than TNFα.

As shown in fig. 2.14, MCP-1 mRNA expression was significantly reduced in fibroblasts that received siTNFα-treated macrophage media (orange triangles) compared to fibroblasts that received fully stimulatory macrophage media (black squares). Control fibroblasts (red circles) experienced significantly smaller changes in MCP-1 expression as a result of LPS dosing, suggesting that cytokine levels, and not LPS, were dominating the gene expression responses to the paracrine media switch. These trends were independent of the t1 and t2 timings used in each experiment. Therefore, we concluded that direct silencing of TNFα in macrophages caused the indirect downregulation of MCP-1. We replicated the experiment with a t1 of 7 hours and a t2 of 18 hours to further validate the result (rightmost points in the second panel of fig. 2.14).

2.3.4 Juxtacrine experiment confirms TNFα knockdown leads to MCP-1 knockdown

In addition to testing gene silencing in paracrine co-culture, we were also interested in examining the effect of gene silencing on macrophages and fibroblasts in physical contact with one another. This type of co-culture, called juxtacrine co-culture, mimics the neighboring cells in the wound bed that not only influence each other chemically through cytokines, but also mechanically through contact cues. The first panel of fig. 2.16 details the timeline of the experiment, wherein the co-culture and the two separate cell lines were dosed with LNPs and LPS. In the second panel of fig. 2.16, 100 nM siTNFα was added to a co-culture as well as the two cell lines separately, and LPS was added to all samples 20 hours later. TNFα mRNA expression (second panel of fig. 2.16) and MCP-1 expression (third panel of fig. 2.16) were then measured 16 hours later. 100 nM siTNFα reduced TNFα expression in the co-culture by 64% and in macrophages alone by 80%. Another experiment wherein mRNA was extracted 4 hours after

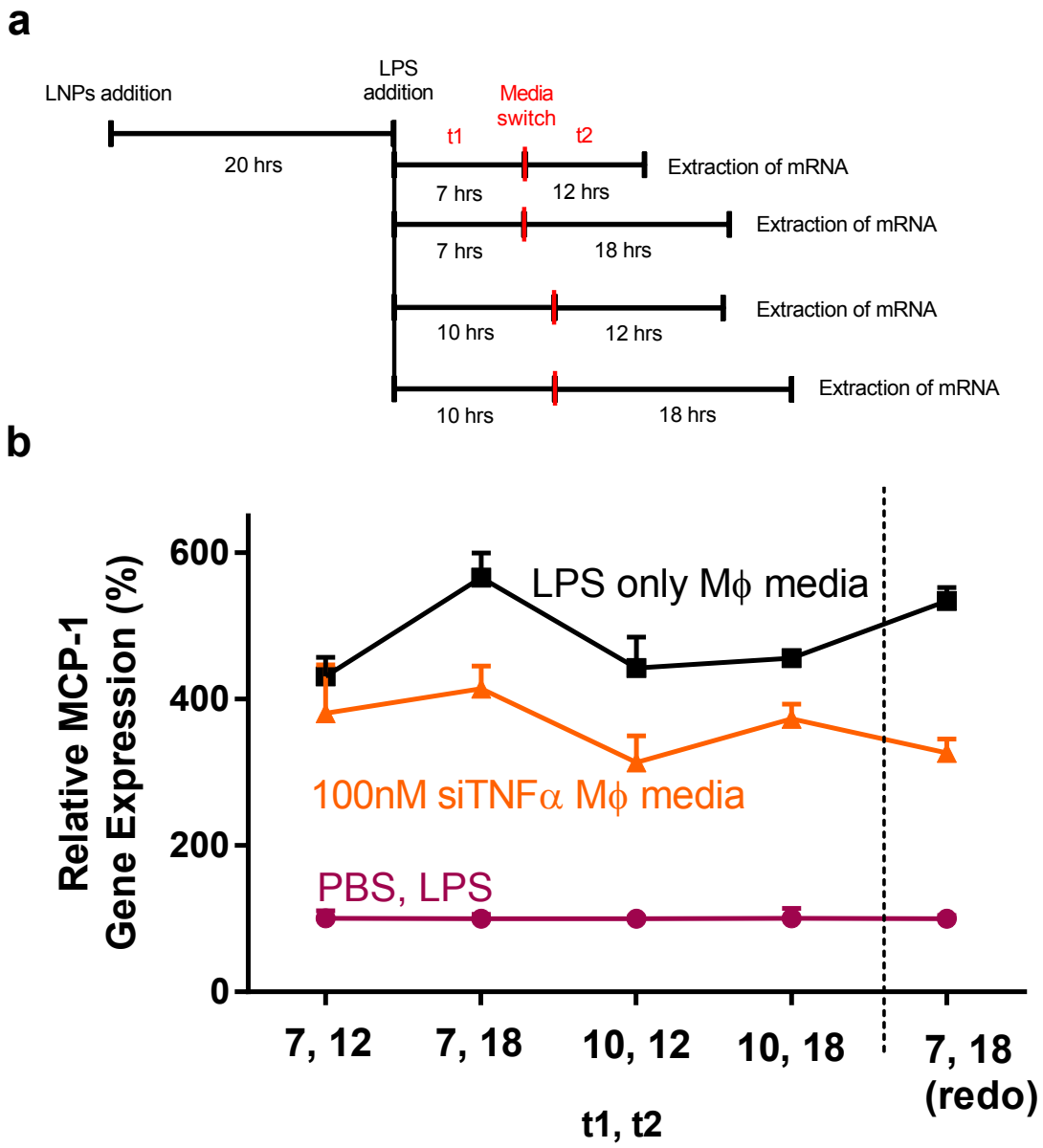

Figure 2.14: **Paracrine co-culture experiments shown that MCP-1 production in fibroblasts in suppressed when TNFα has been silenced in macrophages.** (a) Macrophages were activated with LPS at time zero and, for treated samples, were dosed with siTNFα nanoparticles 20 hours prior. After "t1" hours (either 7 or 10), media was removed from the fibroblasts and replaced with media from the macrophages treated with either LPS or 100 nM siTNFα/LPS. mRNA was then extracted from the fibroblasts "t2" hours after media exchange (either 12 or 18). (b) In all experiments, expression of MCP-1 was downregulated in fibroblasts that had received siTNFα treated macrophage media compared to those that received untreated, activated macrophages media. The result was independent of the t1 and t2 values chosen. The (7,18) result was replicated to further validate the finding. All data points are in comparison to control samples in which PBS and LPS were applied to fibroblasts. Error bars represent s. d. ($n = 3, {}^{*}p < 0.05, {}^{**}p < 0.01$).

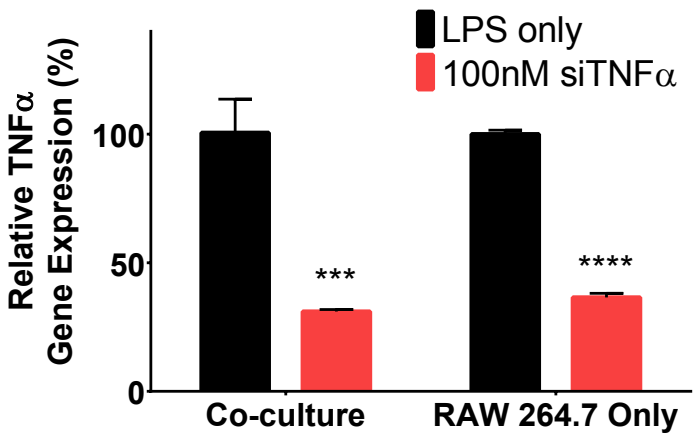

Figure 2.15: **Juxtacrine co-culture demonstrates that TNFα silencing in co-culture is comparable to TNFα silencing in macrophages alone.** Macrophages and fibroblasts plated together were stimulated with LPS, with treated samples receiving LNPs 20 hours prior to LPS addition. mRNA was harvested 4 hours post-LPS addition. 100 nM siTNFα knocked down TNFα by 69% in co-culture and 64% in macrophage only wells 4 hours after LPS stimulation.

LPS addition showed approximately 70% TNFα mRNA reduction in both co-culture and macrophages, demonstrating that the knockdown is independent of time (fig. 2.15). As shown in the third panel of fig. 2.16, 100 nM siTNFα lowered MCP-1 levels in co-culture by 29% and by 65% in macrophages alone. Next, we were interested in comparing the downregulation of MCP-1 upon TNFα silencing with the level of silencing that could be achieved with direct dosing of siMCP-1. In fibroblasts only, 100 nM MCP-1 knocked down MCP-1 by 90%, and in macrophages, by 43%. Interestingly, the indirect downregulation of MCP-1 in co-culture from 100 nM siTNFα dosing was nearly identical to reductions in gene expression seen from direct silencing with 100 nM siMCP-1. This result further confirms the value of using a single siRNA sequence against TNFα to downregulate the expression of both TNFα and MCP-1.

After observing the knockdown patterns in coculture and the cell lines separately, we wanted to assess if combining siMCP-1 and siTNFα in the same nanoparticle might further the synergistic MCP-1 silencing observed. Nanoparticles were formulated at twice the concentration typically observed, with the required volume of siRNA made up of half siTNFα solution and half siMCP-1 solution. Unfortunately there is no means of determining if equal numbers of siTNFα and siMCP-1 molecules were

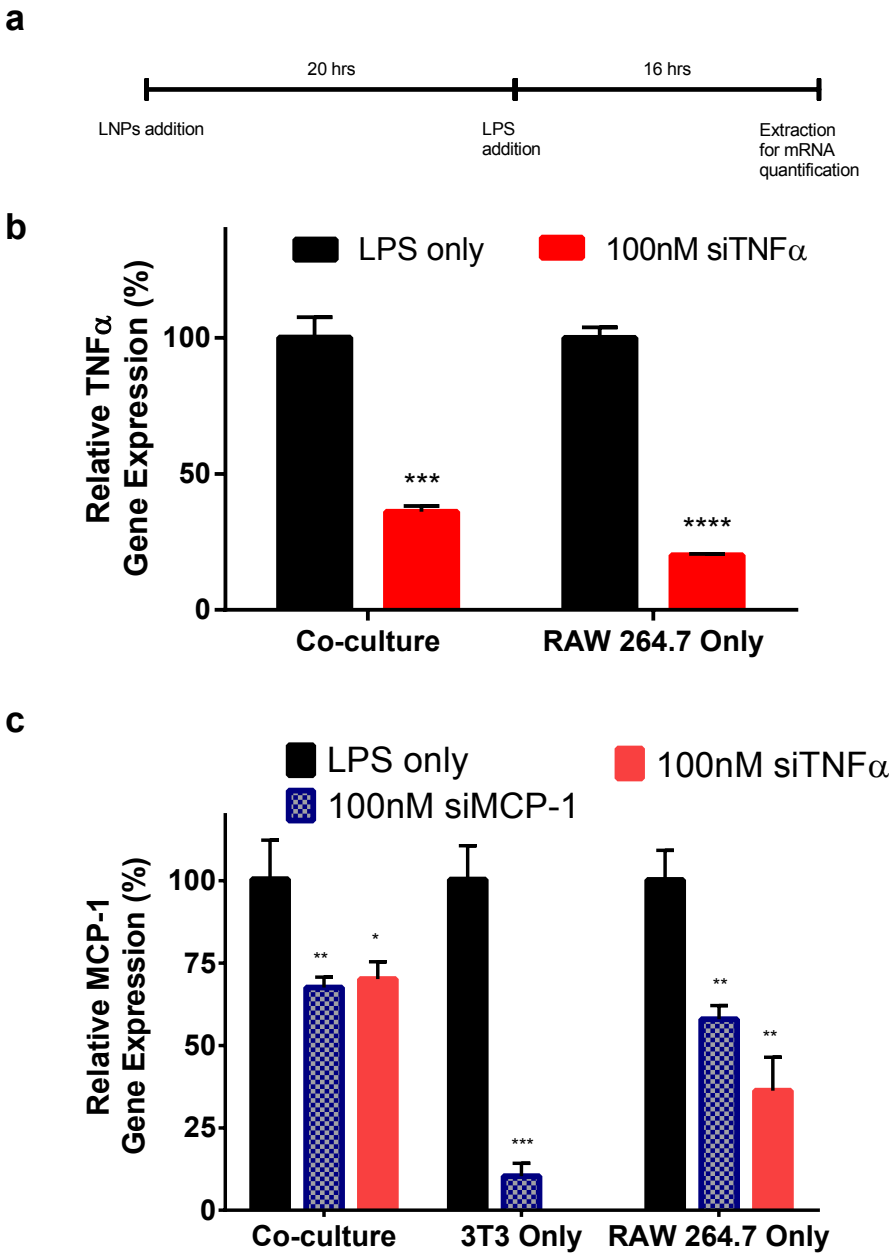

Figure 2.16: **Juxtacrine co-culture demonstrates that silencing TNFα expression in macrophages results in a downregulation of MCP-1 that is comparable to direct silencing of MCP-1.** (a) Macrophages and fibroblasts plated together were stimulated with LPS, with treated samples receiving LNPs 20 hours prior to LPS addition. mRNA was harvested 16 hours post-LPS addition. (b) LNPs loaded with siTNFα silenced TNFα expression in RAW 264.7 macrophages when they were co-cultured with fibroblasts comparably to in macrophage culture alone. (c) TNFα silencing downregulated MCP-1 expression to the same level as when MCP-1 was silenced directly using siMCP-1 loaded nanoparticles. Error bars in all panels represent s. d. ($n = 3, {}^{*}p < 0.05, {}^{**}p < 0.01, {}^{***}p < 0.001, {}^{****}p < 0.0001$).

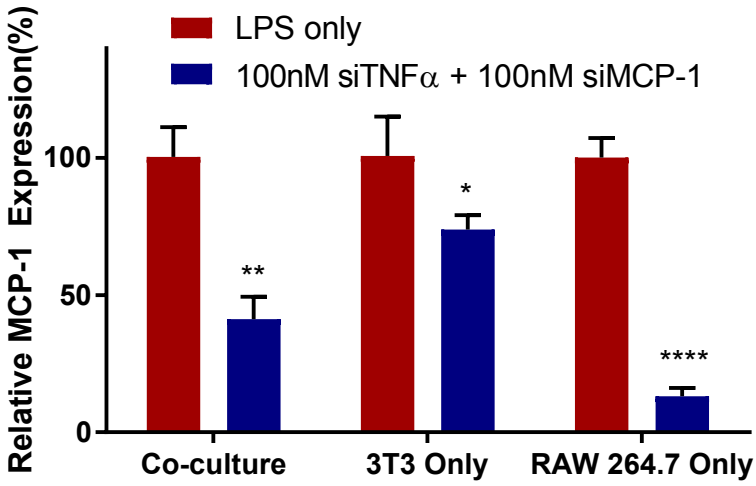

Figure 2.17: **Co-delivery of siMCP-1 and siTNFα improves siMCP-1 knockdown in coculture.** Nanoparticles were formulated at double the concentration with half of the siRNA siMCP-1 and half siTNFα. Coculture, macrophages, and fibroblasts received 200 nM doses (effectively 100 nM siMCP-1 and 100 nM siTNFα) and RNA was harvested 24 hours later. MCP-1 gene expression was 40% in coculture, 73% in fibroblasts alone, and 13% in macrophages alone using this combined nanoparticle. Error bars in all panels represent s. d. ($n = 3, {}^{*}p < 0.05, {}^{**}p < 0.01, {}^{****}p < 0.0001$)

incorporated into each nanoparticle. Macrophages, fibroblasts, and the coculture received this 200 nM dose (100 nM siTNFα and 100 nM siMCP-1 in each nanoparticle) and RNA was extracted 24 hours later (fig. 2.17). An MTT viability assay was also conducted with 200 nM siGFP to ensure that silencing was not due to cell death at this higher siRNA dose (fig. 2.18). MCP-1 gene expression was 40% in coculture, 73% in fibroblasts alone, and 13% in macrophages alone using this combined nanoparticle. This marks a knockdown improvement of 25% in coculture and 40% in macrophages alone as compared to siMCP-1 on its own. However, knockdown was considerably worse in fibroblasts alone, decreasing from 90% knockdown to 25% knockdown. This is possibly due to the fact that siTNFα is futilely utilizing some percentage of the RISC machinery that previously siMCP-1 had exclusive access to. Since fibroblasts do not produce TNFα and thus cannot benefit from the synergistic silencing in the first place, this loss of RISC-siMCP-1 activity results in a loss of gene silencing.

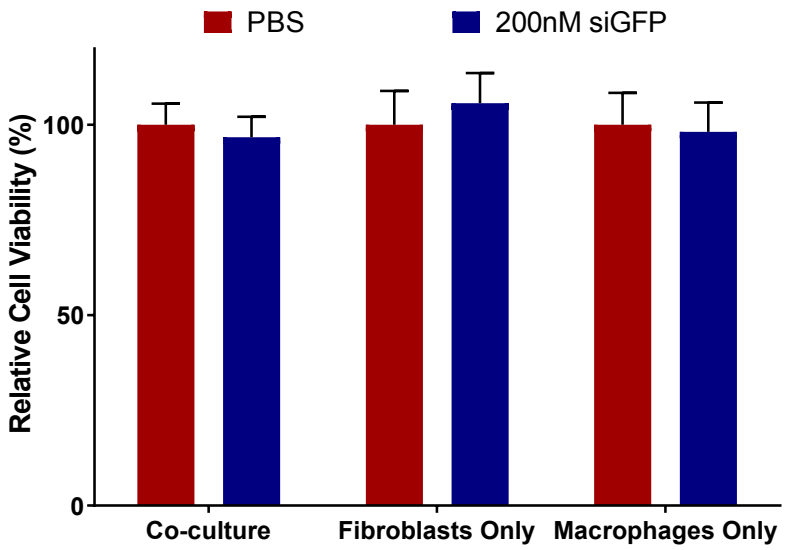

Figure 2.18: **Delivery of 200 nM siRNA doses does not cause cell death.** An MTT assay demonstrated that 200 nM doses of siRNA do not reduce cell viability in coculture or single cell cultures. Thus, silencing observed is more than likely not due to cell death. Error bars in all panels represent s. d. $n = 3$.

2.4 Discussion

Despite the many advantages inherent of siRNA as a therapeutic, its delivery is difficult due to its negative charge and relatively large size [43]. Of the many types of nanoparticles that have been studied as siRNA delivery vehicles, lipid nanoparticles (LNPs) are among the most promising in *in vivo* settings [43, 31]. LNPs have been shown to potently deliver siRNA *in vivo* to several cell types, including hepatocytes, epithelial cells, and difficult to transfect cell lines, including immune cells [33, 44, 45, 46].

One of the challenges in using an *in vitro* model of a diabetic wound is the difficulty in recapitulating a sustained inflammatory environment. In our experiments, we had to activate cytokine production in macrophages using a bacteria-derived stimulant, LPS. The resultant TNFα expression profile was dynamic over a period of 24 hours (fig. 2.10). Macrophages became tolerant of the LPS with repeated LPS dosing (data not shown), as is well-documented in the literature [47]. Nonetheless, LNPs reduced TNFα expression in LPS activated macrophages for as long as the LPS derived inflammation persisted. We anticipate that LNPs will provide longer durations of knockdown in a chronic inflammatory environment in the same way they have been used for prolonged gene silencing in hepatocytes [31] and intestinal epithelial cells [32]. Future *in vivo* experiments using a diabetic chronic wound model will be

used to determine the precise timing needed between siRNA doses to maintain cytokine knockdown.

The macrophage/fibroblast co-culture used in this work helps to capture the intricate cytokine trafficking that occurs in a normal wound bed. The paracrine co-culture represents those cells that are not in physical contact but continue to exchange soluble proteins, while the juxtacrine co-culture introduces physical proximity and contact derived changes to the system. In both co-cultures, TNFα stimulates fibroblasts to take on a proinflammatory phenotype, whereby inflammatory cytokines like MCP-1 and collagen degrading enzymes of the matrix metalloproteinase family are drastically upregulated [48, 38].

Before proceeding with the co-culture model, we sought to decouple the effect of LPS stimulation from the effect of TNFα. This is because LPS stimulates macrophages to produce TNFα, but also triggers fibroblasts to produce MCP-1 [42]. In these experiments, fibroblast only controls were given LPS at the same time that fibroblasts were given macrophage conditioned media in the paracrine experiment (fig. 2.14). This represents the maximum amount of LPS that the fibroblasts could see. There was a threefold upregulation in MCP-1 expression due to LPS application, but this is relatively small compared to the sixteen fold MCP-1 upregulation after application of the TNFα containing macrophage media. Therefore, we concluded that the majority of MCP-1 upregulation in fibroblasts was almost entirely due to TNFα signaling from macrophages, and was not an artifact of using LPS as an inflammatory stimulant.

The most important finding enabled by co-culture experiments is that RNAi-mediated reductions in TNFα, produced by macrophages, concomitantly reduced the expression of MCP-1 in fibroblasts (fig. 2.14 and fig. 2.16). Therefore, a therapeutic that targets TNFα can interfere with two distinct components of the positive inflammatory feedback cycle present in diabetic wounds (fig. 2.1). Together, paracrine and juxtacrine co-culture experiments showed that knocking down TNFα reduced MCP-1 expression in all cell types: macrophages, as well as fibroblasts in close proximity to and further away from the macrophages. Within the juxtacrine co-culture, a 100 nM siTNFα treatment was as effective at knocking down MCP-1 as a 100 nM dose of siMCP-1, speaking to the highly linked nature of the two cytokines. This effect improved when 100 nM siMCP-1 and 100 nM siTNFα were delivered in the same nanoparticle. The comparable effect seen in co-culture and the synergistic effect seen in macrophages

alone may be because MCP-1 gene expression is controlled by NF-κB, which is the same transcription factor involved in the expression of TNFα [49]. The ability to knockdown two genes with a single siRNA sequence is not only more cost-efficient, but also dosing and delivery efficient.

This reduction in not only TNFα but also MCP-1 is desirable because it breaks the cycle of chronic inflammation that exists within diabetic wounds. Lowering the amount of TNFα present in the skin also has the advantage of allowing fibroblasts to retain their insulin sensitivity, as TNFα overproduction in diabetics has been shown to trigger insulin resistance and a downregulation of GLUT4 in fibroblasts [50]. It is the loss of insulin sensitivity and vasculature stability that contributes to the formation of the diabetic ulcer in the first place.

2.5 Conclusion

Diabetic foot ulcers represent a damaging cocktail of chronic inflammation and deregulated healing response on the part of several cell types. Macrophages have been shown to be the most important of these cell types, with their overproduction of tumor necrosis factor α (TNFα) one of the main instigators of the ulcer's chronic inflammation. LNPs loaded with siTNFα are a non-cytotoxic, non-immunostimulatory topical wound healing treatment that may be a compelling alternative to systemically administered anti-TNFα therapy, which is associated with dangerous levels of systemic immune suppression. Furthermore, LNPs induce high levels of silencing in both macrophages and fibroblasts, two very different types of cells present in the wound bed. Most importantly, TNFα silencing therapy was highly effective in a macrophage/fibroblast co-culture, where the paracrine feedback loop between TNFα and monocyte chemotactant protein-1 (MCP-1/CCL2) was very apparent. Together, these data demonstrate the ability of siTNFα loaded lipidoid nanoparticles to downregulate the expression of TNFα and MCP-1 in a wound bed environment and underscore their potential in accelerating the closure of diabetic foot ulcers.

Chapter 3

siTNFα loaded lipidoid nanoparticles improve wound healing in diabetic mice

3.1 Introduction

Diabetes is quickly becoming a major crisis for the health care industry. As the population ages, the number of those affected is rising, with 50% of Americans now suffering from pre-diabetes or diabetes [2]. Many of these individuals are not even aware that they have it, which delays early treatment and intervention. Approximately 90% of diabetics suffer from Type II Diabetes, which can trigger a constellation of negative complication [3]. These complications include ischemia, peripheral neuropathy, atherosclerosis, kidney failure, and impaired wound healing. This study examines the last of those listed, as delayed wound healing can result in the formation of a chronic foot ulcer in up to 25% of diabetics, with many leading to lower limb amputation [4]. Unfortunately, these amputations carry a 50% three year survival rate, so there is an acute need to prevent the formation of the ulcer in the first place [5].

Unlike acute wounds, diabetic foot ulcers do not proceed normally through the three general stages of wound healing: inflammation, re-epithelization, and wound remodeling [6]. Instead, diabetic wound bed cells undergo harmful phenotypic changes that impair their ability to produce and react appropriately to the normal cytokine and growth factor cascade [51, 7]. Additionally, higher than

normal numbers of inflammatory macrophages have been shown to reside within diabetic wounds, where they overproduce tumor necrosis factor α (TNFα), one of the most important inflammatory cytokines [8, 9, 10, 11]. A small, tightly controlled amount of TNFα is required for fibroblast migration, proliferation, and remodeling [12]. When overproduced, however, TNFα damages the wound further by upregulating levels of cellular apoptosis, reactive oxygen species production, and matrix degradation [13, 9, 14, 15, 10]. Currently the most common method of treatment is the use of moisture-retentive bandages, hyperbaric oxygen therapy, and antibiotics [16, 17]. These treatments are often ineffective as they do not address the chronic inflammation and other biological irregularities that caused the ulcer to form. Biomaterials research has focused on correcting these irregularities with a wide variety of nanoparticles, hydrogels, nanofibrous meshes, and dressings capable of delivering a plethora of drugs and growth factors to the wound [52].

Another possible approach is to utilize RNA interference (RNAi) to reduce the levels of problematic proteins. Short interfering RNA (siRNA), a 19-23 nucleotide double-stranded RNA, silences gene expression by cleaving mRNA complimentary to the guide strand [43, 53]. Since the technology can be applied to silence almost any gene in the body, it is promising if currently underutilized in the treatment of diabetic wounds. There have been several reports of improved wound healing outcomes upon gene silencing of matrix metalloproteinases (MMPs) [22, 23, 54] and prolyl hydroxylase domain protein 2 [55, 56]. siRNA loaded in hydrogel dressings has been used to some success when knocking down other relevant gene targets in the diabetic wound, like xanthine dehydrogenase [57] and tumor suppressor gene p53 [58]. In this study, we examined whether siRNA can silence TNFα in the diabetic wound and thus allow the wound to close. Sufferers of other inflammatory diseases, like inflammatory bowel disease and rheumatoid arthritis, have benefited from treatment with antagonists of TNFα [21, 24, 25]. Even diabetic wounds have improved with systemic anti-TNFα therapies [26] and antibody-based neutralization [27], but with an increased risk of infection and severe liver damage [28, 29, 27, 25, 30]. Local downregulation of TNFα may avoid these negative side effects and still correct the chronic inflammation present.

In this paper, we demonstrate a possible therapy using topically applied lipidoid nanoparticles loaded with siRNA against TNFα to improve wound healing both in non-diabetic and diabetic mouse

models. These nanoparticles have been previously used to potently deliver siRNA *in vivo* [31, 32, 33] and control inflammatory feedback loops in an in vitro macrophage-fibroblast coculture [1]. LNPs contain ionizable amine groups that facilitate receptor-mediated endocytosis and endosomal escape under the reduced pH conditions of the endosome [34, 35]. As the major cytokine, TNFα is an especially enticing target as its knockdown should help to fix the inappropriate inflammatory response in the wound. Herein, we show that LNPs can be topically delivered in solution to non-diabetic and diabetic mouse wounds to effect significant levels of TNFα gene expression knockdown.

3.2 Materials and Methods

3.2.1 Nanoparticle formulation

Lipidoids were formulated into nanoparticles in all experiments. The three-tailed version of lipidoid $306O_{13}$ was utilized in all experiments. The $306O_{13}$ lipidoid was synthesized via the Michael addition of 3,3'-Diaminodipropylamine (Acros Organics) to tridecyl acrylate (Pfaltz and Bauer, Waterbury, CT) at a stoichiometric ratio of 1:3 as described previously to create a three-tailed product [1, 32]. The lipidoid was then purified over a silica column on a Teledyne ISCO chromatography system. For nanoparticle formulation, the lipid solution was formed by mixing the lipidoid, distearoyl-sn-glycerol-3-phosphocholine (DSPC, from Avanti Polar Lipids), cholesterol (Sigma Aldrich, St. Louis, MO), and, where noted, C14-PEG (Avanti Polar Lipids) at a molar ratio of 50:10:38.5:1.5 in the presence of ethanol (Sigma Aldrich), and citrate buffer. Silencer Select Pre-Designed siRNA against Tumor Necrosis Factor α (s75248) was purchased (Thermo Fisher). The siRNA was diluted in 10 mM sodium citrate and combined with the lipid solution at a final lipid to siRNA weight ratio of 5:1. The solution was vortexed after each reagent addition, and the lipid solution was added to the siRNA solution before being diluted to the desired final concentration in PBS. Nanoparticles were dialyzed against PBS for at least an hour before use in mice.

3.2.2 Nanoparticle characterization

Nanoparticles were diluted to a final siRNA concentration of 1 μg/mL in PBS. Percent siRNA entrapment was determined via the Quant-iT Ribogreen assay (Invitrogen), as Ribogreen binds to siRNA and fluoresces. Entrapment was determined by comparing the signal from intact LNP solutions to the signal from an LNP solution that had been ruptured with 2% Triton-X surfactant. Nanoparticle size was measured with a Malvern Zetasizer Nano (Malvern Instruments, UK).

3.2.3 Animal studies

All mouse experiments were approved by the Institutional Animal Care and Use Committee (IACUC) at Carnegie Mellon University under protocol number PROTO201700004. C57BL/6 mice were either purchased from Charles River Laboratories (Wilmington, MA, USA) or obtained from an institutionally managed breeding colony. Genetically diabetic BKS.Cg-Dock7 ^{m} +/+ Lepr ^{db} /J mice were purchased from the Jackson Laboratory (Bar Harbor, ME). Mice were housed in cages of fewer than six animals, with controlled temperature (25°C), 12 hour light-dark cycles, and free access to food and water. Mice used in this study were males between the ages of 10-16 weeks. Prior to wounding, the backs of the mice were shaved with electric clippers and circle templates 8 mm in diameter were traced on the right flank (single wound), or both the left and right flanks (double wounds). Surgery was performed under anesthesia and 3 mg/kg bupivacaine was injected in a line block formation around each wound site (6 mg/kg total dose). Two 8 mm full thickness excisional wounds were created with surgical scissors using the template circles. Single wounded mice received either PBS or nanoparticle solution on their single wound immediately after wounding. For double wounded mice, nanoparticle solution and PBS were topically administered to the right and left flank wounds respectively of anesthetized mice twenty-four hours after wounding, and mice were sacrificed twenty-four hours after treatment. Wounds were excised and immediately placed into 2.0 mL homogenizer tubes filled with 800 μL of TRIzol (Thermo Fisher). The homogenizer tubes were pre-filled with 0.5 mm garnet shards and a 6.0 mm in diameter zirconium bead (Laboratory Supply Network). A BeadBug tissue homogenizer (Laboratory Supply Network) was used for 120 seconds at 3000 RPM to homogenize the wounds in TRIzol. The tubes were

then stored at -80°C until RNA extraction.

3.2.4 RNA interference

Experiments conducted in 24 well plates in a previous study [1] were dosed at 25 pmol siRNA/cm^2 well area (100 pmol/cm^3). Assuming the wound is a circle with a radius of approximately 5 mm (the average for a day after wounding) and a height of 1 mm, this gives a predicted wound volume of 0.079 cm^3. Scaling this to the original 100 pmol/cm^3 indicates that 7.85 pmol in the wound would be roughly equivalent to a 100 nM in vitro dose. For a 500 nM in vivo dose, nanoparticles were formulated at a final siRNA concentration of 0.049 mg/mL and 10 μL of solution was topically applied to the wound. This is 39.2 pmol, which is five times 7.85 pmol (a 100 nM dose).

3.2.5 Wound area analysis

Mice were photographed in the same position next to the same object of known length each day of the experiment. Images were then processed using ImageJ to calculate wound area and the change in wound area for each day.

3.2.6 RNA extraction and cDNA creation

RNA extraction and purification from the homogenized wound tissue was accomplished with TRIzol with some modifications from the manufacturer's instructions. A yellow fat layer often formed at the bottom of the tube after isopropanol addition. This layer had to be removed mechanically after one centrifugation step, with the balance of the volume being replaced by more isopropanol. The tube was then re-centrifuged, and the isopropanol replaced with 70% ethanol. RT-PCR was performed with the High Capacity cDNA Reverse Transcription kit (Applied Biosystems) to form 2 μg of cDNA. The quality and quantity of mRNA and cDNA were assessed by the absorbance at 260/280 nm with the Nanodrop 2000 UV-Vis spectrophotometer (Thermo Scientific).

3.2.7 Quantitative PCR

qPCR was performed in a 384-well block on a ViiA^{TM} 7 Real-Time PCR system machine with purchased Taqman Gene Expression Master Mix (Applied Biosystems), along with GAPDH (Mm99999915_g1) and TNFα (Mm00443258_m1) Taqman probes (Thermo Fisher). 10 μL of Master Mix, 1 μL of endogenous control probe, and 1 μL of target gene probe was used per well. All runs utilized the comparative Ct method and the following run protocol: 50°C (2 min), 95°C (10 minutes), 40 cycles of 95°C (15 sec) and 60°C (1 min). qPCR experiments consisted of three to five biological replicates and two technical replicates per each biological. The target gene (TNFα) was normalized to the endogenous control gene (GAPDH) for each sample. Single wounded mice treated with nanoparticles were then normalized to single wounded mice treated with only PBS. For double wounded mice, treated samples were normalized again to the nanoparticle-free control sample for each mouse.

3.2.8 Confocal microscopy

Wounds were treated with Cy5.5 labelled siLuciferase loaded nanoparticles. Two hours after wounding, wounds were excised completely with surgical scissors and immediately fixed in 4% formaldehyde solution. After a period of overnight fixation at 4°C, they were washed with PBS, permeabilized with 0.1% Triton-X100, and incubated for two hours with staining solutions. The staining solution contained DAPI (12 μg/mL, 358 nm/461 nm) to mark nucleic acids, AlexaFluor 488® conjugated phalloidin (5 units/mL, 495 nm/518 nm) to bind actin, and PE-Texas Red® conjugated F4 / 80 antibody (0.15 mg/mL, 565nm/615nm) to identify macrophages. After staining, the wounds were washed three times with PBS, mounted on glass slides, and placed under coverslips. Prepared slides were imaged at 63x magnification using a Zeiss LSM 700 confocal microscope with ZEN 2012 SP1 software. Images were captured using a Plan-Apochromat 63x/1.40 Oil DIC objective and an X-Cite Series 120Q laser source exposing at 405, 488, and 555 nm. Images were captured at room temperature and represent a single time point. Images were approximately 101.61 μm × 101.61 μm. No additional processing or averaging was performed to enhance the resolution of the images. ImageJ (NIH) image processing software was used to prepare confocal images.

3.2.9 Statistical analysis

All mean values are expressed as $\pm$ standard deviation. Unpaired Student's t-tests and one-way ANOVA tests were used where appropriate to evaluate statistical significance. A p value of < 0.05 was considered significant.

3.3 Results

3.3.1 Wound processing

The wound can be a difficult to terrain to image using microscopy. It is riddled with dead and dying cells and other debris, and is not as stable for intact removal as an organ usually is. However the images it does generate can provide at least a qualitative look at how nanoparticles interact with the wound environment. Either PBS or nanoparticles loaded with 5 μM Cy5.5 labelled siLuciferase were topically dosed to an open wound (fig. 3.1). Panels a and c represent wound tissue that only received PBS. While the nuclei and actin skeletons of cells can be clearly seen (fig. 3.1(c)), there is no nanoparticle signal (fig. 3.1(a)). After treatment with nanoparticles for two hours, it appears that nanoparticles can be visualized embedded in the wound tissue (fig. 3.1(b), fig. 3.1(d)). Nanoparticles localize in and around wound bed cells in a pattern that probably conforms to wound bed topology (fig. 3.1(d)).

Having demonstrated that nanoparticles remain in the wound, we investigated if they were capable of causing silencing. Before addressing the silencing results, it is important to note that a good deal of time and effort was spent developing a protocol that would allow for extraction of RNA from wound tissue in sufficient quality and quantity as to be useful for qPCR. The data from this trial and error period is not included in this thesis but the process is as briefly described below.

The two most common methods of RNA extraction from tissues are Qiagen's RNA microcentrifuge spin columns stabilized in β-mercaptoethanol or the use of TRIzol/chloroform centrifugation. The former is easily clogged by fibrous tissues and thus was not an option. The latter theoretically permits the processing of fibrous tissues, such as heart or wound, and so was chosen to proceed.

However, while most internal organs like the colon or spleen can be easily extracted with minimal

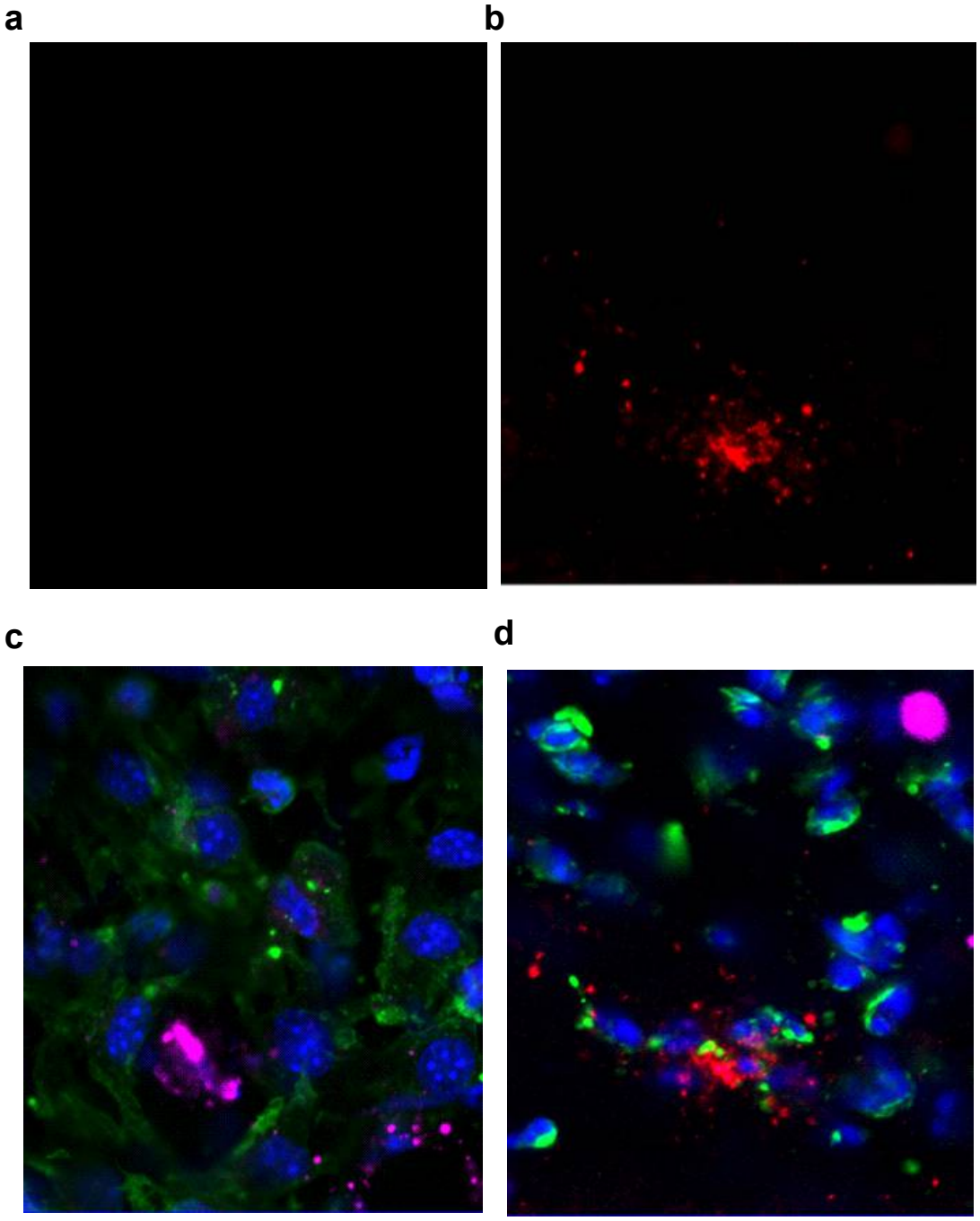

Figure 3.1: **Nanoparticles localize in and around wound bed cells.** Mouse wounds were treated with PBS or 5 μM Cy5.5 labelled siLuciferase. Wounds were excised and stained for DNA (blue), actin (green), and the F4/80 receptor on macrophages (magenta). a) There is no nanoparticle signal in the PBS control treated mouse wound. b) Nanoparticle signal is evident in the nanoparticle treated mouse wound. c) An overlay of all channels reveals the presence of defined wound bed cells. d) Nanoparticles, in red, localize in and around wound bed cells.

effort, attempts to use wound tissue—even chopped into small pieces—was not successful. Mechanical disruption through the typical method of flash freezing in liquid nitrogen and pulverization in a frozen mortar was not feasible due to the distance between the vivarium and the biomolecular lab (tissues must be immediately homogenized and submerged in TRIzol after harvest) and the lack of availability of liquid nitrogen on site. Disruption through force with prolonged vortexing or a scalpel/blunt object pair (both before and after TRIzol addition) was unsuccessful in obtaining quality RNA. Finally, a compact, simple benchtop tissue homogenizer was purchased. Though the original tubes filled only with a zirconium bead were not powerful enough to adequately shred the collagenous tissue, the inclusion of garnet shards was able to reduce the wound to a slurry.

From here, another major problem arose. Though the wound seemed to have been reduced to a manageable consistency, RNA quality was poor. It became clear that an unexpected additional layer was forming during the extraction steps. This yellow layer sank to the bottom and prevented the adherence of most of the RNA pellet during centrifugation. Some probing revealed this layer to be fat that had absorbed pigments from the skin. The addition of chloroform and other organic solvents to perform another extraction—thereby holding the organic fat more securely in the bottom layer while the top aqueous RNA-containing one could be removed—were less than successful. Instead, careful manual removal with a pipette tip and replacement of the lost volume with isopropanol for another extraction was found to be effective.

3.3.2 TNFα silencing in single wounded, non-diabetic mice

Since genetically diabetic mice are expensive, we began with non-diabetic mice to investigate if silencing of TNFα was possible at all in the wound. A single right flank wound was made per mouse, with completely separate PBS and nanoparticle treated mice. Mice were wounded on Day 1, treated with PBS or nanoparticles on Day 2, and the wound was excised for RNA extraction on Day 3. The resultant TNFα gene expression is shown in fig. 3.2. Doses of 200, 400, and 500 nM siTNFα are not significantly different from PBS control mice. This is because the range of TNFα produced by all mice is so broad. Not every mouse is an equal producer of TNFα in general, so it is difficult to say if gene expression is the

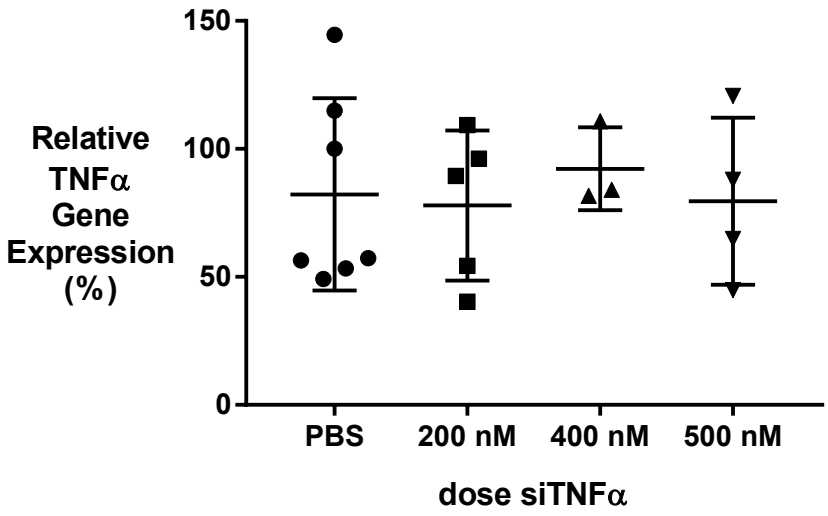

Figure 3.2: **TNFα knockdown is unclear in singly wounded mice.** Mice were wounded on Day 1, treated with PBS or nanoparticles on Day 2, and the wound was excised for RNA extraction on Day 3. TNFα expression is not statistically different between the groups due to variances in natural TNFα production to begin with. Error bars represent s. d. ($n = 3$–7)

value it is due to a lack of knockdown, or if knockdown *did* occur from an even higher value. It became clear that if the nanoparticles were having an effect, it was being obfuscated by the natural variances in TNFα production from one mouse to another.

We surmised that since inflammation was heterogeneous between mice, introducing outside inflammatory stimuli might not only reveal the silencing that was occurring but allow for the creation of an inflammatory (if non-diabetic) wound model. In vitro inflammation is typically caused by LPS, and at least one group utilized this compound in an in vivo setting by injecting LPS into the hind foot of a mouse [59]. We began first by investigating topical versus intraperitoneal delivery, where 500 pg of LPS was administered either directly onto the wound or injected into the abdominal cavity. Neither delivery route substantially changed the expression of TNFα in the wound 24 hours later compared to PBS controls (fig. 3.3).

Having shown that intraperitoneal delivery would not upregulate TNFα, we increased the dose of topically applied LPS in an attempt to increase the inflammatory response seen. As discussed in the previous chapter, in vitro macrophages were treated with 10 ng of LPS during coculture and monoculture experiments. Wounds treated topically with 1 ng or 10 ng of LPS, however, did not produce increased

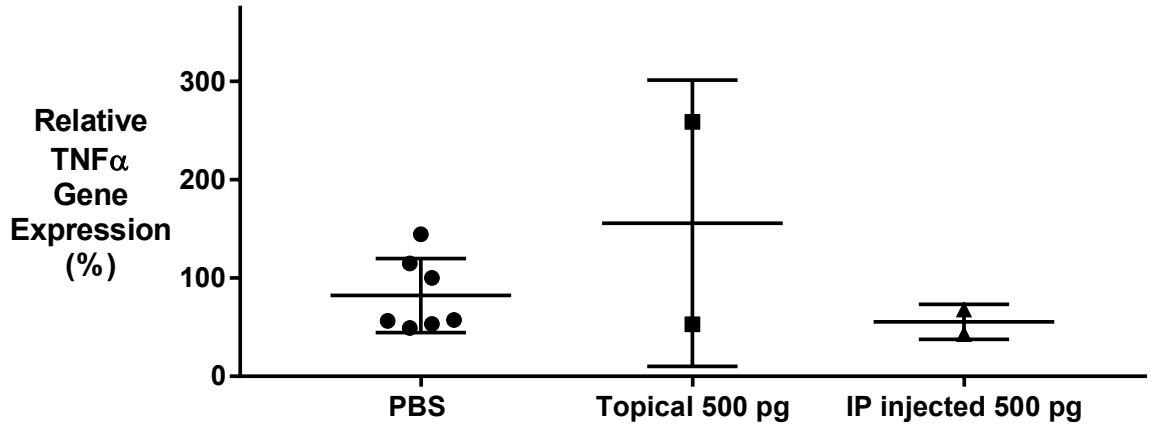

Figure 3.3: **Intraperitoneal delivery of LPS does not upregulate TNFα.** Mice were wounded and 500 pg of LPS diluted in PBS was administered directly to the wound or injected into the abdomen. 24 hours later the wound was excised and processed. IP injections did not upregulate TNFα expression in the wound, while topical delivery's effects were unclear. Error bars represent s. d. ($n = 2$–7)

levels of TNFα 24 hours after treatment (fig. 3.4).

The response to LPS in vitro is examined at short time points, like four hours, because it tends to decrease over time. We believed that waiting the full 24 hours after LPS addition might be why no upregulation of TNFα was seen. Instead, we wounded the mice and waited 24 hours before dosing with 25 ng of LPS. We then harvested the wounds three hours following this 25 ng dose. With this dose increase and time of treatment decrease, there was a statistically increased expression of TNFα 24 hours later (fig. 3.5). Nevertheless, this increase in TNFα expression is only slight compared to the vast increases seen in in vitro LPS usage and real-world inflamed wounds. Repeating the experiment with 500 nM siTNFα being dosed at the time of wounding (and 25 ng of LPS given 24 hours later, with a three hour treatment time) failed to silence the upregulation of TNFα seen in the wound. We believe this is probably due to the timing of nanoparticle addition, as nanoparticles dosed immediately at the creation of the wound would not be taken up by wound cells that arrive at later time points, thus blunting their silencing effect. Nevertheless LPS was not causing the large increase in TNFα we wanted to see, and so we decided on a different approach.

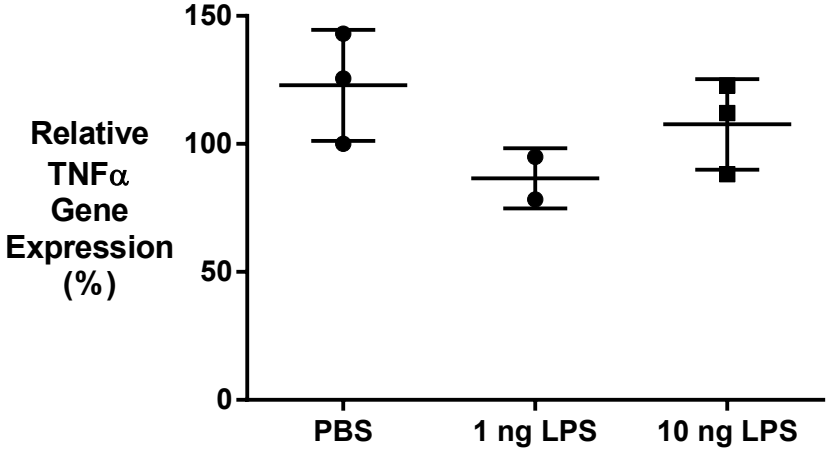

Figure 3.4: **Low levels of LPS do not increase TNFα expression in the wound.** Mice were wounded and dosed immediately with 1 ng or 10 ng of LPS. 24 hours later wounds were excised and processed, revealing no statistically increased level of TNFα in the LPS treated wounds. Error bars represent s. d. ($n = 2$–3)

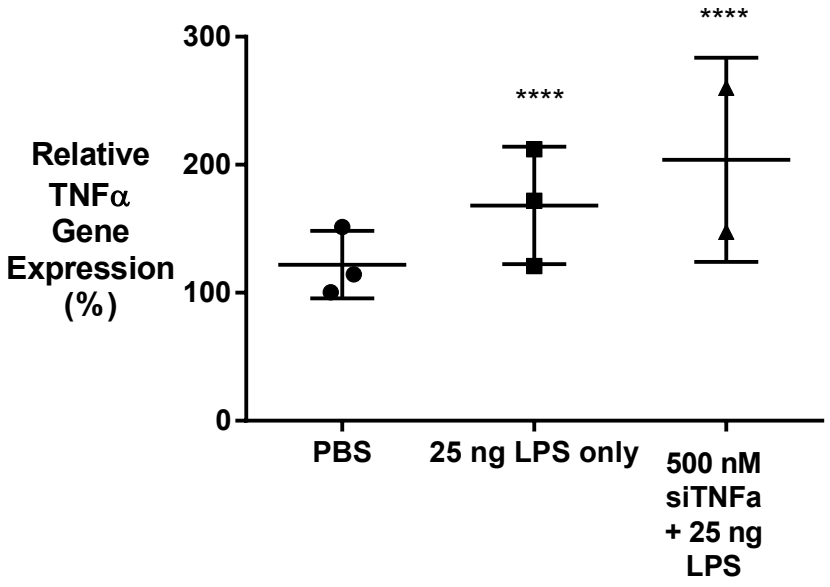

Figure 3.5: **25 ng of LPS upregulates TNFα in the wound.** Mice were wounded and dosed immediately with PBS or 500 nM siTNFα. Twenty-four hours later, they were dosed with 25 ng of LPS. Wounds were excised three hours after LPS addition. Though the 25 ng of LPS was sufficient to upregulate TNFα slightly, the nanoparticles did not silence this upregulation. Error bars represent s. d. ($n = 3, {}^{****}p < 0.0001$)

3.3.3 Double-wounded non-diabetic mouse model

It became abundantly clear that the controls heretofore used were not adequate in accounting for the difference in TNFα produced by different mice. This problem has prompted other groups to switch to a double-wounded mouse model, where mice receive wounds on the left and right flanks. In this model, nanoparticle treated wounds can be compared directly to PBS treated wounds, thus removing the issue of each mouse naturally possessing a different robustness of immune response. We transitioned to a double-wound protocol, with the time between wounding and treatment stretched to 24 hours. Here wounding occurred on Day 1 and harvest on Day 3. The left wound received PBS while the right received nanoparticle treatment. On the whole, area calculations using ImageJ revealed that the wounds closed at roughly the same rate, and were in the process of being pulled open further when the experiment terminated.

Although the TNFα levels in a non-diabetic wound are not as extreme as a diabetic one, it is still possible to use siTNFα to silence it. We dosed with 100, 250, 500, and 1000 nM siTNFα, as well as used a 500 nM siGFP control (fig. 3.6). The siRNA entrapments of those nanoparticles were 73%, 84%, 78-82% (three different occasions), 84%, and 85% respectively as measured by the Ribogreen assay. On average, 100 nM siTNFα reduced TNFα gene expression by 44%, 250 nM by 50%, and 500 nM by 54%. It is possible that silencing maxes out effectively at a dose lower than 250 nM. When compared to PBS, these three doses effected statistically significant silencing. 1000 nM siTNFα doses did not cause statistically significant levels of gene silencing, probably because this extremely high dose of siRNA and lipid was causing inflammation or toxicity. This theory is further supported by the 500 nM siGFP control, which lacks compensatory siTNFα to obfuscate the increase in TNFα gene expression. The difference in silencing between the siTNFα treatment groups is statistically significant as calculated by one-way ANOVA, indicating that a weak dose response is occurring.

Taking the data for the 500 nM siTNFα treated mice and normalizing to only one PBS control value illustrates the spread in TNFα gene expression that prompted the switch to the double wounded model in the first place (fig. 3.7). Here the control and treated wound for each mouse are stacked on top of each other, and it is clear that some mice produce more TNFα in both wounds than others. The spread

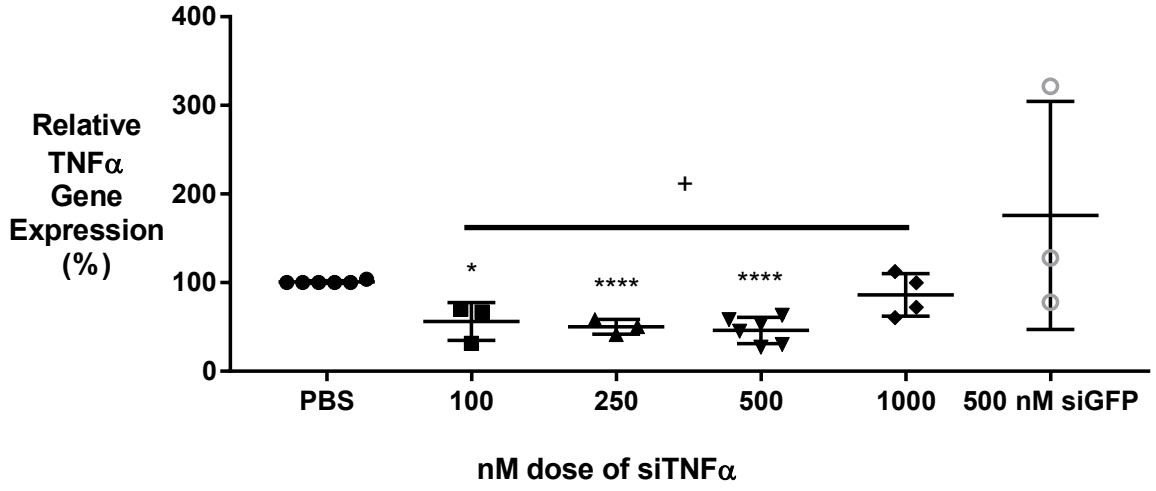

Figure 3.6: **siTNFα reduces gene expression in double-wounded, non-diabetic mice.** On average, 100 nM siTNFα reduced TNFα gene expression by 44%, 250 nM by 50%, and 500 nM by 54%. 1000 nM siTNFα and 500 nM siGFP did not affect gene expression significantly. The doses are statistically different as measured by a one-way ANOVA. Error bars represent s. d. ($n = 3$–$6, {}^{*}p < 0.05, {}^{**}p < 0.01, {}^{****}p < 0.0001,$ + ANOVA $p < 0.05$)

of TNFα gene expression in the control wound can differ by up to three times, with a range from 80% to 225%. The double wounded model helps to account for this intrinsic difference in TNFα expression.

3.3.4 Double-wounded diabetic mice model

After showing that TNFα knockdown was possible in the wound, we purchased BKS.Cg-Dock7 ^{m} +/+ Lepr ^{db} /J mice (homozygous for Lepr ^{db}). This strain is genetically diabetic beginning at four to eight weeks of age and exhibits all the hallmarks of Type II Diabetes in humans: hyperglycemia, obesity, peripheral neuropathy, myocardial disease, and impaired wound healing. As such, they are often utilized in the study of diabetic ulcer treatments.

Two separate kinds of experiments were carried out to probe the efficacy of topically applied siTNFα loaded lipidoid nanoparticles. The first interrogated the gene silencing seen in the initial inflammation phase, while the second allowed the wounds to close to completion to study the effect on wound contraction and healing time. In the former, five eleven week old mice were wounded with two flank wounds as previously described (Day 1). Twenty-four hours later, they were topically dosed with 250

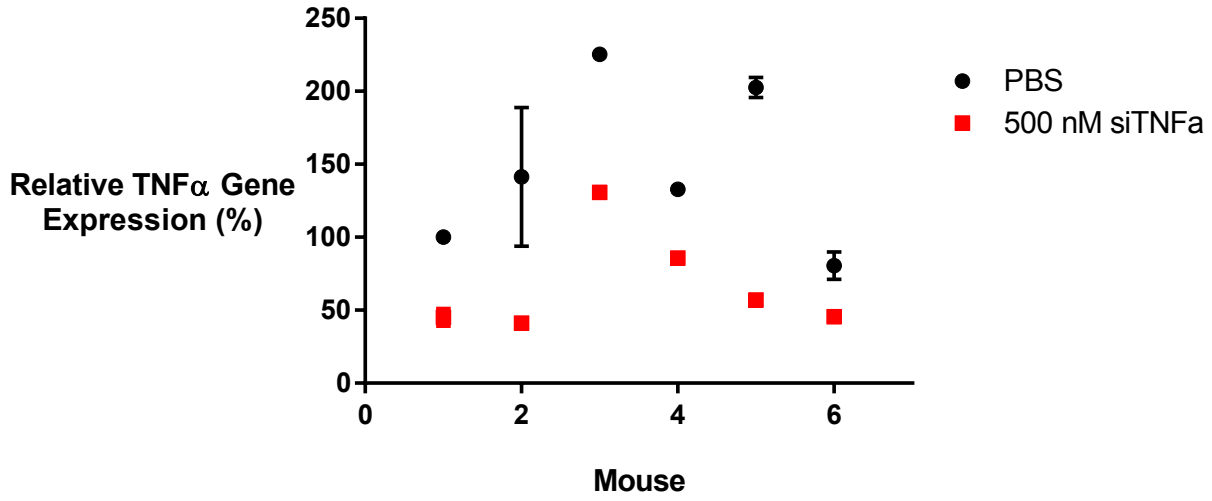

Figure 3.7: **Non-normalized data reveals the large spread of TNFα gene expression.** This is the same 500 nM siTNFα data from fig. 3.6, but without the normalization seen in that graph. Here every wound for both treatment types is normalized to a single PBS control value, to better illustrate the variance in values. Gene expression in control wounds can span from 80% to 225%, and in general, a mouse that produces more TNFα in one wound will produce more in the other as well.

nM siTNFα (10 μL) on their right flank and an equal volume of PBS on their left. Nanoparticles had a Z-average diameter of 124 nm and an siRNA entrapment of 75%. On Day 3, they were dosed a second time, and then wounds were harvested on Day 4. Wounds were photographed each day (fig. 3.8) and areas were calculated with ImageJ (fig. 3.9).

We calculated wound area as a percentage of the initial wound area for each wound, each day. Initial wound area was subtracted from the current size of the wound, and the difference was normalized to the starting wound area. This is shown in fig. 3.10. Here, 100% indicates that the wound is as large as it was on Day 1. Values less than 100% on subsequent days indicate the wound is shrinking. If the wound increased in area after Day 1, the percentage is larger than 100%. Grouping all wound closure percentages for each treatment group together shows that PBS control wounds contract at a much slower rate than nanoparticle treated wounds. By Day 4, this difference in percentage wound closure is statistically significant.

This increased rate of wound contraction for nanoparticle treated wounds is reflected in the silencing data. After excision on Day 4, the wounds were immediately processed and qPCR was performed to

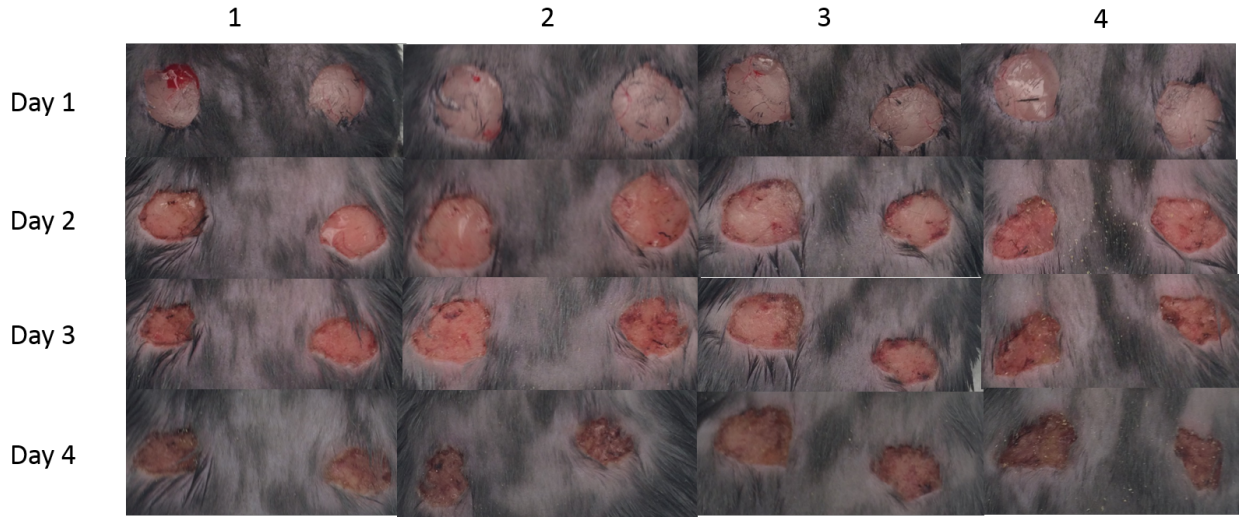

Figure 3.8: **Diabetic mice wounds heal slowly over four days.** Each mouse was photographed every day next to an object of the same known length. Each column is one mouse, while each row represents a day. Mice were wounded on Day 1, received 250 nM siTNFα nanoparticle treatments on Days 2 and 3, and were sacrificed on Day 4. ($n = 4$)

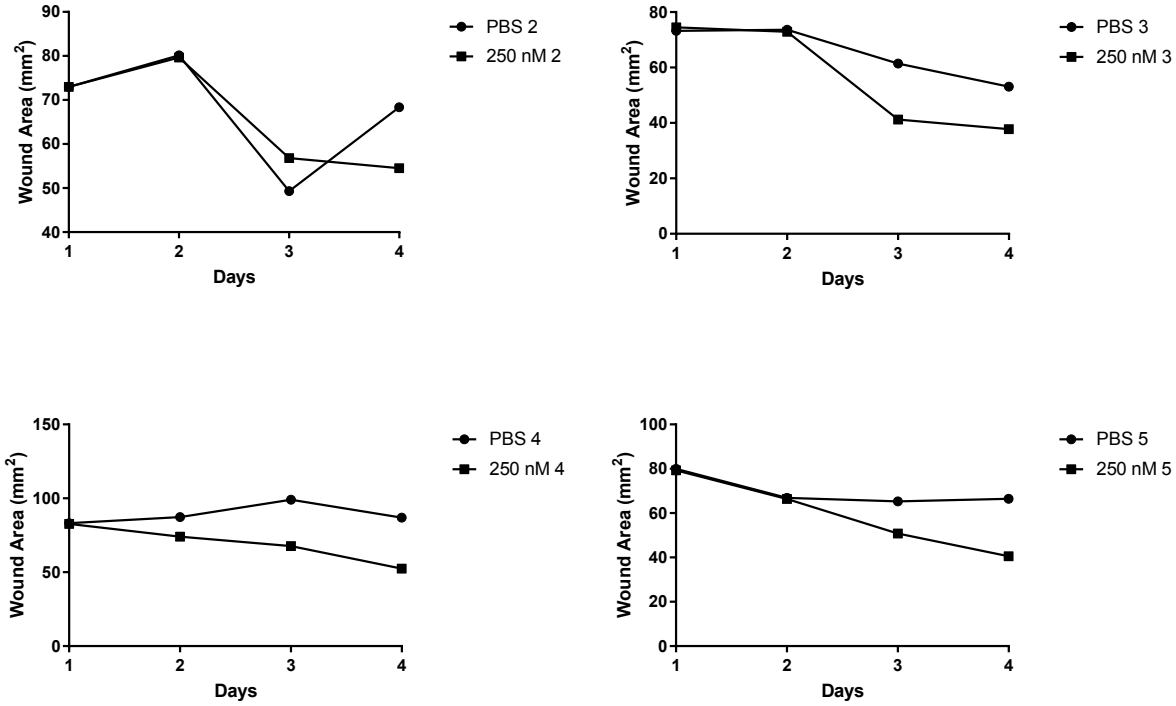

Figure 3.9: **Wound areas decrease at different rates over four days.** Each graph represents a mouse, with PBS and 250 nM siTNFα treated wound areas given for each day. Mice were wounded on Day 1, dosed on Days 2 and 3, and harvested on Day 4. Wound areas were calculated with ImageJ using an object of known length next to all of the mice. ($n = 4$)

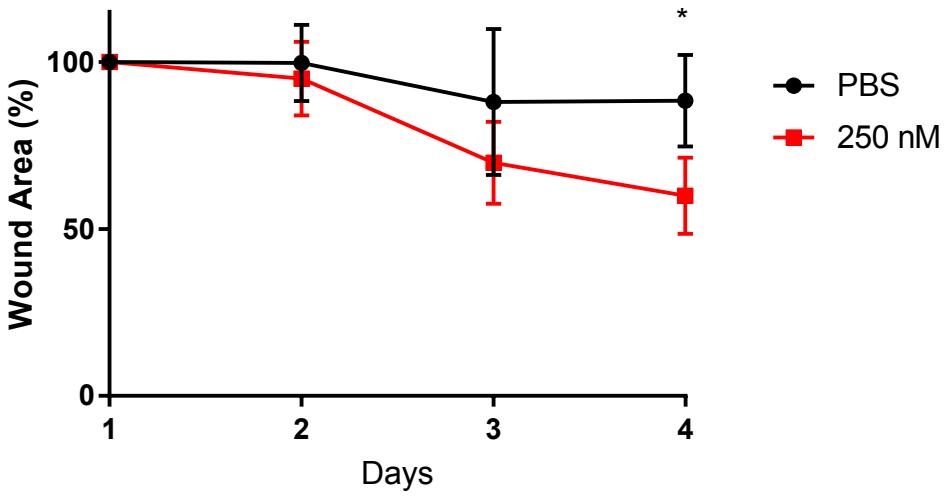

Figure 3.10: **Nanoparticle treated wounds close faster in four days.** The wound area of each treatment group on each mouse is subtracted from the original size of that wound, and the difference is normalized to the original size. 100% indicates the wound has not varied from its original size, while less than 100% indicates the wound is contracting. By Day 4, the difference in wound areas between PBS and nanoparticle treated mice is statistically significant. Error bars represent s. d. ($n = 4, {}^{*}p < 0.05$)

analyze TNFα gene expression. Wounds treated with 250 nM siTNFα saw approximately 42% reduction in TNFα as compared to control wounds (fig. 3.11).

The second wing of experiments was to assess nanoparticle effect on wound healing allowed to proceed to completion. Similar to the RNA interference experiment discussed above, mice were wounded and treated twice with nanoparticles. They were then photographed every day until both wounds had fully healed. While RNA extraction is a terminal procedure and thus could not be incorporated into the experiment, the areas and contraction percentages were calculated to compare the different healing rates. As seen in fig. 3.12, treated wounds heal signficantly faster than control wounds over fourteen days. After Day 8, treated wounds were significantly smaller as compared to original wound area than control wounds. The treated wounds of two mice had completely or almost completely healed by Day 14, while the third mouse had to be sacrificed due to pain management issues from the control wound.

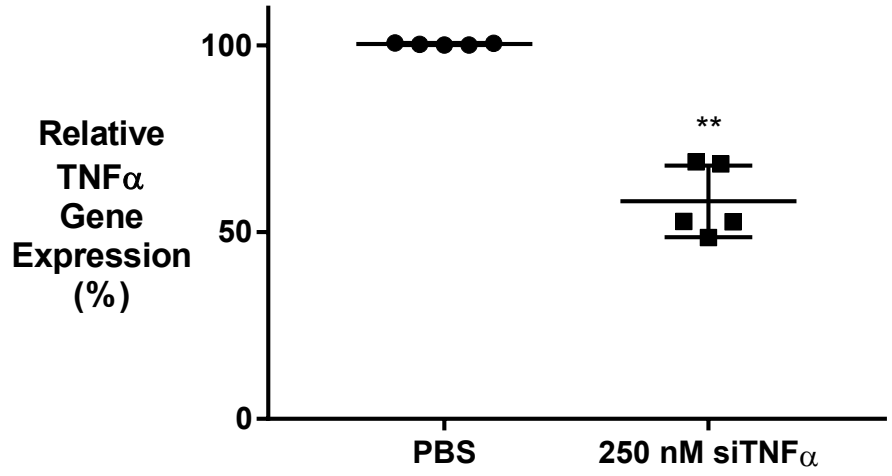

Figure 3.11: **Nanoparticles silence TNFα in diabetic wounds.** Each nanoparticle treated wound is normalized to its paired PBS control wound. Wounds treated with 250 nM siTNFα saw approximately 42% reduction in TNFα as compared to control wounds. Error bars represent s. d. ($n = 5, ^{**}p < 0.01$)

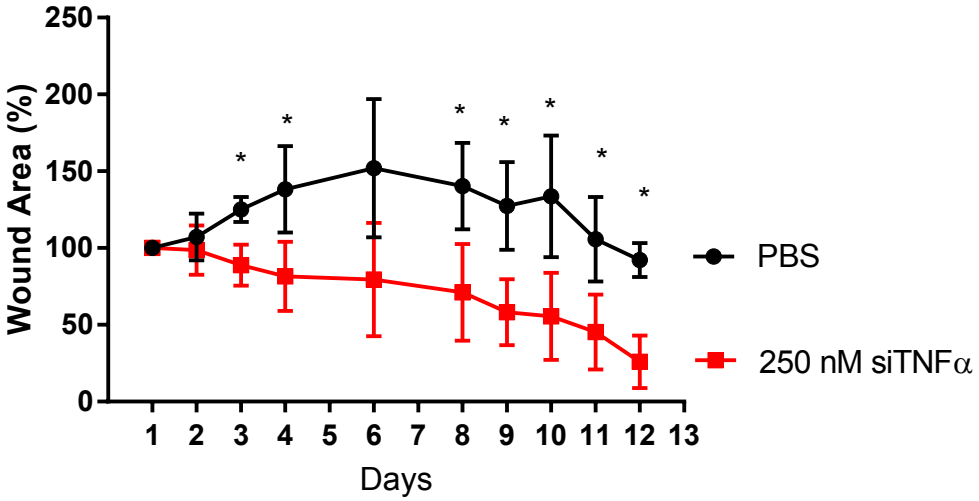

Figure 3.12: **Nanoparticle treated wounds close faster in fourteen days.** The wound area of each treatment group on each mouse is subtracted from the original size of that wound, and the difference is normalized to the original size. 100% indicates the wound has not varied from its original size, while less than 100% indicates the wound is contracting. By Day 8, the difference in wound areas between PBS and nanoparticle treated mice is statistically significant. Treated wounds close within fourteen days. Error bars represent s. d. ($n = 3, ^{*}p < 0.05$)

3.4 Discussion

Although siRNA is very promising as a therapeutic, its use is often complicated by its large size, negative charge, and the need for a delivery vehicle [43]. For these reasons, siRNA has been utilized only sporadically in diabetic wound treatment in the literature, usually delivered with polymer nanoparticles, nanofibrous meshes, or hydrogels [22, 23, 54, 55, 56, 57, 58]. The most common target by far has been members of the matrix metalloproteinase family, as these enzymes prevent healthy tissue reconstruction when upregulated in diabetic ulcers. While this is an important avenue of treatment, addressing the chronic inflammation endemic to diabetic foot ulcers represents another promising method. Other inflammatory models of disease, like plaque psoriasis and arthritis, have utilized polymer carriers for siTNFα to reduce chronic inflammation to good effect [60, 61].

Some diabetic mouse studies have used systemic anti-TNFα treatments, like neutralizing antibodies [27, 62, 9], to hasten wound healing, but to date none have examined the effect of a topically applied compound specifically meant to downregulate TNFα. In this regard, the specificity and local activity of siRNA makes it an ideal choice.

One of the most efficacious types of delivery vehicles are lipid nanoparticles, of which lipidoids are one class [43, 31]. Lipidoid nanoparticles have been shown to potently deliver siRNA *in vivo* to several cell types, including hepatocytes, epithelial cells, and difficult to transfect cell lines, like immune cells [33, 44, 45, 46, 1]. To successfully transfect wound bed cells, lipidoid nanoparticles must remain in the wound tissue without being degraded by enzymes or becoming stuck in wound debris. Confocal images show that they remain in the tissue, most likely conforming to wound bed topology, and manage to avoid degradation long enough to be taken up by cells (fig. 3.1).

Diabetic wound silencing is possible after topical application, with an average of approximately 42% TNFα mRNA reduction observed (fig. 3.11). This knockdown would almost return levels to the baseline seen in a normoglycemic mouse, as TNFα mRNA levels in wounded diabetic mice are up to three times as high as wounded normoglycemic animals [62]. Reducing levels of TNFα not only curb the inflammatory response seen in the wound, but also translate to real reductions in wound area and healing time (fig. 3.10). This improvement in healing extends into the long-term, where treated wounds

closed significantly faster than control wounds and were almost completely healed by Day 14 (fig. 3.12.

One of the challenges of studying inflammation in wound healing is the heterogeneity of the wound environment. Single wounds on non-diabetic mice exhibited TNFα gene expression that could vary up to three times over, thus obscuring any knockdown that was actually occurring (fig. 3.2). A switch to doubly wounded mice is not only prevalent in the literature, but combats this discrepancy by providing another control. Curiously, the non-normalized data indicates that TNFα expression is more closely similar between diabetic mice than non-diabetic mice, differing by less than a factor of two rather than over three. This might be due to the fact that a common etiology is what causes the chronic inflammation in the diabetic mice, whereas non-diabetic mice may or may not be host to a wide variety of other heterogeneities. Non-diabetic mice also did not heal faster from nanoparticle treatment, at least in the short-term RNAi study. Non-diabetic mice do not suffer from an overproduction of TNFα that keeps the wounds open, so this result is not surprising.

Another challenge with diabetic wound healing is finding a model. Although a few options exist, genetically diabetic mice present one of the best in terms of recapitulating features typically seen in human ulcers. Just as wounds remain open in diabetic humans, diabetic animal models develop markedly different wounds compared to normoglycemic animals. The size of normoglycemic excisional mouse wounds is reduced by 50% within 2-3 days, while diabetic mice require a couple weeks to reach the same degree of closure [63]. Nevertheless, mouse and rat models of diabetic wound healing still poorly mimic human wound healing, as unless they are splinted open, they heal primarily by contraction rather than re-epithelialization [64]. Splinting is possible, thus forcing the wound bed cells to proliferate rather than rely on myofibroblasts pulling the edges of the wound closed by force, but it can be difficult and does not make up the majority of the literature.

3.5 Conclusion

Diabetes represents a growing epidemic in the United States, with several deleterious consequences. Hyperglycemia and vascular damage often results in impaired wound healing and the formation of a chronic foot ulcer. While current treatments are largely palliative, RNA interference with siRNA offers

the opportunity to reduce the chronic inflammation in the wound. TNFα silencing is possible with siTNFα loaded lipidoid nanoparticles in both non-diabetic and diabetic mouse wounds. With the expression of TNFα knocked down by almost half, treated wounds were shown to close statistically faster than control wounds. Together this data indicates siTNFα in lipidoid nanoparticles is an alternative therapeutic to address one of the major biological irregularities endemic to the diabetic wound.

Chapter 4

Understanding lipid nanoparticle structure's effect on the immune system

4.1 Introduction

Drug delivery is a complex field, tasked with packaging and transporting a wide variety of compounds across the many barriers in the body. These barriers include blood vessels, the stomach and intestinal lining, as well as cellular, intracellular, and nuclear membranes. Most medicines require delivery vehicles to get where they need to go and do what they need to do, with everything from vaccines to chemotherapeutics depending on a vehicle of some kind. Over the past several decades, hundreds of promising drug delivery systems have been developed and introduced into human clinical trials. Unfortunately, however, very few drug delivery systems in the United States are ultimately approved by the FDA [65].

One of the major hurdles preventing the translation of more drug delivery systems to the clinic is toxicity. Although therapeutic efficacy largely has one end-point and forms the bulk of preclinical testing, safety and toxicity can have many possible endpoints and are largely under-investigated. Rises in liver enzymes, kidney damage, and weight loss are typically monitored as proxies for the complex toxicity response, but they do not communicate the full picture. Another very important type of toxicity, and the focus of this paper, is immunogenicity. Millions of years of evolution have equipped the hu-

man body with the amazing ability to destroy almost anything it encounters, ranging from dangerous pathogens to, unfortunately, beneficial therapeutics. The immune system poses a major challenge to drug delivery researchers for two reasons: 1) the immune system prematurely clears [66] or neutralizes delivery vehicles from the body, which reduces efficacy, and 2) an immune response can cause potentially severe side effects in the patient, including fever, inflammation, and anaphylaxis. Because of this, a significant goal during delivery material development is avoidance of an immune response.

Unfortunately, there is currently a poor understanding of how delivery vehicles interface with and, subsequently, provoke the immune system. There are several important drug delivery vehicle parameters to investigate in this regard, including the size, shape, and surface chemistry of the delivery system [67, 68, 69, 70]. Although some studies have examined the former two parameters, little work has been done to identify the effect of surface chemistry on the complete immune response. One group has extremely recently examined the role of lipidoids as toll-like receptor 4 (TLR4) agonists in vitro [71], but this investigates only a partial effect on the innate immune system, rather than incorporating humoral or adaptive responses. A complete study would investigate not only the innate system, like macrophages, but fully explore the primary and secondary B and T cell responses. By understanding exactly which chemical structures do and do not provoke the immune system, we can choose to incorporate only well-tolerated chemical moieties into our drug delivery vehicles.

The humoral and adaptive responses are reliant upon activated T and B cells. While both are equally important, we first decided to focus on major subtypes of B cells. These include germinal center B cells, plasma cells, and memory B cells. Germinal center B cells are those B cells which have responded to antigen and, three to four days after immunization, begin to form T cell- and dendritic cell-rich regions called germinal centers in secondary lymphoid organs [72]. Overall, these areas are the home-base of the immune response. They are associated with clonal expansion of B cells, affinity maturation of antibodies, destruction of suboptimal B cells, and the generation of memory B cells [73]. Germinal center B cells have many receptors on their surface, but one that can be targeted with flow cytometry is known as B and T cell antigen, or GL-7. Germinal center B cells then can proceed down two different lineages: plasma cells or memory B cells [74]. Plasma cells produce antibody, and while some are generated quickly as a stopgap measure and are intended to die within the first week or two,

others can increase the affinity of their antibody through somatic hypermutation and persist for years in secondary lymphoid organs and the bone marrow [75]. They are identified by CD138 on their cell surface [76]. Memory B cells are intended to persist for years as well, and are responsible for mounting a faster, more robust response upon re-inoculation with the agent [77]. They are identified by CD27 and IgG on their surface [78].

These cells produce a variety of compounds to not only help in their activation but also in their neutralization of antigen. The primary weapon of B cells is their antibody, of which the most abundant type in the blood is IgG. IgG binds to antigen and triggers its destruction by immune cells via the Fc receptor or interactions with the complement system, and thus can majorly decrease therapeutic efficacy [79]. Additionally, cytokines and chemokines produced by B cells, T cells, and macrophages can be detected in the blood and in cell culture of plated cells. One of these is IL-6, which is first produced by the innate immune system but then reaches systemic circulation to induce the differentiation of naïve T cells into helper T_H cells. It also stimulates the differentiation of germinal center B cells into plasma cells [80].

Herein we describe the analysis of all aforementioned compounds in the setting of a primary and secondary immunization of antigen. A library of twenty lipidoids was created to serve as antigen, and the cellular and cytokine responses after repeat injection were analyzed with flow cytometry and ELISA. The library was also tested against RAW 264.7 macrophages and peripheral blood mononuclear cells isolated from healthy volunteers. Special attention was paid to B cell subsets and B cell specific cytokines. We show that not only does a T cell dependent response definitely occur, but plasma cells and memory B cells are generated in significant number. While the amine head group seems to predominately affect the immune response seen, the tail group can modulate inflammation up or down. The presence of a nitrogen ring in the head group seems particularly immunostimulatory, as does the presence of an eleven or twelve carbon acrylate tail.

4.2 Materials and Methods

4.2.1 Lipidoid library synthesis and purification

The lipidoid library was synthesized via the combinatorial Michael addition of four amine head groups to five acrylate tail groups at a stoichiometric ratio of 1:4. The amines included, purchased from Acros Organics, were: 3,3'-Diaminodipropylamine (306), Tris[2-(methylamino)ethyl]amine (304), 1,4-Bis(3-aminopropyl)piperazine (313), and N,N-Diethyldiethylenetriamine (123). These were combinatorically combined with acrylate tails containing 10-13 carbons, as well as with an isodecyl acrylate. Each lipidoid was purified over a silica column on a Teledyne ISCO chromatography system to obtain the fully substituted product.

4.2.2 Nanoparticle formulation

Lipidoids were formulated into nanoparticles for all experiments. For nanoparticle formulation, the lipid solution was formed by mixing the lipidoid, distearoyl-sn-glycerol-3-phosphocholine (DSPC, from Avanti Polar Lipids), cholesterol (Sigma Aldrich, St. Louis, MO), and C14-PEG (Avanti Polar Lipids) at a molar ratio of 50:10:38.5:1.5 in the presence of ethanol (Sigma Aldrich), citrate buffer, and PBS. siRNA against Green Fluorescent Protein (AD18537.13) was obtained from Alnylam. The siRNA was diluted in 10 mM sodium citrate and combined with the lipid solution at a final lipid to siRNA weight ratio of 5:1. The solution was vortexed after each reagent addition, and the lipid solution was added to the siRNA solution. The mixture was vortexed to form nanoparticles.

4.2.3 Nanoparticle characterization

Nanoparticles were diluted to a final siRNA concentration of 1 μg/mL in PBS. Percent siRNA entrapment was determined via the Quant-iT Ribogreen assay (Invitrogen), as Ribogreen binds to siRNA and fluoresces. Entrapment was determined by comparing the signal from intact LNP solutions to the signal from an LNP solution that had been ruptured with 2% Triton-X surfactant. Nanoparticle size was measured with a Malvern Zetasizer Nano (Malvern Instruments, UK).

4.2.4 Cell culture

RAW 264.7 macrophages (ATCC, Manassas, VA) were maintained in High Glucose (4.5 g/L) Dulbecco's Modified Eagle's Medium (Gibco, Carlsbad, CA), 10% Fetal Bovine Serum (Invitrogen, Carlsbad, CA), and 1% Penicillin-Streptomycin (Invitrogen) at 37°C and 5% carbon dioxide. Macrophages were used below passage 9. Isolated splenocytes were plated in RPMI 1640 medium, 10% Fetal Bovine Serum, and 1% Penicillin-Streptomycin at 37°C and 5% carbon dioxide.

4.2.5 RNA extraction and cDNA synthesis

RNA extraction and purification from macrophages was accomplished with the QIAshredder and RNeasy Mini Kit (Qiagen, Valencia, CA). RT-PCR was performed with the High Capacity cDNA Reverse Transcription kit (Applied Biosystems) to form 2 μg of cDNA. The quality and quantity of mRNA and cDNA were assessed by the absorbance at 260/280 nm with the Nanodrop 2000 UV-Vis spectrophotometer (Thermo Scientific).

4.2.6 Quantitative PCR

qPCR was performed in a 384-well block on a ViiA^{TM} 7 Real-Time PCR system machine with purchased Taqman Gene Expression Master Mix (Applied Biosystems), along with GAPDH (Mm99999915_g1), TNFα (Mm00443258_m1), IL-6 (Mm00446190_m1), and IL-1β (Mm00434228_m1) Taqman probes (Thermo Fisher). 10 μL of Master Mix, 1 μL of endogenous control probe, and 1 μL of target gene probe was used per well. All runs utilized the comparative Ct method and the following run protocol: 50°C (2 min), 95°C (10 minutes), 40 cycles of 95°C (15 sec) and 60°C (1 min). qPCR experiments consisted of three biological replicates and two technical replicates per each biological. The target gene was normalized to the endogenous control gene (GAPDH) for each sample, and then normalized again to the nanoparticle-free control sample.

4.2.7 Human peripheral blood mononuclear cells

Human blood experiments were conducted at the Indian Institute of Bombay, in Professor Rahul Purwar's lab. Blood was collected at the on-site hospital from healthy volunteers and brought on ice to the lab. Peripheral blood mononuclear cells were separated with Ficoll histopaque (Sigma Aldrich) according to manufacturer's directions. Cells were plated in 12-well plates in 500 μL of media and dosed with 100 nM siGFP formulated with each lipidoid. 24 hours later, cell culture supernatant was collected and aliquotted for ELISA analysis. ELISA kits to detect IL-2, IL-6, TNFα, IFNγ, and IL-1β were purchased from BD Biosciences and run according to manufacturer's directions.

4.2.8 Animal studies

All mouse experiments were approved by the Institutional Animal Care and Use Committee (IACUC) at Carnegie Mellon University under protocol number PROTO201600048. C57BL/6 mice were either purchased from Charles River Laboratories (Wilmington, MA, USA) or obtained from an institutionally managed breeding colony. Mice were housed in cages of fewer than six animals, with controlled temperature (25°C), 12 hour light-dark cycles, and free access to food and water. Mice used in this study were females between the ages of 7-10 weeks at the beginning of the study, and had never received a nanoparticle injection or treatment before. They were divided into treatment groups of four animals per lipidoid tested per time point, with six separate animals serving as controls per time point. Each mouse was injected with a 1 mg/kg dose of siGFP loaded into the appropriate nanoparticle for their treatment group and allowed to rest for four weeks. After four weeks, they were re-injected with 1 mg/kg siGFP in the same kind of nanoparticle previously tested. Either two or seven days later, mice were sacrificed via carbon dioxide inhalation. A blood sample was taken via postmortem cardiac puncture and the spleens were excised. Blood was aliquotted and frozen at -80°C until ELISA analysis could be performed.

4.2.9 Flow cytometry of splenocytes

Spleens were excised and placed immediately into PBS. Shortly thereafter, they were strained through 70 μm cell strainers (Fisher Scientific) and non-white blood cells were lysed with 1X RBC Lysis Buffer

(Thermo Fisher) per the manufacturer's instructions. They were washed twice with media and counted. Per sample, the volume to yield two sets of 1×10^6 cells was removed, spun down, and decanted. Two staining buffers were made. The first staining buffer contained 5 μL per sample each of PE Rat Anti-Mouse T- and B-Cell Activation Antigen - Clone GL7 (BD Biosciences), APC Rat anti-Mouse CD138 - Clone 281-2 (BD Biosciences), PerCP Hamster Anti-Mouse CD3e - Clone 145-2C11 (BD Biosciences), and FITC Rat Anti-Mouse CD45R/B220 - Clone RA3-6B2 (BD Biosciences), with 80 μL per sample of Flow Cytometry Staining Buffer (Thermo Fisher). The second staining buffer contained 5 μL per sample each of APC Hamster Anti-Mouse CD27 (BD Biosciences), PE Rat Anti-Mouse IgG1 - Clone A85-1 (BD Biosciences), PerCP Hamster Anti-Mouse CD3e - Clone 145-2C11 (BD Biosciences), and FITC Rat Anti-Mouse CD45R/B220 - Clone RA3-6B2 (BD Biosciences), with 80 μL per sample of Flow Cytometry Staining Buffer. One set of splenocytes from each lipidoid tested received 100 μL of stain 1, while the second set received 100 μL of stain 2. Cells were immersed in staining solution for 30 minutes before being centrifuged and decanted. They were washed twice with Flow Cytometry Staining Buffer and finally resuspended in 500 μL of Flow Cytometry Staining Buffer. Flow cytometry was immediately performed on a BD Biosciences Accuri-Intellicyt Flow Cytometer running ForeCyt software. Plots were generated using FlowJo software.

4.2.10 Splenocyte stimulation

Splenocytes not prepped for flow cytometry were plated in two 24 well plates, 1×10^6 cells in 1 mL of media per sample. One well plate received a 20 ng/mL dose of Lipopolysaccharide (LPS) from *E. coli* 0111:B4 (Sigma-Aldrich). The other plate received 10 ng/mL dose of Phorbol 12-myristate 13-acetate (PMA) (Sigma Aldrich) and 500 ng/mL dose of ionomycin (Thermo Fisher). 24 hours later cell culture supernatant was harvested from both plates, and immediately aliquotted and frozen at -80°C until ELISA analysis could be performed.

4.2.11 ELISA analysis

Blood samples were thawed and IL-6 (Thermo Fisher, 88-7064-76) and Total IgG (Abcam, ab157719) ELISAs were run according to the manufacturer's instructions. Cell culture supernatants from cells treated with LPS were tested using the uncoated TNFα ELISA plate kit (Thermo Fisher, 88-7324-77) while culture from cells treated with PMA/ionomycin were tested with the uncoated IL-2 ELISA kit (Thermo Fisher, 88-7024-22). All ELISAs were run following the manufacturer's instructions.

4.2.12 Factor VII silencing

Lipidoids were formulated with siRNA specific against Factor VII (Alnylam). They were injected at 0.4 mg/kg dose into mice, three per treatment group. Two days later blood was taken via submandibular bleed and a Biophen Factor VII activity assay was run (Aniara, Inc., Westchester, OH) according to manufacturer's directions. Factor VII silencing was calculated using a calibration curve generated from dilutions of a control sample. To establish repeat efficacy, a month after the first injection 304O13 was reformulated with the same siRNA and reinjected into the same mice, and the process was repeated.

4.2.13 Statistical Analyses

All mean values are expressed as $\pm$ standard deviation. Unpaired Student's t-tests and one-way ANOVA tests were used where appropriate to evaluate statistical significance. A p value of < 0.05 was considered significant.

4.3 Results

4.3.1 Lipidoid structures

Four amines were combinatorically matched with five tail groups to create a library of twenty lipidoids. The amines are known by the numbers (123, 304, 306, and 313) they were given during their first utilization at the Massachusetts Institute of Technology. Four of the tail groups were acrylates including ten,

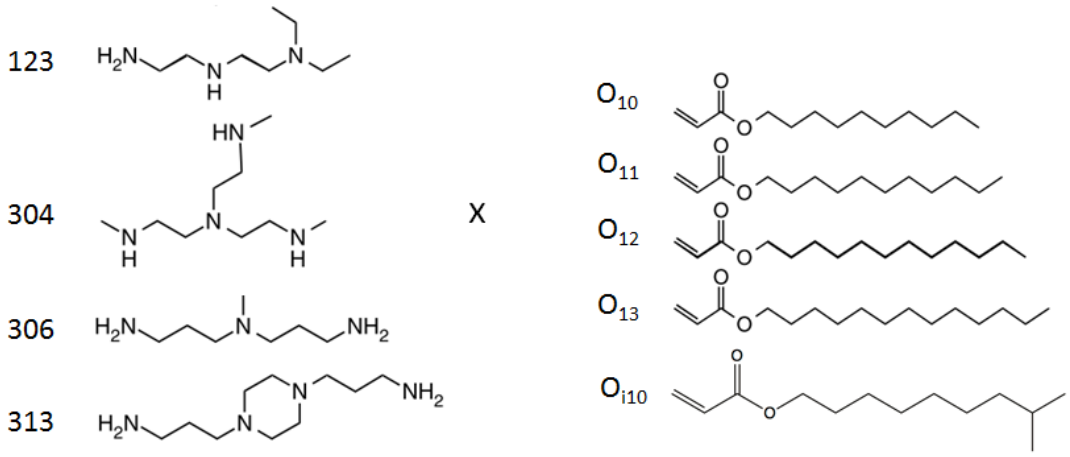

Figure 4.1: **Four head groups and five tail groups were combined to produce the lipidoid library.**

eleven, twelve, and thirteen carbons (O10, O11, O12, and O13). The structures of these compounds are given in fig. 4.1. The fifth tail included an isodecyl acrylate group (Oi10) rather than a straight carbon chain. These tertiary amines are capable of adding three to four tails and the final products form via solvent free Michael addition. Tails were added to amines in a ratio to favor the production of fully substituted lipidoid products, and were allowed to react under constant mixing at ninety degrees centigrade for two days. The crude lipidoid products were purified on a silica column using a Teledyne Isco flash chromatography system in order to isolate the fully substituted version of these compounds. When possible and present in great enough quantity, the compound with one fewer tail was also collected.

Purity of the lipidoid compounds was assessed in two ways. The first was thin layer chromatography, where each fraction generated by flash chromatography was tested on a glass-backed silica plate for the presence of multiple compounds. We combined fractions that possessed the same single compound and removed solvent via rotary evaporation. The exact chemical nature of each combined product was determined with electrospray mass spectrometry.

Once formulated into nanoparticles, the liposomes are stable in the refrigerator on the order of months. However, they are far more stable when lyophilized into a powder and stored at -80°C, and can be shipped to India without a loss of function. Therefore, the library was made into nanoparticles

and divided up into smaller aliquots in the Whitehead Lab. Each of the seven aliquots contained roughly 15 experiments worth of nanoparticles, providing enough materials in total for seven months of work. Each aliquot could be easily reconstituted in DI water and used in a variety of experiments for one to two months.

4.3.2 Cell culture and the lipidoid library

Fifteen of the lipidoid nanoparticles were tested in a RAW 264.7 cell line model. These are mouse macrophages, and constitute an ideal first pass to examine the innate cytokine response. Tumor necrosis factor α (TNFα) was chosen as the first cytokine to be examined, as it is the master cytokine of the macrophage mediated inflammatory cascade. Fortunately, the levels of other cytokines, such as IL-1β or IL-6, can be measured in the future using the DNA harvested from all experiments. In initial experiments with a different previously made library, extensive time courses were carried out to examine the gene expression of TNFα in response to several nanoparticles at different time points. Expression was measured every 2 to 4 hours for a full day (fig. 4.2), and the time point of ten hours was chosen as an ideal comparison point for going forward.

Experiments going forward were performed with the library discussed in the previous section, and with the knowledge gained with the time course experiments discussed above. Cells were plated and received a dose of 100 nM siGFP loaded lipidoid nanoparticles. Green fluorescent protein (GFP) was chosen as the dummy target since it is not expressed in this cell line. RNA was harvested ten hours later and TNFα gene expression quantified via qPCR. Fig. 4.3 represents the same data organized in two different manners. The data is arranged by amine head group in fig. 4.3(a), while fig. 4.3(b) is arranged by tail group. Individual asterisks indicate whether TNFα expression is significant compared to that provoked by the PBS control, while the large black bars indicate if values within a particular head or tail group are significantly similar to or different from each other.

All lipidoids with the amine groups 123, 313, and 306 generated a significant TNFα immune response in vitro, as seen by the asterisks over each group in fig. 4.3(a). Changing the tail group did not largely affect TNFα production, indicating that the amine group head was a larger determining factor.

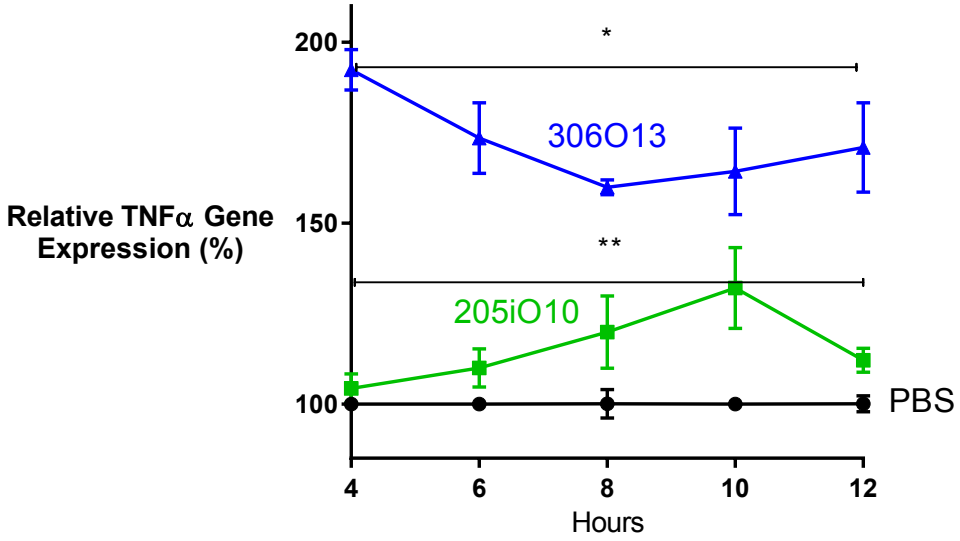

Figure 4.2: **Different lipidoids yield different kinetics of TNFα production over 12 hours.** Using a previously made library, an initial experiment was performed to determine the optimal time to measure TNFα in in vitro experiments. Two different lipidoids were tested, 306O13 and 205iO10. They had different response profiles, with peak production of TNFα occurring at different times. However, ten hours was chosen as the time point for future experiments. The overarching bars are one-way ANOVAs indicating that the TNFα expression at each time point is indeed different and time-dependent. Error bars are s. d. ($n = 3, {}^{*}p < 0.05, {}^{**}p < 0.01$)

This is also seen in fig. 4.3(b), where lipidoids might all possess the same tail group, but their TNFα expression was wildly different. Nevertheless, the tail group can modulate the immune response slightly, as seen in fig. 4.3(a).

4.3.3 Human peripheral blood mononuclear cells

In March 2017, I visited and worked with the Purwar Lab at IIT Bombay. The raw materials for fabricating the lipidoid nanoparticles were shipped ahead of time, and I formulated seventeen different nanoparticle solutions in person. Nanoparticles were tested on seven different specimens of human-derived PBMCs, and the levels of several key immune proteins in their culture supernatant were measured. These included IL-6, TNFα, IL-1β, IFNγ, and IL-2. The first three are graphed by amine head group family in fig. 4.4, as the latter two targets were not identified in the supernatant of any samples. Although many of the lipidoids provoked rises in the healthy blood samples, three in particular

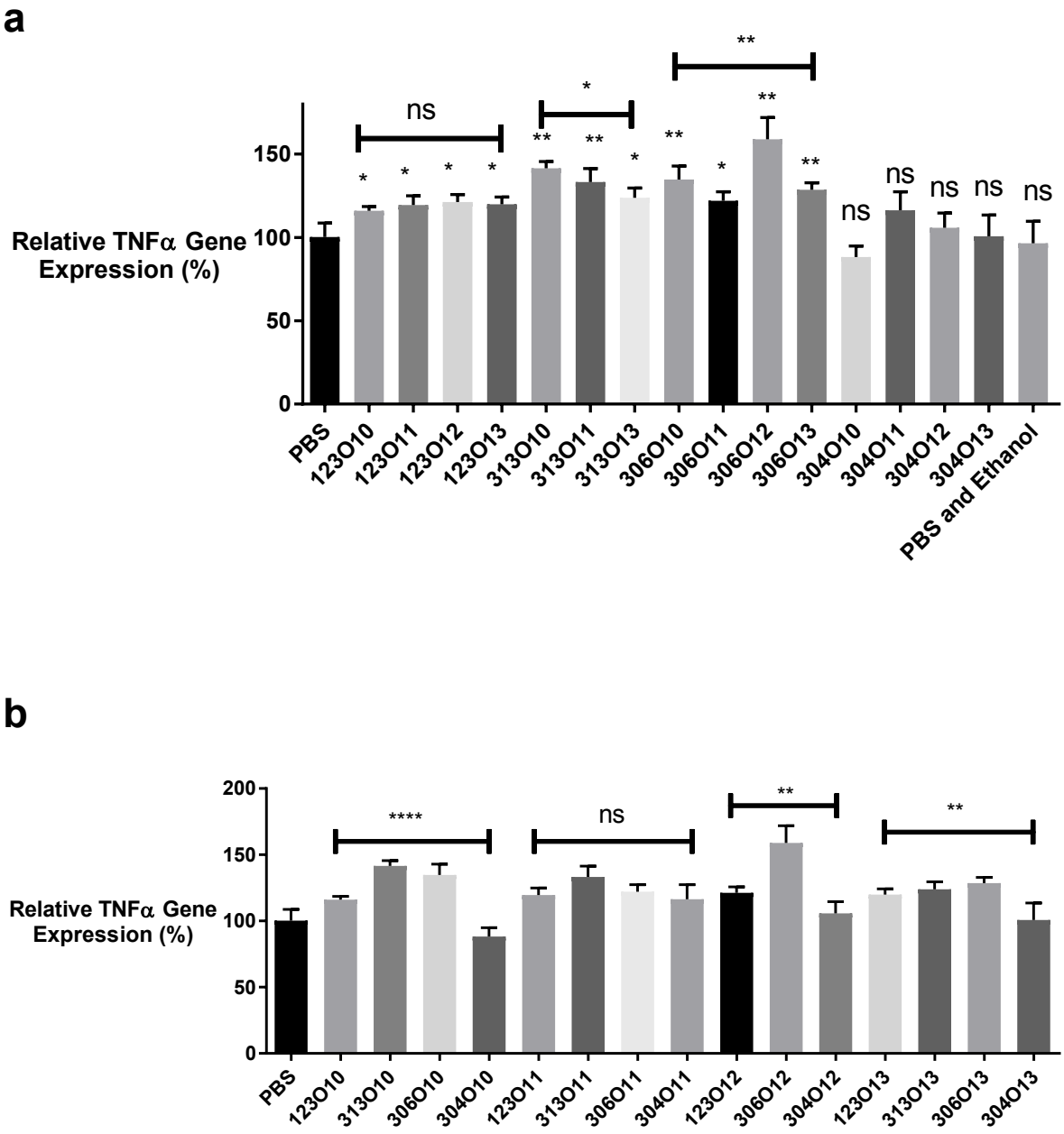

Figure 4.3: **Head group seems to determine the immune response, but tail group can modulate.** Both graphs represent the same data, just graphed in a slightly different way. a) Data is organized by head group, with t-test significance compared to controls given over each bar. The large black bars overhead are one-way ANOVAs, examining how different the values within one head group are. Changing the tail group resulted in only slight differences in TNFα production. b) Lipidoids are grouped together by tail. Changing the head group significantly changes TNFα production, indicating head is a larger determining factor. (Error bars represent s. d. $n = 3$, $^{*}p < 0.05$, $^{**}p < 0.01$, $^{****}p < 0.0001$)

provoked enough of a rise to be statistically significant. 123O10, 306O11, and 306O12 exhibited statistically significant rises in IL-6 or TNFα, with many other lipidoids, like 304O10 or 313O12, giving nearly significant results. 306O12 also caused a significant rise in IL-1β. In this instance, significance refers only to the fact that cells from all tested volunteers reacted; many of the lipidoids gave rises in three out of four, or four out of five, of the volunteers. The 306 family is graphed in fig. 4.4(a). Small changes in the structure—in this case the addition or deletion of a carbon from the acrylate tail—generated a very different immune response. 306O11 and 306O12 both saw rises in these two inflammatory cytokines, while 306O10 and 306O13 did not. The response is similar for most other families pictured.

4.3.4 Two day time-point

Mice ($n = 4$–6) were injected with 1 mg/mL siGFP formulated with each lipidoid in the library and allowed to rest for four weeks. They were then reinjected, and two days later blood samples and spleens were taken for ELISA and flow cytometry respectively. As discussed in the chapter introduction, three main types of B cells were targeted, representing different lineages possible in the immune response. Flow cytometry gives the percentages of each subtype as a portion of total splenocytes sampled (fig. 4.5). Fig. 4.5(a) gives the numbers of germinal center B cells, and only 313Oi10 and 306O11 are increased in number. These lipidoids also show increased numbers of plasma cells in fig. 4.5(b), along with several other members of the 313 and 306 head group families. Fig. 4.5(c) shows the robust memory B cells response that occurred, with nearly all lipidoids showing an increase in that type of B cell.

The increase in antibody producing cells, like plasma and memory B cells, is mirrored in the increase in total IgG seen in mouse blood samples as measured by ELISA (fig. 4.6). Except for 306O12 (which is debatable, due to its wide error bars), 304O11, and 304Oi10, all lipidoids showed an increase in total IgG.

We also looked at levels of IL-6 in the same blood samples (fig. 4.7). IL-6 is involved in T cell activation and the transition from germinal center B cells to plasma cells. Members of the 313 and 306 amine group families again had increases in protein concentration, though 304 did as well.

After isolation, cells were plated and stimulated with LPS. ELISA was used on the cell culture

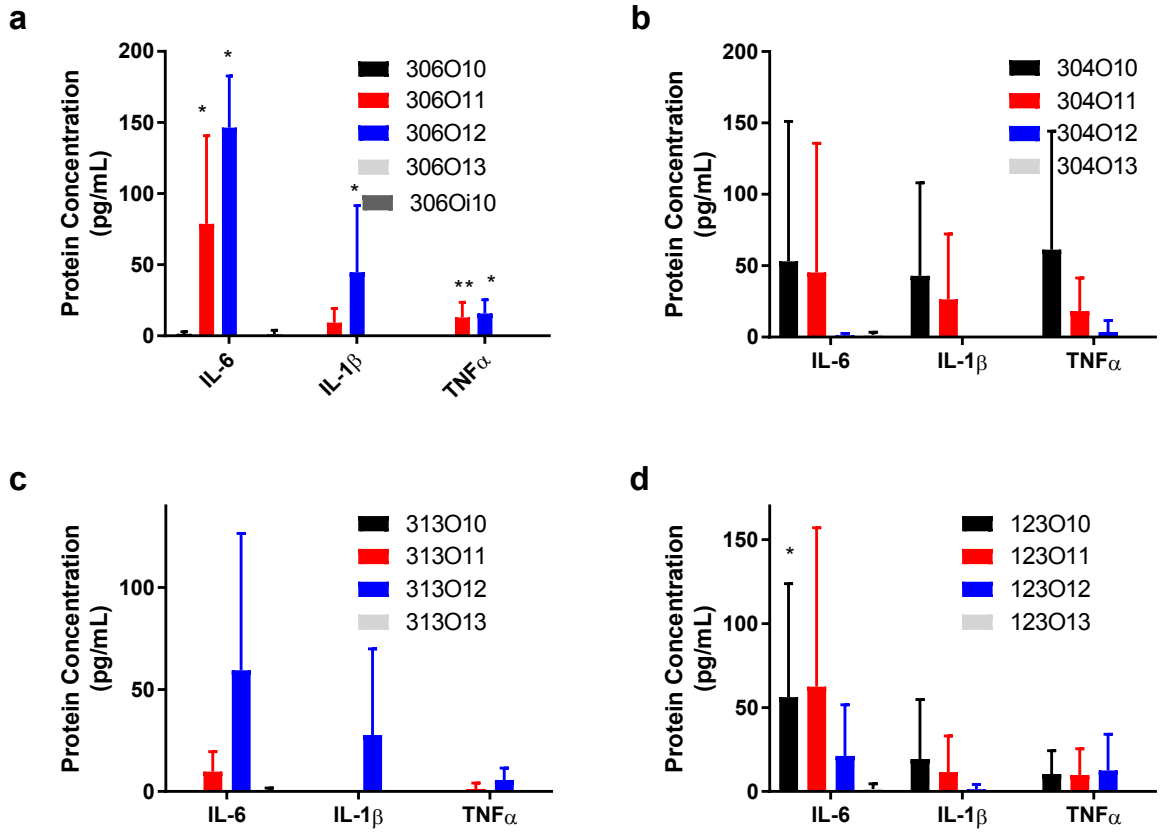

Figure 4.4: **Small changes in structure result in large changes in immune response.** PBMCs isolated from healthy donors were exposed to the full lipidoid library. 24 hours later cell culture supernatant was collected and analyzed for cytokines via ELISA. Pictured here are all families of amines. a) 306O11 and 306O12 both gave significant rises in IL-6 and IL-1β, while 306O10 and 306O13 did not. b) While none of these gave hits in all volunteers, 304O10 and 304O11 consistently did react. c) 313O12 gives the largest response for all targets. d) 123O10, 123O11, and 123O12 are reactive while 123O13 is not.

supernatant to assay for TNFα (fig. 4.8). Although every sample was not collected for various reasons, those that were collected indicated marked upregulation of soluble TNFα. Only 123O12 and 313O11 did not produce higher levels than control values. Cells exposed to nanoparticles produced 5-15 times more TNFα than control cells, implying an already high baseline number and activity of immune cells.

Cells were also stimulated with PMA/ionomycin to assess the T cell response. Future work will involve testing these aliquotted and frozen samples for IL-2 and IFNγ.

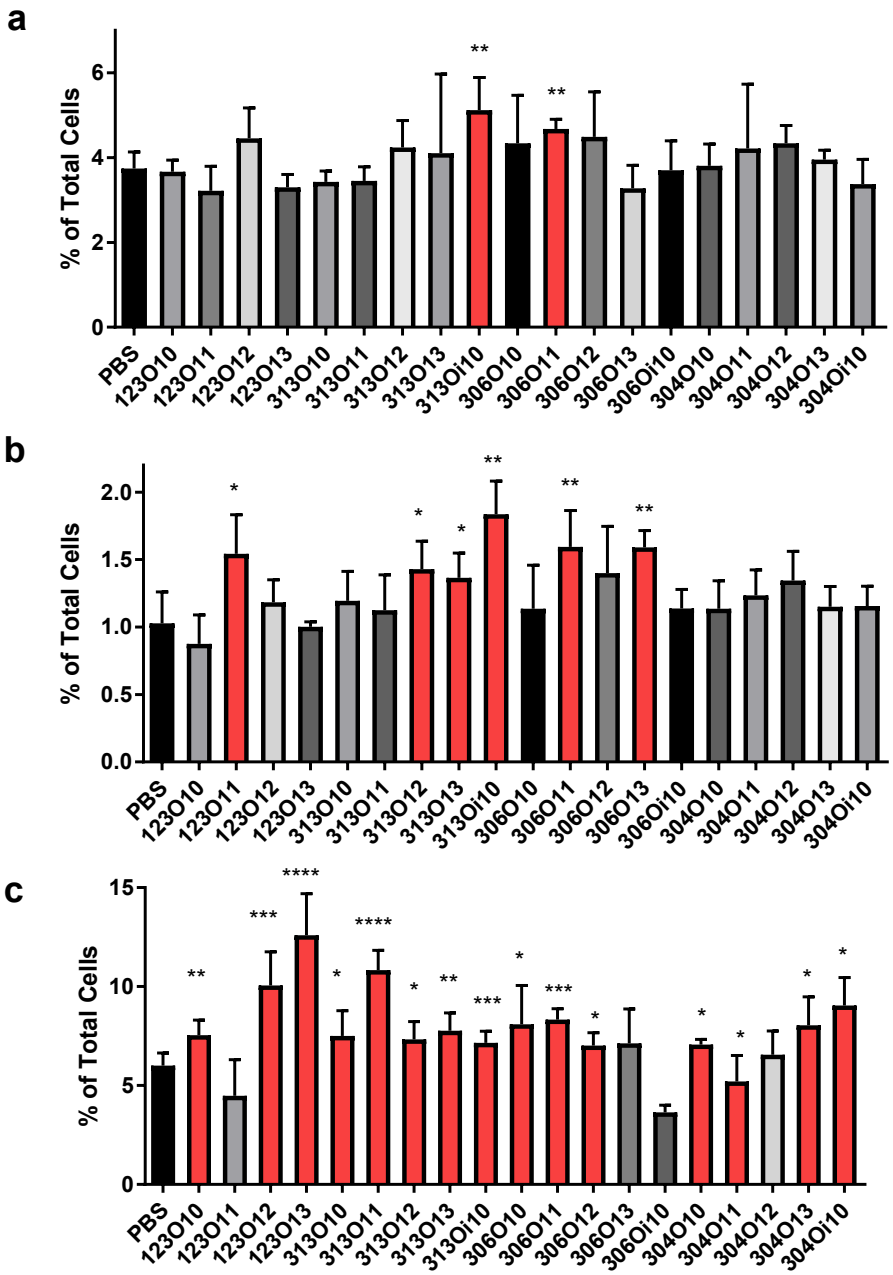

Figure 4.5: **A vigorous memory B cell response exists two days post-second injection.** All panels represent a different subtype of B cell, with data from all three analyzed at the same time for each sample. Red bars are those that have higher numbers of cell percentages than controls. a) Germinal center B cells are only slightly increased in number for 313Oi10 and 306O11. b) Plasma cells are more upregulated, with several members of the 313 and 306 head groups affected. c) Memory B cells are increased in number almost across the board. Error bars represent s. d. ($n = 4$–$6, {}^{*}p < 0.05, {}^{**}p < 0.01, {}^{***}p < 0.001, {}^{****}p < 0.0001$)

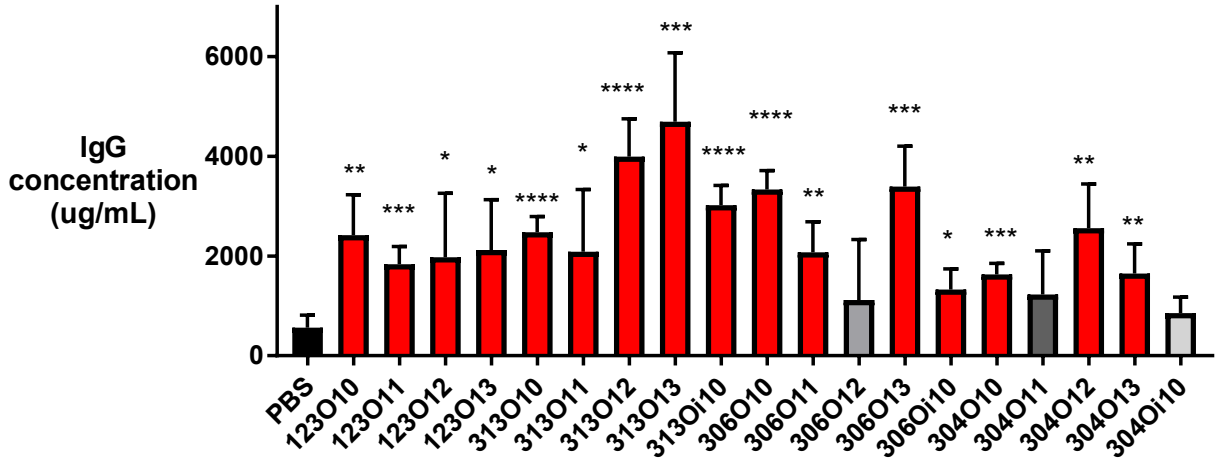

Figure 4.6: **Antibody levels are higher in mice that received nanoparticles.** ELISA was used to measure the free total IgG levels in the blood for all mice at the time of sacrifice. Only three lipidoids did not show an increase in IgG: 306O12, 304O11, and 304Oi10. Error bars represent s. d. ($n = 4$–6, $^{*}p < 0.05$, $^{**}p < 0.01$, $^{***}p < 0.001$, $^{****}p < 0.0001$)

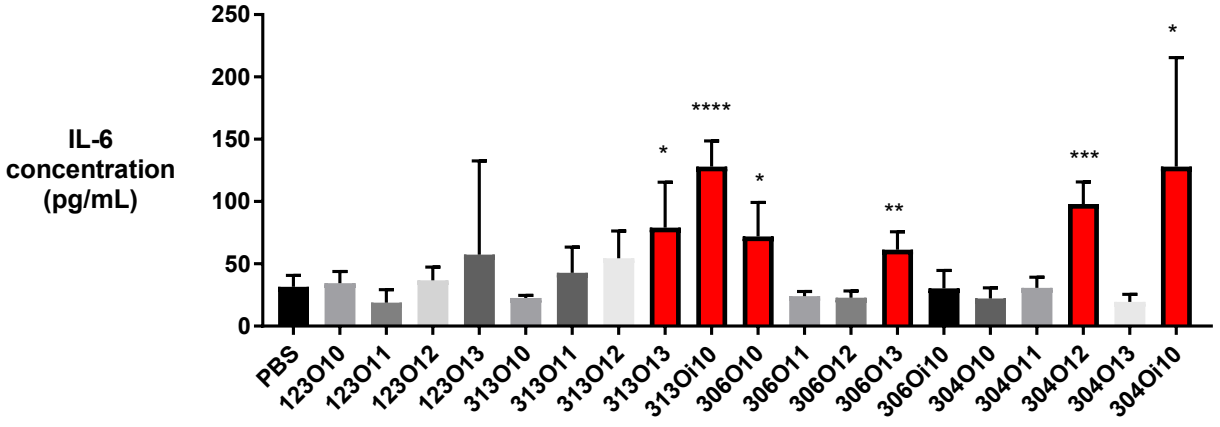

Figure 4.7: **IL-6 is increased in several lipidoid treatment categories.** Mouse blood was assayed via ELISA for IL-6. 313O13, 313Oi10, 306O10, 306O13, 304O12, and 304Oi10 saw increases in levels. Error bars represent s. d. ($n = 4$–6, $^{*}p < 0.05$, $^{**}p < 0.01$, $^{***}p < 0.001$, $^{****}p < 0.0001$)

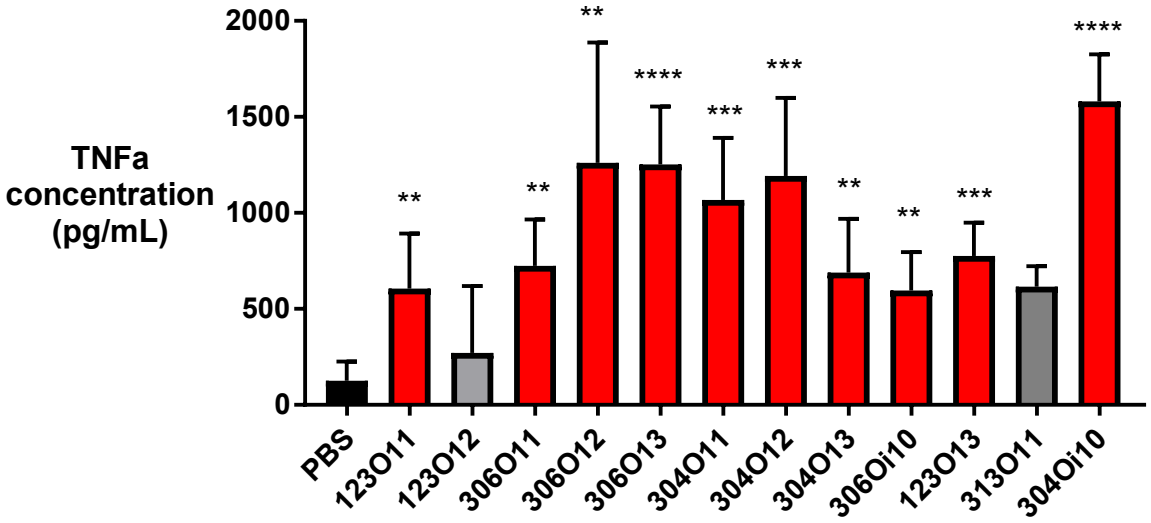

Figure 4.8: **TNFα is produced in greater amounts by almost all lipidoids tested.** Cells exposed to nanoparticles produced 5-15 times the level of TNFα mRNA than control cells. (n = 4–6, $^{*}p < 0.05$, $^{**}p < 0.01$, $^{***}p < 0.001$, $^{****}p < 0.0001$)

4.3.5 One week time-point

The above experiments were repeated in a different set of mice, but this time with a week following the second injection instead of two days. Flow cytometry was performed to analyze the levels of germinal center B cells, plasma cells, and memory B cells (fig. 4.9). The 306 and 304 family were not included in the graph, as they are currently being repeated due to problems with the antibodies used. Germinal center B cells were not statistically different in number among any of the treatment groups (fig. 4.9(a)). Among plasma cells, only 123O10 showed an increase in number (fig. 4.9(b)) a week after the second injection. Some were lower in number, the significance of which is unclear. Memory B cells showed fewer increases than at two days, with 123O11, 123O12, 313O11, and 313O12 not giving significant rises (fig. 4.9(c)). Notably, the Oi10 tail group seemed to encourage a robust memory B cell response.

ELISAs are will be performed to assess IgG and IL-6 content in mouse blood samples, along with TNFα, IL-2, and IFNγ in cell culture supernatant.

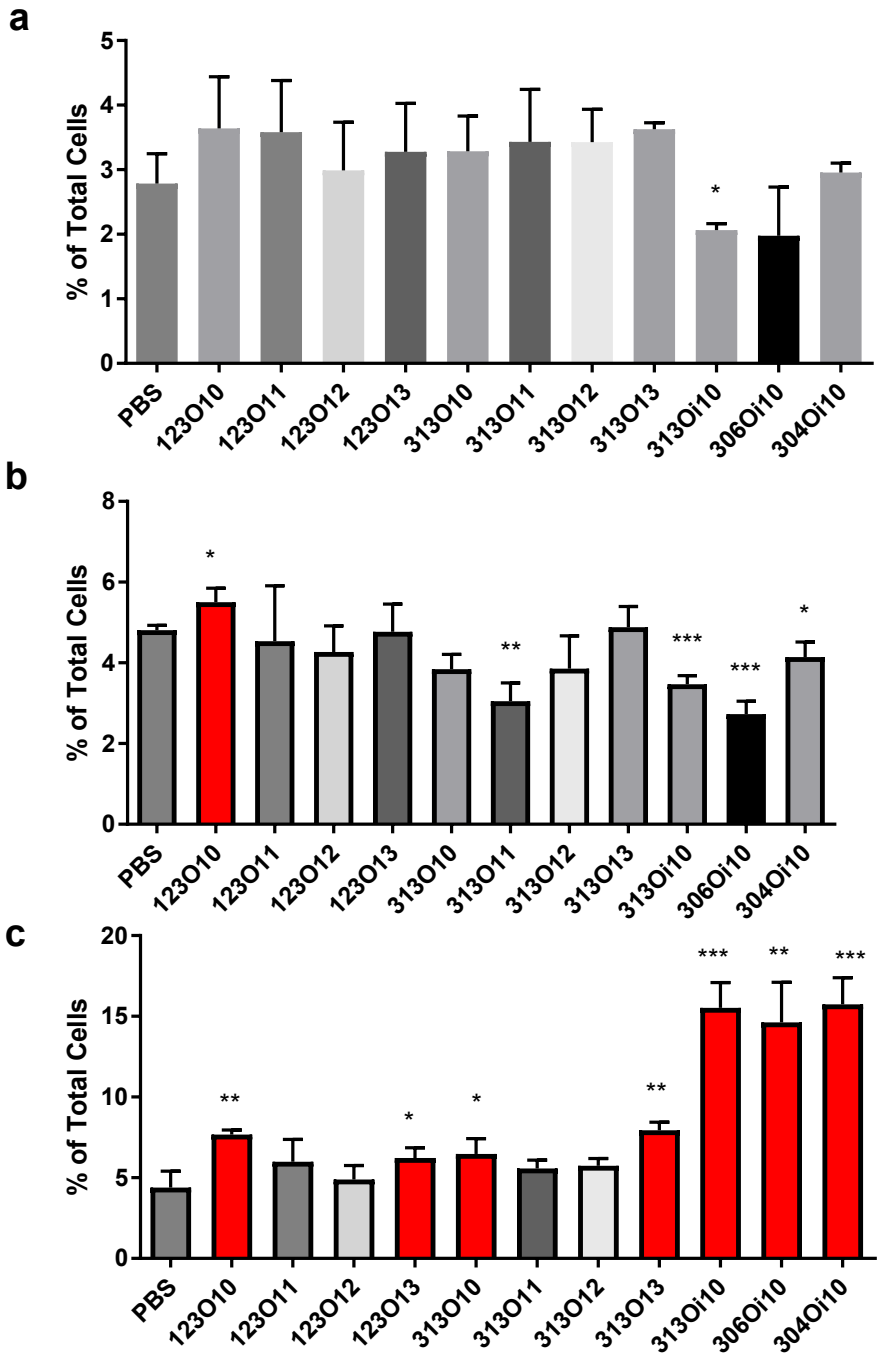

Figure 4.9: **Fewer lipidoids show increases in B cell percentages one week after repeat dosing.** Mice were injected, allowed to rest for a month, and injected again with lipidoid nanoparticles. One week after the second injection they were sacrificed and flow cytometry was performed. a) Germinal center B cells do not differ in number from controls. b) Only 123O10 shows an increase in plasma cell percentages. c) Memory B cells are higher than controls for some lipidoids, but fewer than at two days post repeat injection. Error bars are s. d. ($n = 4$–6, $^{*}p < 0.05$, $^{**}p < 0.01$, $^{***}p < 0.001$)

4.4 Discussion

One prong of this study is to analyze the immune response caused by lipidoid nanoparticles on human cells, as this provides the specificity to human cells required to gauge human immune response. The most direct means of obtaining human white blood cells is to isolate peripheral blood mononuclear cells (PBMCs) from the blood of healthy volunteers. This population of white blood cells includes macrophages, T cells, B cells, and several other types of immune cells, all of which contribute to both the innate and antibody-driven immune response. However, because these cells are seeing the nanoparticles for the first time, only a primary response could be seen, not a secondary response.

Additionally, because the odds of finding a B and a T cell reactive against the same epitope, not to mention a dendritic cell capable of presenting, in this small population is low, the response engendered is probably innate in origin. This is seen in fig. 4.4, where no targets provoked a rise in IFNγ or IL-2. From the IL-6 and TNFα response, 306O11 and 306O12 might possibly look like some natural epitope many people are exposed to and trained against, since this would be a virgin response and largely innate dominated. The results of the macrophage experiments (fig. 4.3) match up nicely with the results seen in PBMCs, strengthening the data by comparing across two species and systems. As in the mouse in vitro experiments, 123O10, 306O11, and 306O12 all provoked a rise in TNFα, with 306O12 generating a highly significant rise.

This increase in IL-6 might be due to the lipidoids' position as an agonist of toll-like receptor 4. Usually TLR4 responds to double-stranded RNA and lipopolysaccharide, but it has been shown that the lipidoids interact with it as well [71]. TLR4 involvement would increase IL-6 and encourage the production of plasma cells from germinal center B cells, both effects which our study demonstrated.

Our study also indicates that the immune response has to be T cell dependent, or else plasma and memory B cells would not be present. The fact that germinal center B cell numbers are the same as controls for most of the lipidoids makes sense, as they typically peak in the first couple weeks after initial inoculation. As for plasma cells, they are especially long-lived, but they do eventually relocate to the bone marrow. This might be seen as the reduction of spleen plasma cells at two days and at one week post second injection. The memory B cell response is the most robust, with nearly every

lipidoid showing increased numbers as compared to control. Once repeat efficacy of each nanoparticle is established with an assay that measures Factor VII in the blood, the clinical significance of these rises can be studied.

The human PBMC data underestimates the immune response, as it cannot account for the secondary humoral response. However, 306O11 and 306O12 gave statistically increased rises in various cytokines in human PBMCs, and then went on to show increases in plasma and memory B cells in mice as well. In general, the O11 and O12 tails provoked responses in human PBMCs as well as mice, the latter of which is reflected in increases in immune cells across several amine head groups.

That 313Oi10 and 306O11 show germinal center B cell response weeks after initial inoculation indicates either a new primary response or an exceptionally long persistence of germinal center B cells. These two lipidoids show increases in all types of cells, however, thus speaking to the development of a robust immune response. Other lipidoids have exhibited a preference for the plasma cell linage rather than memory B cell, like 123O11 and 306O13. While it might be natural to assume an increase in IL-6 should lead to an increase in plasma cells, there are some exceptions, such as 123O11. Other cells only show a memory B cell response, like 304O13.

We unfortunately have to test for total IgG rather than an antibody more specific for our delivery vehicles, as no antibody can be made for the lipidoids and they cannot be affixed to the bottom of a plate for ELISPOT analysis. However, all mice were exposed to the same environmental conditions, and the amount of antibody roughly matches up to the increase in antibody producing cells.

The average data from each test has been plotted in a heat map to better see trends (fig. 4.10). In this case, the PBS control values were set as the lowest values on the spectrum, and are considered green for "good." The highest values in each row (corresponding to the values for all the same test) are in the brightest shade of red, indicating immunostimulation. It is difficult to establish exactly how in-between values should be ranked, as the negative influence of increased values is unclear. To put it another way, it is unclear how bad certain metrics have to become before they begin to show systemic effects or losses of efficacy.

Despite the overall immunogenicity of lipidoids, 306Oi10 has proven to be among the safest and most efficacious. Conversely, 313Oi10 has the worst track record, along with the rest of 313 group. This

	PBS	123O10	123O11	123O12	123O13	313O10	313O11	313O12	313O13	313Oi10
Germinal Center B cells (%)	3.74	3.67	3.22	4.45	3.30	3.43	3.45	4.24	4.11	5.12
Plasma cells (%)	1.03	0.88	1.54	1.18	1.00	1.20	1.13	1.43	1.37	1.84
Memory B Cells (%)	6.00	7.55	4.48	10.06	12.60	7.51	10.83	7.33	7.77	7.16
IgG (ug/mL)	561.89	2416.46	1834.39	1974.49	2122.17	2479.02	2088.29	3990.63	4692.57	3016.33
IL-6 (pg/mL)	31.57	34.51	18.81	36.84	57.38	22.69	42.78	54.38	78.99	128.07

	306O10	306O11	306O12	306O13	306Oi10	304O10	304O11	304O12	304O13	304Oi10
Germinal Center B cells (%)	4.34	4.68	4.49	3.28	3.70	3.81	4.21	4.34	3.95	3.37
Plasma cells (%)	1.14	1.60	1.40	1.59	1.14	1.14	1.24	1.35	1.15	1.16
Memory B Cells (%)	8.10	8.33	7.02	7.14	3.65	7.07	5.21	6.56	8.05	9.05
IgG (ug/mL)	3331.10	2075.85	1119.58	3394.58	1324.95	1629.56	1225.73	2557.53	1649.71	853.08
IL-6 (pg/mL)	71.95	24.13	22.86	61.28	30.25	22.27	30.74	98.08	19.58	128.01

Figure 4.10: **A heat map of the average values for each metric for every lipidoid.** The PBS control values were set as the lowest values on the spectrum, and are considered green for "good." The red indicates higher than control values for each metric.

could be due to the presence of the nitrogen ring, similar to a piperazine. Other data (unpublished) from our lab indicates piperazines can be quite toxic to cells when unmodified, and this study indicates they could be potentially provoking the immune system as well. The 306 head group also seems particularly stimulatory, while the 123 head group is less so. O12 and O13 tails tend to provoke stimulation for every head group, while 306O11 yielded stimulation hits in almost every metric tried.

4.5 Conclusion

Since efficacy is often the most studied aspect of a therapeutic, safety and toxicity can go understudied. One form of toxicity often ignored is immune stimulation, as it comes in many forms and encompasses many different cell types. This study has focused on the secondary response to lipidoid nanoparticle treatment, analyzing the relative amounts of germinal center B cells, plasma cells, and memory B cells to characterize the humoral response. Overall, certain chemical moieties were found to be more triggering than others, such as a nitrogen ring or a tail with O11 or O12 carbons. Additionally, the memory B cell response seems to be the most robust, but plasma cells were clearly involved as well for several lipidoids tested. The increased numbers of antibody producing cells also translated to real increases in antibody in the blood. Whether these increases in immune cells translate to a real loss of efficacy is next to be analyzed.

Chapter 5

Conclusion

Delivery vehicles are necessary for many therapeutics which otherwise would not be able to overcome the various challenges in their path. Vehicles allow them to carry out their therapeutic effect, but also can encourage inappropriate immune responses that might decrease efficacy. It is clear that the relationship between delivery vehicles and the immune system is a complex one, where depending on the context either uptake or evasion might be desired.

There are many diseases which involve the immune system, and are cases where therapeutic uptake by immune cells is a desirable outcome. Delivery vehicles must then be designed to best facilitate this in a controlled manner. One such delivery vehicle is the lipidoid nanoparticle, and it has been shown to be potent in several cell types and target organs. This thesis details the first time lipidoids have been used for wound delivery, and demonstrates the successful silencing of inflammatory protein, TNFα, in the context of diabetic ulcers. Knockdown is seen in an in vitro macrophage-fibroblast coculture model, as well as in non-diabetic and diabetic mice wound models. Lipidoids can silence roughly half of the TNFα gene expression in the diabetic wound and have been shown to help the wound close faster than untreated controls.

Of course, therapeutics being delivered to anything but the immune system have immune evasion as one of their primary goals. Immune activation can decrease therapeutic efficacy or trigger dangerous reactions in the patient. Learning more about what chemical moieties cause an immune response would allow for the design of a particle that could better resist immune clearance and avoid the creation

of a secondary response. Conversely, incredibly reactive moieties could possibly be used in the creation of vaccines or other pro-stimulatory applications. This thesis investigated the effect of a lipidoid library on the immune system using a two pronged approach. The lipidoids were first tested against human peripheral blood mononuclear cells and then were injected into mice to probe the in situ immune response. Several types of B cells were examined in this latter case, namely germinal center B cells, plasma cells, and memory B cells. A T cell dependent response occurred, with a preponderance of memory B cells for most of the lipidoids tested. There was an increase in free antibody in the blood that reflected this increase in antibody producing cells. Human immune cells were also reactive to several of the formulations, implying innate activation (possibly through toll-like receptor 4). Nitrogen rings and carbon tail lengths of eleven and twelve carbons were particularly reactive, though it does seem to be that the amine head group determines immune response more than tail. Further work will analyze whether a loss of efficacy is occurring because of these increases in immune cells, as current ramifications are unclear. An in-depth T cell subset analysis with flow cytometry would also help complete the picture.

Overall, the work sought to investigate the various aspects of the interaction between lipidoid nanoparticles and the immune system. Therapeutic treatment, evasion, and stimulation are all possible, and depend on the specific chemistry chosen.

References

[1] Lisa N. Kasiewicz and Kathryn A. Whitehead. “Silencing TNFα with lipidoid nanoparticles downregulates both TNFα and MCP-1 in an in vitro co-culture model of diabetic foot ulcers”. In: *Acta Biomaterialia* 32 (2016), pp. 120–128. ISSN: 18787568. DOI: 10.1016/j.actbio.2015.12.023.

[2] Andy Menke et al. “Prevalence of and Trends in Diabetes Among Adults in the United States, 1988-2012”. In: *The Journal of the American Medical Association* 314.10 (2015), p. 1021. ISSN: 0098-7484. DOI: 10.1001/jama.2015.10029.

[3] Jing Wang et al. “Dietary Energy Density Predicts the Risk of Incident Type 2 Diabetes: The European Prospective Investigation of Cancer (EPIC)-Norfolk Study”. In: *Diabetes Care* 31.11 (2008). DOI: 10.2337/dc08-1085..

[4] SD Ramsey et al. “Incidence, outcomes, and cost of foot ulcers in patients with diabetes”. In: *Diabetes Ca* 22.3 (1999), pp. 382–7. ISSN: 00257206.

[5] Ezio Faglia, Fabrizio Favales, and Alberto Morabito. “New ulceration, new major amputation, and survival rates in diabetic subjects hospitalized for foot ulceration from 1990 to 1993: A 6.5-year follow-up”. In: *Diabetes Care* 24.1 (2001), pp. 78–83. ISSN: 01495992. DOI: 10.2337/diacare.24.1.78.

[6] Geoffrey C Gurtner et al. “Wound repair and regeneration.” In: *Nature* 453.7193 (May 2008), pp. 314–21. ISSN: 1476-4687. DOI: 10.1038/nature07039.

[7] Jenny E Kanter et al. “Diabetes promotes an inflammatory macrophage phenotype and atherosclerosis through acyl-CoA synthetase 1.” In: *Proceedings of the National Academy of Sciences of the United States of America* 109.12 (Mar. 2012), E715–24. ISSN: 1091-6490. DOI: 10.1073/pnas.1111600109.

[8] A.M. Loots et al. “Differences in cellular infiltrate and extracellular matrix of chronic diabetic and venous ulcers versus acute wounds”. In: *Journal of Investigative Dermatology* 111.5 (1998), pp. 850–857. ISSN: 0022202X. DOI: 10.1046/j.1523-1747.1998.00381.x.

[9] Rongkun Liu et al. “Tumor necrosis factor-alpha mediates diabetes-enhanced apoptosis of matrix-producing cells and impairs diabetic healing.” In: *The American Journal of Pathology* 168.3 (2006), pp. 757–764. ISSN: 00029440. DOI: 10.2353/ajpath.2006.050907.

[10] Fanxing Xu, Chenying Zhang, and Dana T. Graves. “Abnormal cell responses and role of TNF-a in impaired diabetic wound healing”. In: *BioMed Research International* 2013 (2013). ISSN: 23146133. DOI: 10.1155/2013/754802.

[11] Rita E. Mirza and Timothy J. Koh. “Contributions of cell subsets to cytokine production during normal and impaired wound healing”. In: *Cytokine* 71.2 (2015), pp. 409–412. ISSN: 10434666. DOI: 10.1016/j.cyto.2014.09.005.

[12] Johannes Frank et al. “In vivo effect of tumor necrosis factor alpha on wound angiogenesis and epithelialization”. In: *European Journal of Trauma* 29.4 (2003), pp. 208–219. ISSN: 14390590. DOI: 10.1007/s00068-003-1284-6.

[13] Y P Han et al. “TNF-alpha stimulates activation of pro-MMP2 in human skin through NF-(kappa)B mediated induction of MT1-MMP.” In: *Journal of cell science* 114.Pt 1 (2001), pp. 131–139. ISSN: 0021-9533. DOI: 10.1016/j.bbi.2008.05.010.

[14] Shuo Sun et al. “DOPE facilitates quaternized lipidoids (QLDs) for in vitro DNA delivery.” In: *Nanomedicine : nanotechnology, biology, and medicine* 9.7 (Oct. 2013), pp. 849–54. ISSN: 1549-9642. DOI: 10.1016/j.nano.2013.01.006.

[15] Savita Khanna et al. “Macrophage dysfunction impairs resolution of inflammation in the wounds of diabetic mice.” In: *PloS one* 5.3 (Jan. 2010), e9539. ISSN: 1932-6203. DOI: 10.1371/journal.pone.0009539.

[16] Liane I. F. Moura et al. “Recent advances on the development of wound dressings for diabetic foot ulcer treatment–a review.” In: *Acta biomaterialia* 9.7 (July 2013), pp. 7093–114. ISSN: 1878-7568. DOI: 10.1016/j.actbio.2013.03.033.

[17] Margaret A. Fonder et al. “Treating the chronic wound: A practical approach to the care of non-healing wounds and wound care dressings.” In: *Journal of the American Academy of Dermatology* 58.2 (Feb. 2008), pp. 185–206. ISSN: 1097-6787. DOI: 10.1016/j.jaad.2007.08.048.

[18] Paola Losi et al. “Fibrin-based scaffold incorporating VEGF- and bFGF-loaded nanoparticles stimulates wound healing in diabetic mice.” In: *Acta biomaterialia* 9.8 (Aug. 2013), pp. 7814–21. ISSN: 1878-7568. DOI: 10.1016/j.actbio.2013.04.019.

[19] Liane I F Moura et al. “Chitosan-based dressings loaded with neurotensin–an efficient strategy to improve early diabetic wound healing.” In: *Acta biomaterialia* 10.2 (Feb. 2014), pp. 843–57. ISSN: 1878-7568. DOI: 10.1016/j.actbio.2013.09.040.

[20] Lucília da Silva et al. “Neurotensin downregulates the pro-inflammatory properties of skin dendritic cells and increases epidermal growth factor expression.” In: *Biochimica et biophysica acta* 1813.10 (Oct. 2011), pp. 1863–71. ISSN: 0006-3002. DOI: 10.1016/j.bbamcr.2011.06.018.

[21] Kenneth A. Howard et al. “Chitosan/siRNA nanoparticle-mediated TNF-alpha knockdown in peritoneal macrophages for anti-inflammatory treatment in a murine arthritis model.” In: *Molecular therapy : the journal of the American Society of Gene Therapy* 17.1 (Jan. 2009), pp. 162–8. ISSN: 1525-0024. DOI: 10.1038/mt.2008.220.

[22] Na Li et al. “Cationic star-shaped polymer as an siRNA carrier for reducing MMP-9 expression in skin fibroblast cells and promoting wound healing in diabetic rats.” In: *International journal of nanomedicine* 9 (Jan. 2014), pp. 3377–87. ISSN: 1178-2013. DOI: 10.2147/IJN.S66368.

[23] H S Kim and H S Yoo. “Matrix metalloproteinase-inspired suicidal treatments of diabetic ulcers with siRNA-decorated nanofibrous meshes.” In: *Gene therapy* 20.4 (Apr. 2013), pp. 378–85. ISSN: 1476-5462. DOI: 10.1038/gt.2012.49.

[24] Raymond M Schiffelers et al. “Effects of treatment with small interfering RNA on joint inflammation in mice with collagen-induced arthritis.” In: *Arthritis and rheumatism* 52.4 (Apr. 2005), pp. 1314–8. ISSN: 0004-3591. DOI: 10.1002/art.20975.

[25] H. E. Seymour et al. “Anti-TNF agents for rheumatoid arthritis”. In: *British Journal of Clinical Pharmacology* 51.3 (2001), pp. 201–208. ISSN: 03065251. DOI: 10.1046/j.1365-2125.2001.00321.x.

[26] Myriam Aouadi et al. “Gene silencing in adipose tissue macrophages regulates whole-body metabolism in obese mice.” In: *Proceedings of the National Academy of Sciences of the United States of America* 110.20 (May 2013), pp. 8278–83. ISSN: 1091-6490. DOI: 10.1073/pnas.1300492110.

[27] Itamar Goren et al. “Systemic anti-TNFα treatment restores diabetes-impaired skin repair in ob/ob mice by inactivation of macrophages.” In: *The Journal of investigative dermatology* 127.9 (Sept. 2007), pp. 2259–67. ISSN: 1523-1747. DOI: 10.1038/sj.jid.5700842.

[28] Enzo Ierardi et al. “Onset of liver damage after a single administration of infliximab in a patient with refractory ulcerative colitis”. In: *Clinical Drug Investigation* 26.11 (2006), pp. 673–676. ISSN: 11732563. DOI: 10.2165/00044011-200626110-00008.

[29] Ravish Parekh and Nirmal Kaur. “Liver Injury Secondary to Anti-TNF-Alpha Therapy in Inflammatory Bowel Disease: A Case Series and Review of the Literature.” In: *Case reports in gastrointestinal medicine* 2014 (2014), p. 956463. ISSN: 2090-6528. DOI: 10.1155/2014/956463.

[30] Susan M. Goodman. “TNF Inhibitors and Severe Hepatic Injury”. In: *Drug Safety Quarterly* 4.1 (2009).

[31] Kathryn A. Whitehead et al. “Degradable lipid nanoparticles with predictable in vivo siRNA delivery activity.” In: *Nature communications* 5 (Jan. 2014), p. 4277. ISSN: 2041-1723. DOI: 10.1038/ncomms5277.

[32] Rebecca L. Ball, Christopher M. Knapp, and Kathryn A. Whitehead. “Lipidoid Nanoparticles for siRNA Delivery to the Intestinal Epithelium: In Vitro Investigations in a Caco-2 Model”. In: *Plos One* 10.7 (2015), e0133154. ISSN: 1932-6203. DOI: 10.1371/journal.pone.0133154.

[33] Kathryn A. Whitehead et al. “The in Vitro – in Vivo Translation of Lipid Nanoparticles for Hepatocellular siRNA Delivery”. In: *ACS nano* 6.8 (2012), pp. 6922–6929. DOI: 10.1021/nn301922x.The.

[34] Muthusamy Jayaraman et al. “Maximizing the Potency of siRNA Lipid Nanoparticles for Hepatic Gene Silencing In Vivo”. In: *Angewandte Chemie International Edition* 51.34 (2012), pp. 8529–8533. ISSN: 14337851. DOI: 10.1002/anie.201203263.

[35] Gaurav Sahay et al. “Efficiency of siRNA delivery by lipid nanoparticles is limited by endocytic recycling.” In: *Nature biotechnology* 31.7 (2013), pp. 653–8. ISSN: 1546-1696. DOI: 10.1038/nbt.2614.

[36] Jiyeon Yang et al. “Role of MCP-1 in tumor necrosis factor-alpha-induced endothelial dysfunction in type 2 diabetic mice”. In: *American Journal of Physiological Heart Circulation* 297 (2009), pp. 1208–1216. DOI: 10.1152/ajpheart.00396.2009..

[37] Craig W. Younce, Asim Azfer, and Pappachan E. Kolattukudy. “MCP-1 (Monocyte Chemotactic Protein-1)-induced protein, a recently identified zinc finger protein, induces adipogenesis in 3T3-L1 pre-adipocytes without peroxisome proliferator-activated receptor”. In: *Journal of Biological Chemistry* 284.40 (2009), pp. 27620–27628. ISSN: 00219258. DOI: 10.1074/jbc.M109.025320.

[38] K Murao et al. “TNF-alpha stimulation of MCP-1 expression is mediated by the Akt/PKB signal transduction pathway in vascular endothelial cells.” In: *Biochemical and biophysical research communications* 276.2 (2000), pp. 791–796. ISSN: 0006-291X. DOI: 10.1006/bbrc.2000.3497.

[39] René Rodríguez et al. “TNF triggers mitogenic signals in NIH 3T3 cells but induces apoptosis when the cell cycle is blocked”. In: *European Cytokine Network* 18.4 (2007), pp. 172–180. ISSN: 11485493. DOI: 10.1684/ecn.2007.0106.

[40] Hajime Kanda et al. “MCP-1 contributes to macrophage infiltration into adipose tissue, insulin resistance, and hepatic steatosis in obesity”. In: *Journal of Clinical Investigation* 116.6 (2006). DOI: 10.1172/JCI26498DS1.

[41] David M Mosser et al. “Activation of Murine Macrophages”. In: *Current Protocols in Immunology* Chapter 14 (2008), Unit 14.2. ISSN: 1934-368X. DOI: 10.1002/0471142735.im1402s83.Activation.

[42] Dolly J Holt, Lisa M Chamberlain, and David W Grainger. “Cell-cell signaling in co-cultures of macrophages and fibroblasts.” In: *Biomaterials* 31.36 (Dec. 2010), pp. 9382–94. ISSN: 1878-5905. DOI: 10.1016/j.biomaterials.2010.07.101.

[43] Kathryn A. Whitehead, Robert Langer, and Daniel G Anderson. “Knocking down barriers: advances in siRNA delivery.” In: *Nature reviews. Drug discovery* 8.2 (Feb. 2009), pp. 129–38. ISSN: 1474-1784. DOI: 10.1038/nrd2742.

[44] Yizhou Dong et al. “Lipopeptide nanoparticles for potent and selective siRNA delivery in rodents and nonhuman primates”. In: *Proceedings of the National Academy of Sciences* 111.15 (2014), pp. 5753–5753. ISSN: 0027-8424. DOI: 10.1073/pnas.1404711111.

[45] Ming Wang et al. “Combinatorially Designed Lipid-like Nanoparticles for Intracellular Delivery of Cytotoxic Protein for Cancer Therapy”. In: *Angewandte Chemie* 126.11 (Mar. 2014), pp. 2937–2942. ISSN: 00448249. DOI: 10.1002/ange.201311245.

[46] Tatiana I Novobrantseva et al. “Systemic RNAi-mediated Gene Silencing in Nonhuman Primate and Rodent Myeloid Cells”. In: *Molecular Therapy — Nucleic Acids* 1.1 (2012), e4. ISSN: 2162-2531. DOI: 10.1038/mtna.2011.3.

[47] Subhra K Biswas and Eduardo Lopez-Collazo. “Endotoxin tolerance: new mechanisms, molecules and clinical significance.” In: *Trends in immunology* 30.10 (Oct. 2009), pp. 475–87. ISSN: 1471-4981. DOI: 10.1016/j.it.2009.07.009.

[48] Diana Ta Ploeger et al. “Cell plasticity in wound healing: paracrine factors of M1/ M2 polarized macrophages influence the phenotypical state of dermal fibroblasts.” In: *Cell communication and signaling : CCS* 11.1 (2013), p. 29. ISSN: 1478-811X. DOI: 10.1186/1478-811X-11-29.

[49] Belete Teferedegne et al. “Mechanism of action of a distal NF-kappaB-dependent enhancer.” In: *Molecular and cellular biology* 26.15 (2006), pp. 5759–5770. ISSN: 0270-7306. DOI: 10.1128/MCB.00271-06.

[50] E. Oliver et al. “Co-culture of adipocytes with macrophages inhibits insulin action and promotes a pro-inflammatory state in adipocytes that is modulated by long-chain n-3 PUFA”. In: *Proceedings of the Nutrition Society* 67.OCE7 (2008), E232. ISSN: 0029-6651. DOI: 10.1017/S0029665108008951.

[51] M Loots. “Fibroblasts derived from chronic diabetic ulcers differ in their response to stimulation with EGF, IGF-I, bFGF and PDGF-AB compared to controls”. In: *European Journal of Cell Biology* 81.3 (2002), pp. 153–160. ISSN: 01719335. DOI: 10.1078/0171-9335-00228.

[52] Lisa N. Kasiewicz and Kathryn A. Whitehead. “Recent advances in biomaterials for the treatment of diabetic foot ulcers”. In: *Biomater. Sci.* 5.10 (2017), pp. 1962–1975. ISSN: 2047-4830. DOI: 10.1039/C7BM00264E.

[53] Rosemary Kanasty et al. “Delivery materials for siRNA therapeutics.” In: *Nature materials* 12.11 (Nov. 2013), pp. 967–77. ISSN: 1476-1122. DOI: 10.1038/nmat3765.

[54] Steven A. Castleberry et al. "Self-Assembled Wound Dressings Silence MMP-9 and Improve Diabetic Wound Healing in Vivo". In: *Advanced Materials* 28.9 (2016), pp. 1809–1817. ISSN: 15214095. DOI: 10.1002/adma.201503565.

[55] Meredith Wetterau et al. "Topical prolyl hydroxylase domain-2 silencing improves diabetic murine wound closure". In: *Wound Repair and Regeneration* 19.4 (2011), pp. 481–486. ISSN: 10671927. DOI: 10.1111/j.1524-475X.2011.00697.x.

[56] John R. Martin et al. "Local Delivery of PHD2 siRNA from ROS-Degradable Scaffolds to Promote Diabetic Wound Healing". In: *Advanced Healthcare Materials* 5.21 (2016), pp. 2751–2757. ISSN: 21922659. DOI: 10.1002/adhm.201600820.

[57] Andrew L. Weinstein et al. "Normalizing dysfunctional purine metabolism accelerates diabetic wound healing". In: *Wound Repair and Regeneration* 23.1 (2015), pp. 14–21. ISSN: 10671927. DOI: 10.1111/wrr.12249.

[58] Phuong D. Nguyen et al. "Improved diabetic wound healing through topical silencing of p53 is associated with augmented vasculogenic mediators". In: *Wound Repair and Regeneration* 18 (2010), pp. 553–559. ISSN: 10671927. DOI: 10.1111/j.1524-475X.2010.00638.x.

[59] Abdulaziz M Aldayel et al. "Acid-Sensitive Sheddable PEGylated PLGA Nanoparticles Increase the Delivery of TNF-α siRNA in Chronic Inflammation Sites". In: *Molecular Therapy—Nucleic Acids* 5.7 (2016), e340. ISSN: 2162-2531. DOI: 10.1038/mtna.2016.39.

[60] Pinaki R Desai et al. "Topical delivery of anti-TNFα siRNA and capsaicin via novel lipid-polymer hybrid nanoparticles efficiently inhibits skin inflammation in vivo." In: *Journal of controlled release : official journal of the Controlled Release Society* 170.1 (Aug. 2013), pp. 51–63. ISSN: 1873-4995. DOI: 10.1016/j.jconrel.2013.04.021.

[61] Qin Shi et al. "In vivo therapeutic efficacy of TNFα silencing by folate-PEG-chitosan-DEAE/siRNA nanoparticles in arthritic mice". In: *International Journal of Nanomedicine* 13 (2018), pp. 387–402. ISSN: 11782013. DOI: 10.2147/IJN.S146942.

[62] M F Siqueira et al. "Impaired wound healing in mouse models of diabetes is mediated by TNF-alpha dysregulation and associated with enhanced activation of forkhead box O1 (FOXO1)." In: *Diabetologia* 53.2 (Feb. 2010), pp. 378–88. ISSN: 1432-0428. DOI: 10.1007/s00125-009-1529-y.

[63] David M Ansell et al. "A statistical analysis of murine incisional and excisional acute wound models". In: *Wound Repair and Regeneration* 22 (2014), pp. 281–287. DOI: 10.1111/wrr.12148.

[64] Louise Dunn et al. "Murine model of wound healing." In: *Journal of visualized experiments : JoVE* 75 (2013), e50265. ISSN: 1940-087X. DOI: 10.3791/50265.

[65] Samir Mitragotri, Paul A. Burke, and Robert Langer. "Overcoming the challenges in administering biopharmaceuticals: formulation and delivery strategies". In: *Nature reviews: Drug discovery* 13.9 (2015), pp. 655–672. DOI: 10.1038/nrd4363.Overcoming.

[66] Heather Herd Gustafson et al. "Nanoparticle uptake: The phagocyte problem". In: *Nano Today* 10.4 (2015), pp. 487–510. ISSN: 1878044X. DOI: 10.1016/j.nantod.2015.06.006.

[67] Sunny Kumar et al. "Shape and size-dependent immune response to antigen-carrying nanoparticles". In: *Journal of Controlled Release* 220 (2015), pp. 141–148. ISSN: 18734995. DOI: 10.1016/j.jconrel.2015.09.069.

[68] Gaurav Sharma et al. “Polymer particle shape independently influences binding and internalization by macrophages”. In: *Journal of Controlled Release* 147.3 (2010), pp. 408–412. ISSN: 01683659. DOI: 10.1016/j.jconrel.2010.07.116.

[69] N Schöler et al. “Effect of lipid matrix and size of solid lipid nanoparticles (SLN) on the viability and cytokine production of macrophages”. In: *Int. J. Pharm* 231 (2002), pp. 167–76.

[70] Naomi Benne et al. “Orchestrating immune responses: How size, shape and rigidity affect the immunogenicity of particulate vaccines”. In: *Journal of Controlled Release* 234 (2016), pp. 124–134. ISSN: 18734995. DOI: 10.1016/j.jconrel.2016.05.033.

[71] Anne Marit de Groot et al. “Immunogenicity Testing of Lipidoids In Vitro and In Silico: Modulating Lipidoid-Mediated TLR4 Activation by Nanoparticle Design”. In: *Molecular Therapy - Nucleic Acids* 11.June (2018), pp. 159–169. ISSN: 21622531. DOI: 10.1016/j.omtn.2018.02.003.

[72] S. M. Shinall et al. “Identification of Murine Germinal Center B Cell Subsets Defined by the Expression of Surface Isotypes and Differentiation Antigens”. In: *The Journal of Immunology* 164.11 (2000), pp. 5729–5738. ISSN: 0022-1767. DOI: 10.4049/jimmunol.164.11.5729.

[73] Yang Zhang, Laura Garcia-Ibanez, and Kai Michael Toellner. “Regulation of germinal center B-cell differentiation”. In: *Immunological Reviews* 270.1 (2016), pp. 8–19. ISSN: 1600065X. DOI: 10.1111/imr.12396.

[74] Dan Suan, Christopher Sundling, and Robert Brink. “Plasma cell and memory B cell differentiation from the germinal center”. In: *Current Opinion in Immunology* 45 (2017), pp. 97–102. ISSN: 18790372. DOI: 10.1016/j.coi.2017.03.006.

[75] Mark J. McCarron, Pyong Woo Park, and David R. Fooksman. “CD138 mediates selection of mature plasma cells by regulating their survival”. In: *Blood* 129.20 (2017), pp. 2749–2759. ISSN: 15280020. DOI: 10.1182/blood-2017-01-761643.

[76] Fionnuala P. O’Connell, Jack L. Pinkus, and Geraldine S. Pinkus. “CD138 (Syndecan-1), a Plasma Cell Marker”. In: *American Journal of Clinical Pathology* 121.2 (2004), pp. 254–263. ISSN: 0002-9173. DOI: 10.1309/617DWB5GNFWXHW4L.

[77] Kim L. Good-Jacobson and David M. Tarlinton. “Multiple routes to B-cell memory”. In: *International Immunology* 24.7 (2012), pp. 403–408. ISSN: 09538178. DOI: 10.1093/intimm/dxs050.

[78] Kazunaga Agematsu et al. “CD27: A memory B-cell marker”. In: *Immunology Today* 21.5 (2000), pp. 204–206. ISSN: 01675699. DOI: 10.1016/S0167-5699(00)01605-4.

[79] Rick Kapur, Helga K. Einarsdottir, and Gestur Vidarsson. “IgG-effector functions: “The Good, The Bad and The Ugly””. In: *Immunology Letters* 160.2 (2014), pp. 139–144. ISSN: 18790542. DOI: 10.1016/j.imlet.2014.01.015.

[80] Toshio Tanaka, Masashi Narazaki, and Tadamitsu Kishimoto. “Il-6 in inflammation, Immunity, And disease”. In: *Cold Spring Harbor Perspectives in Biology* 6.10 (2014), pp. 1–16. ISSN: 19430264. DOI: 10.1101/cshperspect.a016295.